Doctoral Thesis

Neuromusculoskeletal Modeling and Computer Simulation of Human Locomotion Considering the Multi-Segmental Motion of the Trunk

March 2021

Doctoral Program in Sport and Health Science
Graduate School of Sport and Health Science
Ritsumeikan University

KUDO　Shoma

Doctoral Thesis Reviewed
by Ritsumeikan University

Neuromusculoskeletal Modeling and Computer Simulation of Human Locomotion Considering the Multi-Segmental Motion of the Trunk

（体幹部の多自由度運動を考慮した筋骨格モデルの構築と歩行動作のシミュレーション）

March 2021

2021 年 3 月

Doctoral Program in Sport and Health Science
Graduate School of Sport and Health Science
Ritsumeikan University
立命館大学大学院スポーツ健康科学研究科
スポーツ健康科学専攻博士課程後期課程
KUDO Shoma
工藤将馬
Supervisor: Professor NAGANO Akinori
研究指導教員：　長野明紀　教授

Contents

Figures

Tables

List of abbreviations

ADDBR:	M. adductor brevis
ADDLO:	M. adductor longus
ADDMA:	M. adductor magnus
AIC:	Akaike's information criterion
AICc:	Bias-corrected Akaike's information criterion
ANOVA:	Analysis of variance
AR:	Axial rotation
ASIS:	Anterior superior iliac spine
BIFEL:	M. biceps femoris caput longum
BIFES:	M. biceps femoris caput brevis
C7:	Seventh cervical vertebra
CE:	Contractile element
COM:	Center of mass
CV:	Coefficients of variation
DOF:	Degree of freedom
DP:	Dorsi flexion and planter flexion
EXTOB1:	Anterior part of m. external oblique
EXTOB2:	Middle part of m. external oblique
EXTOB3:	Posterior part of m. external oblique
FCE:	Contractile element force
FE:	Flexion and extension
FHAL:	M. flexor hallucis longus
FMAX:	Maximal isometric muscle force

FSEE:	Series elastic element
FT:	First twitch fibers
GASL:	M. gastrocnemius lateralis
GASM:	M. gastrocnemius medialis
GMAXI:	M. gluteus maximus
GMEDI:	M. gluteus medius
GMINI:	M. gluteus minimus
GRF:	Ground reaction force
HAT	Rigid-body segment lumped together with the head, arm, and trunk
IE:	Internal and external rotation
ILIA:	M. iliacus
ILIOCLUMB_LUMB:	M. iliocostalis lumborum par lumbrum
ILIOCLUMB_THOR1:	Lower part of m. iliocostalis lumborum par thorasis
ILIOCLUMB_THOR2:	Upper part of m. iliocostalis lumborum par thorasis
INTOB1:	Anterior part of m. internal oblique
INTOB2:	Middle part of m. internal oblique
INTOB3:	Posterior part of m. internal oblique
L3:	Third lumber vertebra
LB:	Lateral bending
LCE:	Fiber length
LONGISTHOR_LUMB:	M. longissimus thoracis pars lumborum
LONGISTHOR_THOR1:	Lower part of m. longissimus thoracis pars thoracis
LONGISTHOR_THOR2:	Upper part of m. longissimus thoracis pars thoracis
LONGISTHOR_THOR_RIB1:	Lower rib part of m. longissimus thoracis pars thoracis

LONGISTHOR_THOR_RIB2:	Upper rib part of m. longissimus thoracis pars thoracis
LSEE:	Length of SEE
MLL:	Maximized logarithmic likelihood
MULFID:	M. multifidus
ODE:	Ordinary differential equation
PCSA:	Physiological cross-sectional area
PE:	Position error
PEE:	Parallel elastic element
PERL:	M. peroneus longus
PERLB:	M. peroneus brevis
PIRI:	M. piriformis
PSIS:	Posterior superior iliac spine
PSOASM:	M. psoas major
QUAD:	M. quadratus femoris
QUADLUMB_ANT:	Anterior part of m. quadratus lumborum
QUADLUMB_MID:	Middle part of m. quadratus lumborum
QUADLUMB_POST:	Posterior part of m. quadratus lumborum
RECABD:	M. rectus abdominis
RECTF:	M. rectus femoris
S1:	First sacral vertebra
SD:	Standard deviation
SEE:	Series elastic element
SEMM:	M. semimembranosus
SEMT:	M. semitendinosus

SOLEU:	M. soleus
STIM:	Stimulation input of a muscle
STM:	Simultaneous transformation matrix
T12:	Twelfth thoracic vertebra
T3:	Third thoracic vertebra
T6:	Sixth thoracic vertebra
T9:	Ninth thoracic vertebra
TE:	Thorax extension
TF:	Thorax flexion
TIBAN:	M. tibialis anterior
TIBPOS:	M. tibialis posterior
VASI:	M. vastus intermedialis
VASL:	M. vastus lateralis
VASM:	M. vastus medialis
VCE:	Shortening velocity of muscle
WBE:	Whole body energy expenditure

Chapter 1: *General Introduction*

1.1. *Background*

Designing an effective intervention for improving human physical activity and healthy life-expectancy needs the understanding of biomechanics of the neurological–muscular–skeletal system for controlling human whole-body motion. Specifically, a theory on human motor functions is necessary to be established by elucidating the mechanisms of physical activity from a set of experimental data; moreover, the effects of the interventions can be evaluated by examining the causal relationship between the neuromusculoskeletal system and human motion based on such a theory. In the field of biomechanics, both inverse and forward dynamics analyses have been used as effective methods to realize these requirements, and several researchers have greatly contributed toward advancing these analytical systems for a better understanding of the neuromusculoskeletal system and its effect on human motion.

A computer simulation with the neuromusculoskeletal model has been recognized as an effective way to predict the causal relationship between the neuromusculoskeletal system and human motion without using an experimental dataset (Anderson and Pandy, 1999, 2001b; Gerritsen et al., 1998; Nagano and Gerritsen, 2001; Nagano et al., 2005a). Although most studies have used the neuromusculoskeletal simulation system to report the musculoskeletal contribution of the lower and upper extremities of human bodies in controlling human movements, there is limited knowledge regarding the trunk of the human body, which is considered to have a significant effect on the stability and mobility of the entire body. Therefore, the lack of knowledge regarding the biomechanics of the human trunk has been a major barrier limiting the understanding of the comprehensive control mechanism of our entire body toward achieving human movement.

The possible reason of this limitation in understanding the musculoskeletal contribution of the

trunk on the control of human movements may be posed by the effectivity of the neuromusculoskeletal model to optimally represent the complex movement for the trunk, which is yet to be revealed. As the trunk has a multi-segmental structure, comprising the cervical, thoracic, and lumbar spines and numerous muscles, a specific formation allows the trunk to deform complexly during human movements. Although the control of stability and mobility of the human body is acknowledged to be imparted by the composite actions of the multi-segmental trunk structures, the trunk has often been modeled as a single fixed-segment ignoring the possible multi-segmental contributions, forces developed by individual muscles, and the torque generated about the joints in the trunk (Cappozzo, 1983; MacKinnon and Winter, 1993; Winter, 1995). For instance, only a few studies have segmented separate components for addressing trunk movements (Breloff and Chou, 2017; Crosbie et al., 1997a, b) instead of separately interpreting the thoracic and pelvic movements for the analysis of human movements, as suggested by previous studies (Crosbie et al., 1997b; Hurt et al., 2010; Stokes et al., 1989; Swinnen et al., 2013; Vogt and Banzer, 1999). Therefore, the optimal musculoskeletal model representing the multi-segmental movements of the trunk has not yet been revealed, and this is one of the vital factors toward analyzing the dynamics of human movement with considerations of the musculoskeletal contribution of the trunk.

1.2. *Focus of this dissertation*

The development of an optimal model of the trunk representing its multi-segmental movements will enable researchers to objectively quantify the neuromusculoskeletal contribution of the trunk for controlling human body movements. Therefore, the goal of this dissertation was to establish a neuromusculoskeletal computer simulation system to enable a three-dimensional motion analysis on the musculoskeletal contribution of the trunk. Thus, a musculoskeletal model of the trunk was constructed to optimally represent the neuromuscular activities of the trunk muscles and the multi-

segmental movements.

The studies described in this dissertation focused on human locomotion (i.e., walking and running), which is one of the most common activities of daily life; thus, the preservation and improvement of the locomotor function are of considerable importance for extending healthy life-expectancy. In this respect, the importance of the trunk has been widely recognized to contribute considerably to achieving and controlling human locomotion by serving as a linking segment between the lower and upper limbs (Arvin et al., 2016; Cappozzo, 1983; MacKinnon and Winter, 1993; Winter, 1995). As a result, irregular trunk movements can serve as indicators of muscular issues in the limbs. For example, the Duchenne or Trendelenburg gait, which is marked by increased trunk movements, is considered to be a compensatory mechanism for hip abductor muscle weakness during human locomotion (Böhm et al., 2013; Schmid et al., 2013). These excessive trunk movements have also been shown to increase the cost of locomotion (Salami et al., 2017) and may cause back pain. However, the causal relationship between the neuromusculoskeletal activity of the trunk and such compensatory motion remains unknown due to the lack a model to optimally assess the musculoskeletal activity of the trunk. To address this problem, a musculoskeletal computer simulation would be helpful in elucidating the causal relationships between the muscular activities of the trunk and the stability and mobility of the human body during locomotion. The utility of such a simulation served as the motivation for this dissertation, and the simulation system established herein is accordingly able to optimally assess the human locomotion function and accurately detect any abnormalities.

1.3. *Literature review*

1.3.1. *Model of skeletal system and kinematic description of the trunk*

The trunk has a multi-segmental structure—comprising the cervical, thoracic, and lumbar spines—that takes up specific formations to allow its flexible deformation during dynamic movements

(Bazrgari et al., 2011; Breloff and Chou, 2015; Frigo et al., 2003). In three-dimensional movement analyses, the trunk segment has often been simplified to a single or small number of rigid segments to reduce the complexity of its flexible multi-segmental structure (Cappozzo, 1983; de Leva, 1996; Frigo et al., 2003). However, such simplifications may overlook the flexible deformation of the trunk (Campos et al., 2015; Leardini et al., 2009; Syczewska et al., 1999); therefore, the extent of this deformation during human locomotion is yet to be verified, and the quantitative assessment of the geometric deformation is essential to facilitate the construction of the optimal musculoskeletal model of the trunk.

Several studies have reported significant multi-segmental motion undergoing in the trunk during human locomotion, thus stating the inadequacy of a single rigid-body representation to optimally describe its movements (Breloff and Chou, 2015; Breloff and Chou, 2017; Crosbie et al., 1997b; Preuss and Popovic, 2010). Moreover, a few studies have reported kinematic and kinetic descriptions of the trunk during human locomotion using multi-segmental linked rigid-body representations, but these studies utilized various linked rigid-body representations of the trunk that adopted several rigid-body segments (Breloff and Chou, 2015; Breloff and Chou, 2017; Callaghan et al., 1999; Crosbie et al., 1997b; Needham et al., 2016; Preuss and Popovic, 2010). For instance, Breloff et al. (2015, 2017) modeled the trunk with seven rigid-bodies, and Callagham et al. (1999) and Needham et al. (2016) modeled the trunk with the pelvis, abdomen, and thorax segments. In this regard, Leardini et al. (2009) and Schinkel-Ivy and Drake (2015) reported that different linked rigid-body representations of the trunk result in different patterns of angular displacement for each segment and range of motion during human locomotion (Leardini et al., 2009; Schinkel-Ivy and Drake, 2015). Therefore, the number of rigid-body segments used in the trunk model significantly affected the resultant kinematics of the trunk, which would be a conclusive factor for describing its multi-segmental motion during human locomotion.

A multi-segmental rigid-body model can provide a better representation of the trunk compared to a small number of rigid-body models in terms of the goodness-of-fit of the model, but there is a tradeoff between fitting the data and the generalizability of the model. In fact, a larger number of segments are generally used to assess the detailed multi-segmental movements of the trunk during human body-movements (Breloff and Chou, 2017; Christophy et al., 2012; de Zee et al., 2007; Leardini et al., 2011; Preuss and Popovic, 2010). However, a greater degree of freedom (DOF) further complicates the model and impairs its ability to be generalized by being extremely specific for a particular dataset of participants (Hicks et al., 2015). Moreover, the computational complexity for the analysis increases with higher DOFs (Hicks et al., 2015; Rajagopal et al., 2016; Zhang, 2001). Therefore, undue model complexity and participant-specificity should be avoided to create a more generalizable model, even though the goodness-of-fit is benefited from increased model complexities.

1.3.2. *System of neuromusculoskeletal computer simulation*

Research and development in the domain of neuromusculoskeletal computer simulation have surged in the last 30 years (Anderson and Pandy, 1999, 2001a; Anderson and Pandy, 2003; Delp et al., 2007; Gerritsen et al., 1998; Nagano and Gerritsen, 2001; Nagano et al., 2005a; Yamaguchi and Zajac, 1990). In particular, the development of numerous software packages for musculoskeletal simulation, as represented by Opensim and proposed by Delp (1990) has contributed immensely to the advancement of studies attempting to understand the effect of the neuromusculoskeletal system on human body motion (Delp et al., 2007; Delp and Loan, 1995). Although these software packages enable convenient assessment of the effect of the neuromusculoskeletal system on human body motion, it is difficult to adjust the model structure and simulation parameters freely based on the objective of the study, due to the specification of these individual packages. This represents a significant problem during modeling the multi-segmental structure of the trunk.

To overcome these problems, Nagano and coworkers have developed and provided computer programing codes to aid the modeling of a whole-body skeleton and a muscle–tendon complex for humans (Nagano, 2003; Nagano and Gerritsen, 2001; Nagano et al., 2005c). Specifically, these programming codes constructed a neuromusculoskeletal system including a skeleton and muscular model using Autolev (OnLine Dynamics, Stanford, CA, USA)—a commercial package that generates C-language code. Using this coding methodology based on C-language for neuromusculoskeletal modeling, the overall architecture of the programing codes can be checked thoroughly, and the structure and parameters of the simulation system can be adjusted freely to fit the objectives of the study. Therefore, such programing methods would be greatly helpful in understanding the overall architecture of the neuromusculoskeletal computer simulation system as well as to freely construct the skeletal and muscle–tendon models of the trunk reflecting the aims of this dissertation.

Furthermore, the computational efficiency of the musculoskeletal simulation system should be considered during its establishment. In context, several whole-body musculoskeletal models—consisting a detailed structure with numerous muscles—have been developed to accurately estimate muscular activities and the force developed by the muscles (Bayoglu et al., 2019; Bayoglu et al., 2017a, b; Christophy et al., 2012; de Zee et al., 2007; Raabe and Chaudhari, 2016); however, the models are not always suitable in terms of computational efficiency. Additionally, as mentioned in the previous subsection, a higher number of muscles and DOFs complicates the model and impairs its ability to be generalized by being too specific for a particular dataset of participants (Hicks et al., 2015). This problem would be more serious when "predicting" human body motion generated by estimated muscle activations in a forward dynamics simulation than in the inverse dynamics simulation, because the latter fits the musculoskeletal model to a set of kinematic data observed experimentally and estimates the muscular activity from its kinematic and kinetic data. Therefore, a consideration of balance between the factors of goodness-of-fit, generalizability, and computational efficiency is essential for

establishing a neuromusculoskeletal computer simulation system that is adaptive for both inverse and forward dynamics simulation.

1.3.3. *Summary*

Three limitations of existing systems for the motion analysis of the trunk were identified in the literature review. First, it is unclear to what extent the trunk acts through multi-segmental movements during human movements. Second, although the optimal number of linked rigid-bodies of the trunk should be determined considering the balance between the goodness-of-fit and generalizability of the model, assessments of such modeling parameters have not yet been quantitatively undertaken. Third, a forward simulation system (model) to assess the effect of trunk muscles on controlling body movements has not yet been established. These limitations have constrained the ability of researchers to understand how the trunk controls the human body during dynamic movements. Addressing these three limitations therefore represents a crucial opportunity to augment the range of biomechanical analyses of human movements traditionally based only on the musculoskeletal systems of the lower extremities.

1.4. *Specific aims*

Considering the limitations of the previous studies reviewed in subsections 1.3.1 and 1.3.2, this study was undertaken in pursuit of five defined objectives, each which is listed and briefly discussed below.

(1) <u>To quantify the geometric deformation of the trunk during human locomotion.</u>

The trunk has a multi-segmental structure comprising the cervical, thoracic, and lumbar spines surrounded by soft tissue elements that allows it to deform flexibly during human

locomotion. The extent of this flexible deformation needs to be evaluated before determining the optimal number of rigid-bodies required in depicting the musculoskeletal model of the trunk. Therefore, this study quantitatively assessed the time-varying geometric deformation of the trunk during human locomotion.

(2) To assess the effects of trunk deformability on the resultant kinematics for different number of rigid-body segments in the trunk model.

The number of rigid-body segments used to model the trunk significantly affects the trunk kinematics represented during human locomotion. The optimally linked rigid-body representation of the trunk should be determined based on the objectives and the accuracy required to adequately describe the complex trunk movement in the analysis; thus, the quantitative assessment of the effects of trunk deformability on the resultant trunk kinematics was conducted with different numbers of rigid-body segments in the trunk model.

(3) To determine the optimal number of linked rigid bodies required to represent trunk movements during walking

The optimal number of linked rigid-bodies of the trunk required to appropriately represent the multi-segmental movements during walking was determined using a quantitative measure for model evaluation. The musculoskeletal model was developed by optimizing its complexity and generalizability to simulate human locomotion for study. In general, a multi-segmental rigid-body model represents the trunk better than a single rigid-body model with regard to goodness-of-fit. However, the computational efficiency and generalizability of the model decreases with increasing model complexity. Thus, this study aimed to determine the optimal number of rigid-body segments during walking using a quantitative measure that fulfills the goodness-of-fit and

generalizability factors for the model based on Akaike's information criterion.

(4) To establish a neuromusculoskeletal computer simulation system considering the multi-segmental structure of the trunk

The musculoskeletal model system, including a skeleton model, muscular model, and an external environment interaction model (i.e., ground reaction force) was constructed using MotionGenesis (Motion Genesis LCC, Stanford, CA, USA)—a commercial package which generates C-language code. Moreover, the whole-body skeleton was modeled considering the multi-segmental structure of the trunk.

(5) To simulate human walking motion and assess the validation of the neuromusculoskeletal computer simulation system

The motion of walking normally on level ground was simulated using the theory of forward dynamics simulation; the kinematic and kinetic data simulated by using forward dynamics computer simulation were compared with those derived using the inverse dynamics approach (Newton–Euler methods) to assess the validity of the musculoskeletal computer simulation system constructed in this dissertation.

1.5. *Significance and originality of this dissertation*

This study presents the first considerations of assessing the neuromusculoskeletal contribution of the human trunk in locomotion that has not been clarified by previous studies. In addition, the current study establishes a framework that will enable researchers to analyze the human body motion on the aforementioned considerations by determining the optimal neuromusculoskeletal model of the trunk. Furthermore, the novelty of this research was highlighted with the use of a quantitative measure

on the model assessment to determine the optimal number of linked rigid-body segments required to adequately represent the trunk during human locomotion. Finally, the neuromusculoskeletal model was programmed using C-language that can be coded independently of any commercial package for such simulations, and this is further helpful in understanding the overall architecture of the neuromusculoskeletal computer simulation system.

1.6. *Thesis overview*

Chapter 2 presents a quantitative assessment of the geometric deformation of the trunk during human locomotion. This chapter includes material coauthored with Dr. Masahiro Fujimoto, Dr. Tadao Isaka, and Dr. Akinori Nagano. Chapter 3 describes the effects of deformability on the resultant trunk kinematics for numerous rigid-body segments that helps in assessing the appropriateness of the linked rigid-body models in representing the flexible deformations of the trunk during walking. This chapter includes material coauthored with Dr. Masahiro Fujimoto, Dr. Takahiko Sato, and Dr. Akinori Nagano. Chapter 4 presents a study to determine the optimal number of rigid-body segments required to adequately represent walking. In this chapter, Akaike's information criterion was used to assess the relative quality of the linked rigid-body trunk models, considering the balance between goodness-of-fit and generalizability of the model; the optimal number of linked rigid-body models was determined based on this criterion. This chapter includes material coauthored with Dr. Masahiro Fujimoto, Dr. Takahiko Sato, and Dr. Akinori Nagano. Chapter 5 describes the musculoskeletal modeling and the aspects of defining musculoskeletal models. Chapter 6 presents the simulation of walking; furthermore, the validity of the musculoskeletal computer simulation system was assessed. Chapter 7 highlights the conclusions drawn from the major findings of each study. The limitations of the studies were discussed with suggestions for future research. The appendices—included after the bibliography—presents detailed derivations of the equations and parameters of the musculoskeletal model used in each study.

Chapter 2: *Quantitative assessment of trunk deformation during human locomotion*

2.1. *Introduction*

The trunk has a multi-segmental structure, composed of the cervical, thoracic, and lumbar spines and surrounded by soft tissue elements, which attains a specific formation that allows flexible deformations during dynamic movements (Bazrgari et al., 2011; Breloff and Chou, 2015; Frigo et al., 2003). The trunk segment has often been simplified to a single or small number of rigid segments in three-dimensional movement analyses to reduce the complexity of its flexible multi-segmental structure (Cappozzo, 1983; de Leva, 1996; Frigo et al., 2003). However, such simplifications may overlook the flexible deformation of the trunk (Campos et al., 2015; Leardini et al., 2009; Syczewska et al., 1999). Therefore, considering the trunk as a deformable segment rather than a single rigid-body segment would be more appropriate. In this regard, it is necessary to quantify the actual trunk deformation resulting from its multi-segmental musculoskeletal structure during human locomotion.

Therefore, the purpose of this study was to quantitatively assess the trunk deformation occurring during human locomotion. The trunk was divided into small areas with forty reflective markers to identify the geometrical deformations in three dimensions. The changes in distance between the markers and the directional changes of the small areas were used to quantify the translational and angular deformations, respectively. The amount of deformation on a particular position can be hypothesized to depend on the corresponding location on the trunk, and the variation of this deformation would increase with the running speed.

2.2. *Methods*

2.2.1. *Participants*

Ten male collegiate students participated in this study (mean age: 21.5 ± 1.0 y, mean height: 172.0 ± 5.5 cm, mean body mass: 66.8 ± 8.5 kg). All participants reviewed and signed an informed consent form, and the study was approved by the Institutional Review Board at Ritsumeikan University, Biwako-Kusatsu Campus, Japan.

2.2.2. *Data collection*

The participants ran on a treadmill at four different speeds: 8, 10, 12, and 14 km/h. Three-dimensional kinematic data were recorded using a sixteen-camera motion capture system at 250 Hz (MAC3D, Motion Analysis Corporation, CA, USA); the recorded data was smoothed using a fourth-order Butterworth filter with a cutoff frequency of 8 Hz. The system and equipment used in this study was capable of achieving sub-millimeter accuracy, and the residual systematic error was less than 0.5 mm at the instant of calibration. Forty reflective markers were placed on the participants' backs at regular intervals to define 56 triangular areas. The markers were placed between the acromioclavicular joint and posterior superior iliac spine (PSIS) levels (Figure 2.1). Additional markers were placed at the anterior superior iliac spine (ASIS) to define the pelvic reference frame; ankle, toe, and heel joint markers were used to define gait cycles.

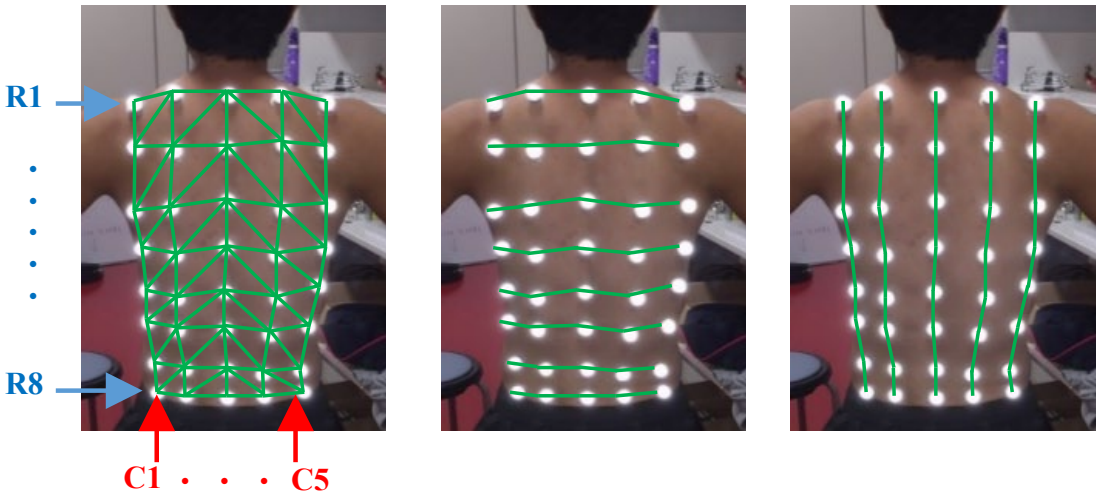

Figure 2.1 Placement of the markers.

Markers were placed between the acromioclavicular joint and posterior superior iliac spine levels. A two-way ANOVA (position and running speed) was used to investigate main and interaction effects on the CVs and SD. (a) For the SD of the normal vectors, area (56 triangular areas, seven rows by eight columns) and speed (four running speeds) were used as the factors. (b) For the CV of the horizontal length, location (32 locations of the horizontal length, eight rows by four columns) and speed (four running speeds) were used as the factors. (c) For the CV of the vertical length, location (35 locations of vertical length, seven rows by five columns) and speed (four running speeds) were used as the factors.

2.2.3. *Data analysis*

The deformation of the trunk was quantified as translational and angular deformations. The translational deformation was quantified based on the horizontal and vertical lengths between two adjacent markers, which were calculated as the Euclidean distance. In addition, the coefficient of variation (CV) during a gait cycle was calculated to assess the amount of translational deformation.

On the contrary, the angular deformation was quantified based on the normal vector of the triangular area defined by the adjacent markers. The standard deviation (SD) of the angle of the normal vector on each plane during a gait cycle was used as a measure of the angular deformation. The changes in the direction of the normal vectors were quantified based on the angle between the normal vectors and the axes of the pelvic reference frame with respect to the frontal, sagittal, and transverse planes (Figure 2.2). The pelvic reference frame was defined using the ASIS and the midpoint of the markers placed at the PSIS level. The medial–lateral axis (y-axis) was defined along the ASIS markers. The vertical axis (z-axis) was defined as a vector orthogonal to the area defined by the ASIS markers and the midpoint of the markers placed at the PSIS level (Leardini et al., 2011). The posterior–anterior axis (x-axis) was defined as a vector orthogonal to the other two axes. The instant of heel strike was detected based on the vertical velocity of the midfoot (O'Connor et al., 2007) and was used to define a gait cycle. The data obtained from five gait cycles were averaged for each subject. The CVs of the horizontal and vertical lengths and the SD of the normal vectors were respectively measured as the translational and angular deformation and visualized as two-dimensional color-coded images. The entire data was processed using MATLAB software (The MathWorks, Natick, MA, USA).

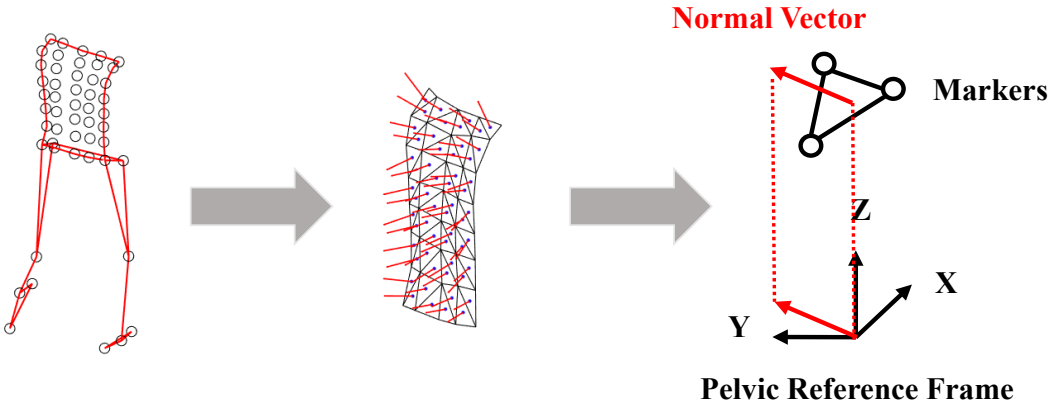

Figure 2.2 The direction of the normal vector was evaluated using the angle between the normal vector and the axes of the pelvic reference frame.

2.2.4. *Statistical analysis*

The main effects and interactions of the translational and angular deformation were investigated through a statistical analysis consisting of a two-way repeated measures analysis of variance (ANOVA) (Ekuseru-Toukei 2015; Social Survey Research Information Co., Ltd., Tokyo, Japan). The area (56 triangular areas, seven rows by eight columns: Figure 2.1a) and speed (four running speeds) were used as the factors to obtain the SD of the normal vectors (angular deformation). The locations (32 locations of the horizontal length, four rows by eight columns: Figure 2.1b; 35 locations of vertical length, five rows by seven columns: Figure 2.1c) and speed (four running speeds) were used as the factors to determine the CVs of the horizontal and vertical length (translational deformation). The level of significance was set at 0.05.

2.3. *Results*

The movement of each triangular plane on the trunk during running is shown in Figure 2.3.

2.3.1. *Translational deformation*

The significant interactions occurring between the location and speed were observed on the CV of the horizontal and vertical lengths ($p<0.001$). The largest amplitudes were found on the medial and lower sides for the horizontal length and on the lateral and upper sides for the vertical length (Figure 2.4 and 2.5). The CV ranged from 0.7–14.3% for the horizontal length and from 0.5–12.6% for the vertical length (Table 2.1).

2.3.2. *Angular deformation*

The significant main effects of the area and running speed were observed on the SD of the normal vectors in the sagittal plane, and significant interactions were also detected in the transverse and frontal planes ($p<0.001$). The largest amplitudes were found on the medial and upper areas for the transverse and frontal planes (Figure 2.6–2.8). The SD ranged from 0.01–0.31 rad (1°–18°), 0.02–0.11 rad (1°–6°), and 0.03–1.36 rad (1°–78°) for the transverse, sagittal, and frontal plane, respectively (Table 2.1).

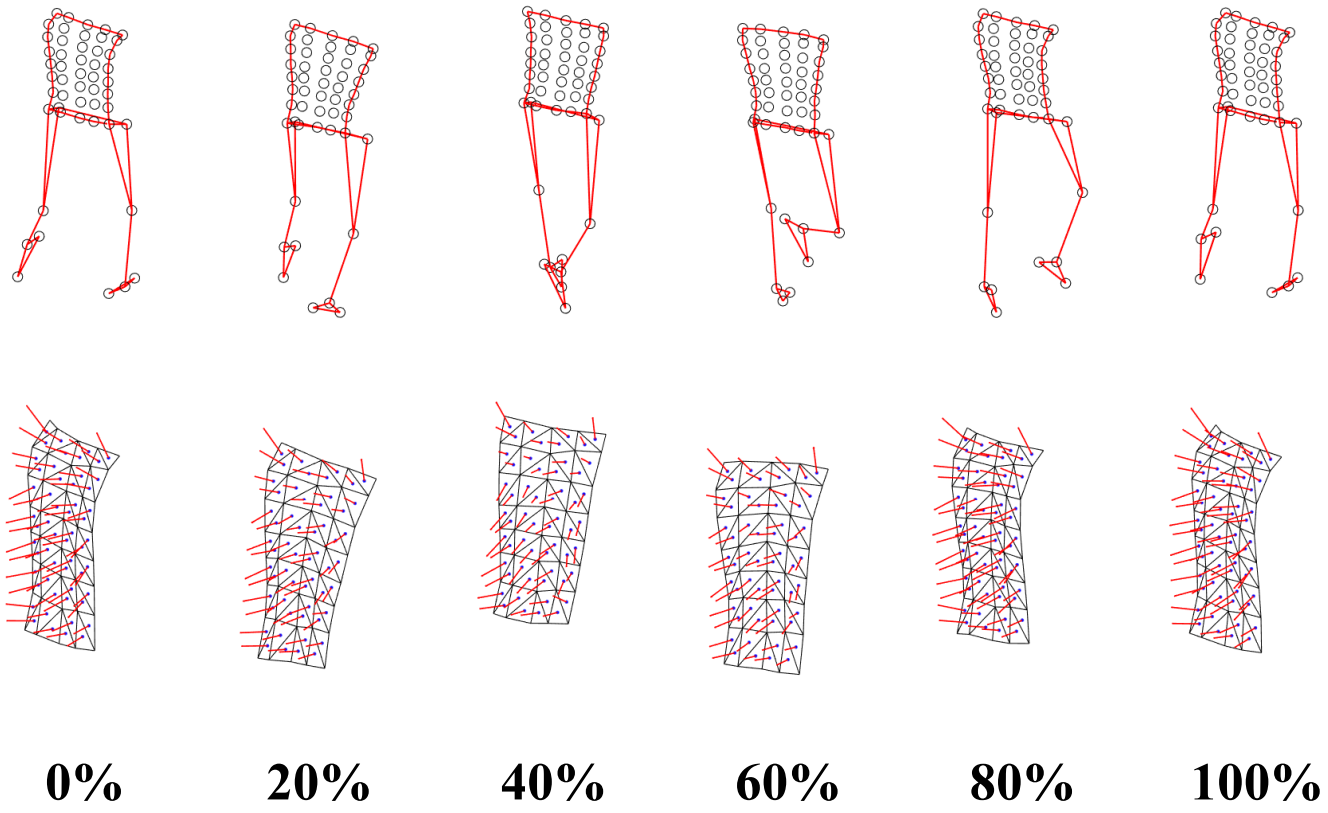

Figure 2.3 Snapshots of the movement of each triangular plane on the trunk during running, in which the percentages indicate progress through a complete running stride.

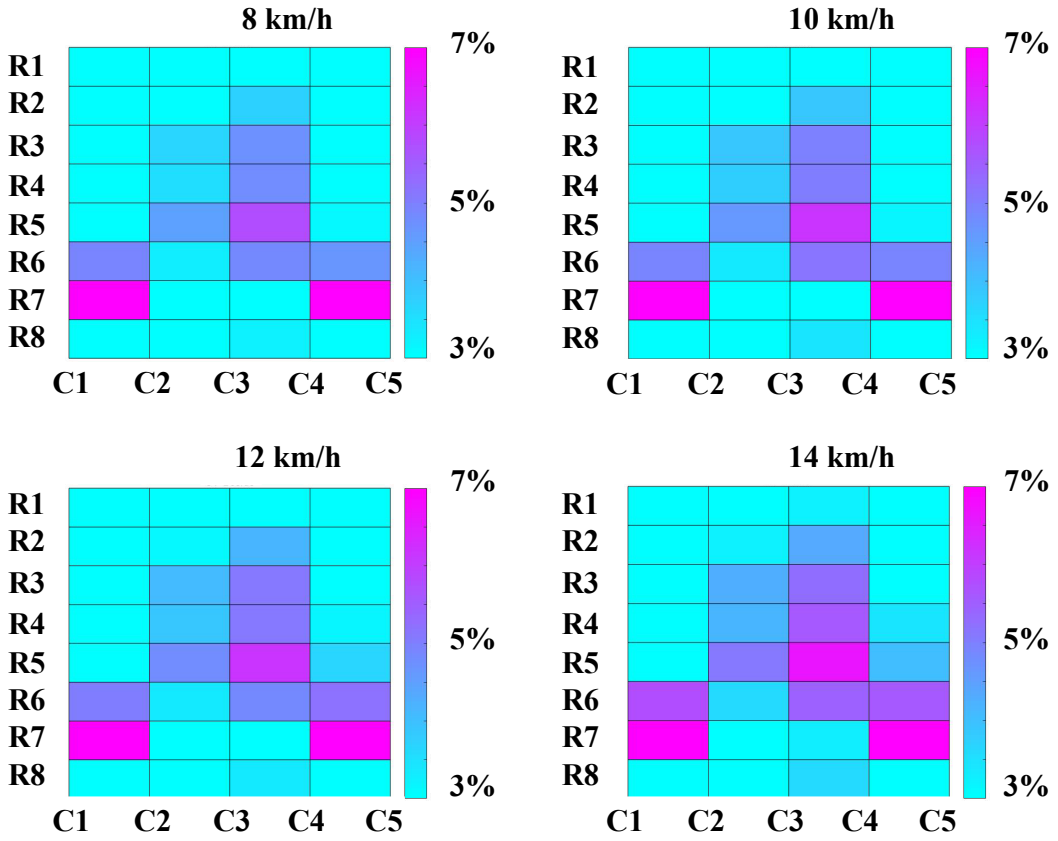

Figure 2.4 Variation in horizontal length (R: row; C: column).

The magnitude of change is represented by a color map (the blue color corresponds to small changes and the red color corresponds to large changes).

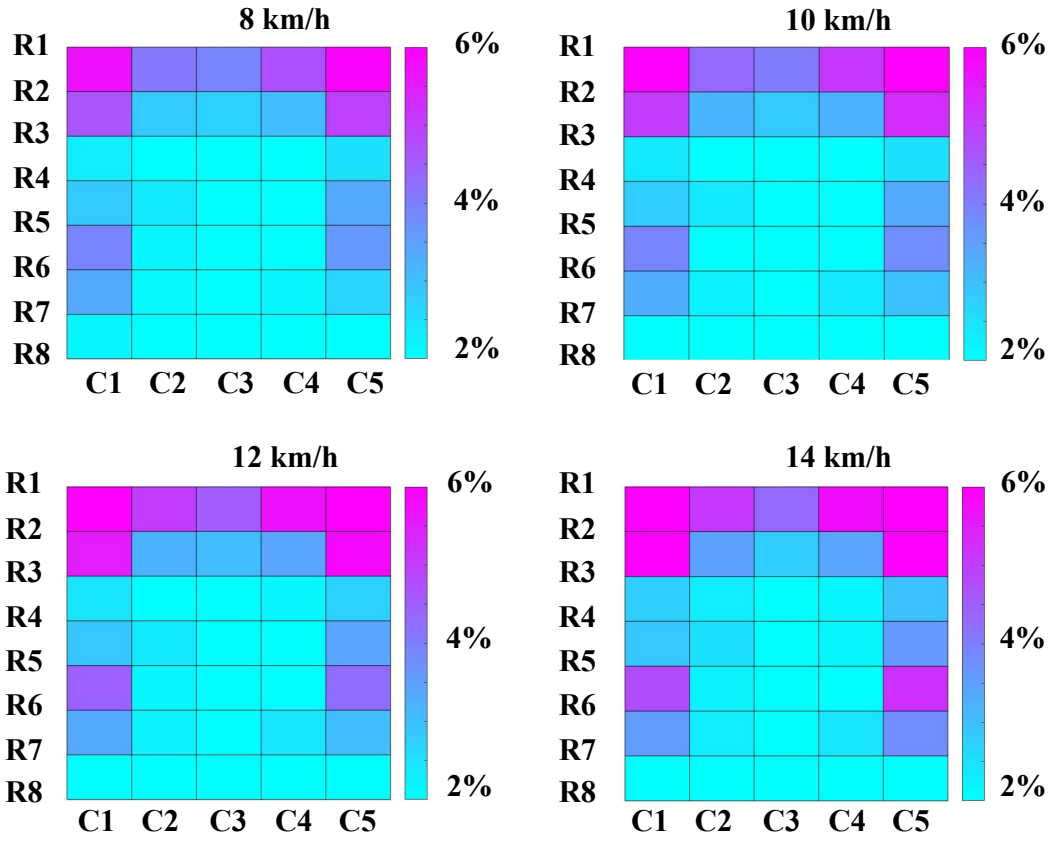

Figure 2.5 Variation in vertical length.

Table 2.1 The minimum and maximum values of the CVs of the horizontal and vertical lengths.

	CV (%, Horizontal)		CV (%, Vertical)	
Condition	min	max	min	max
8 km/h	0.7	11.2	0.6	8.9
10 km/h	0.7	13.0	0.5	8.7
12 km/h	0.8	12.8	0.5	8.9
14 km/h	1.0	14.3	0.6	12.6

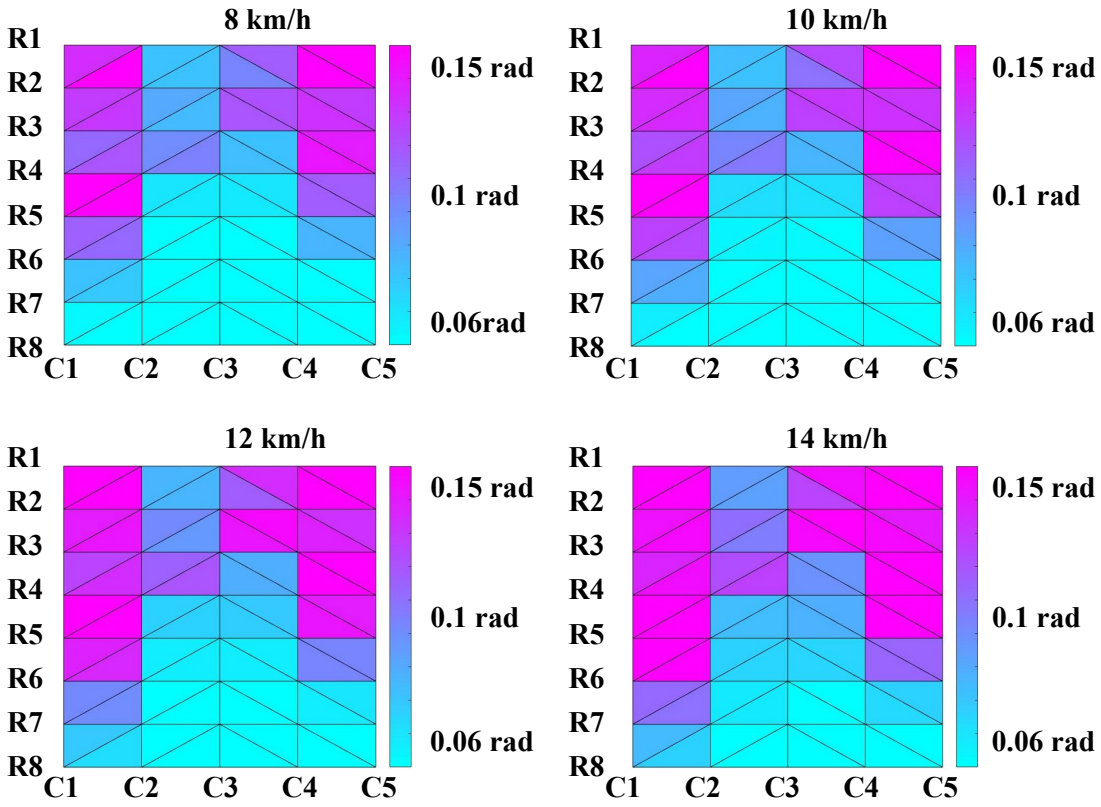

Figure 2.6 Variation in the direction of the normal vector for each area in the transverse plane.

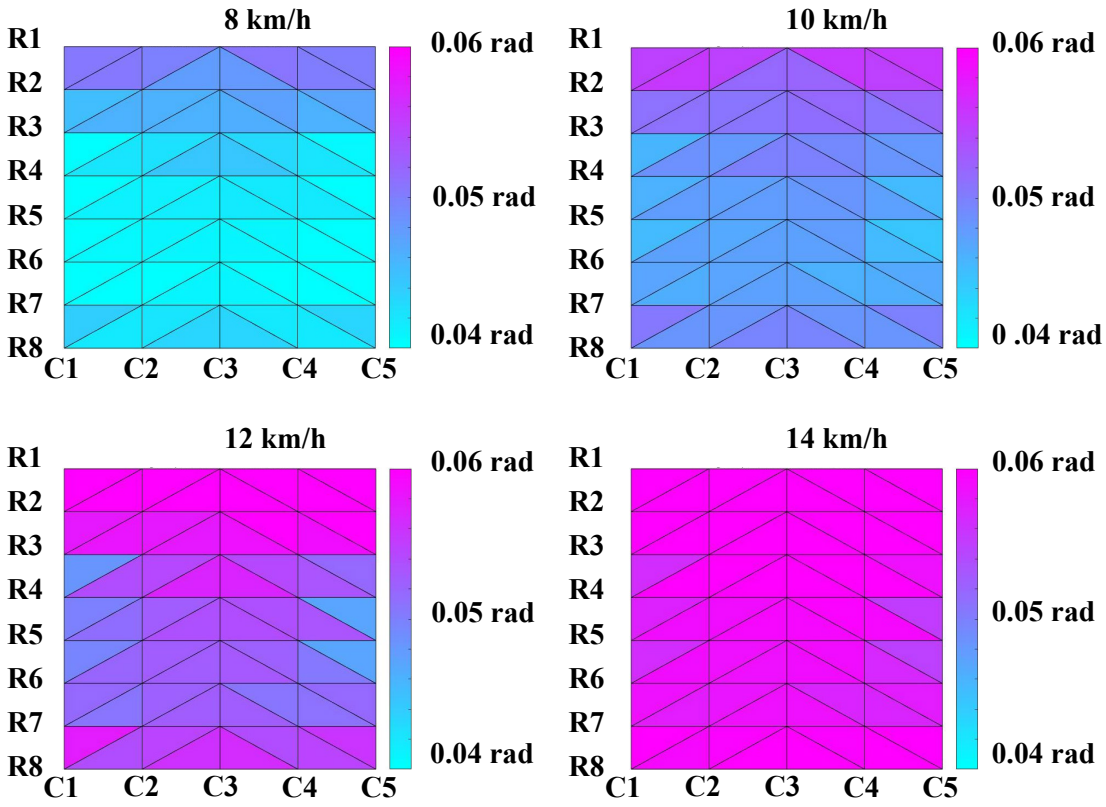

Figure 2.7 Variation in the direction of normal vector for each area in the sagittal plane.

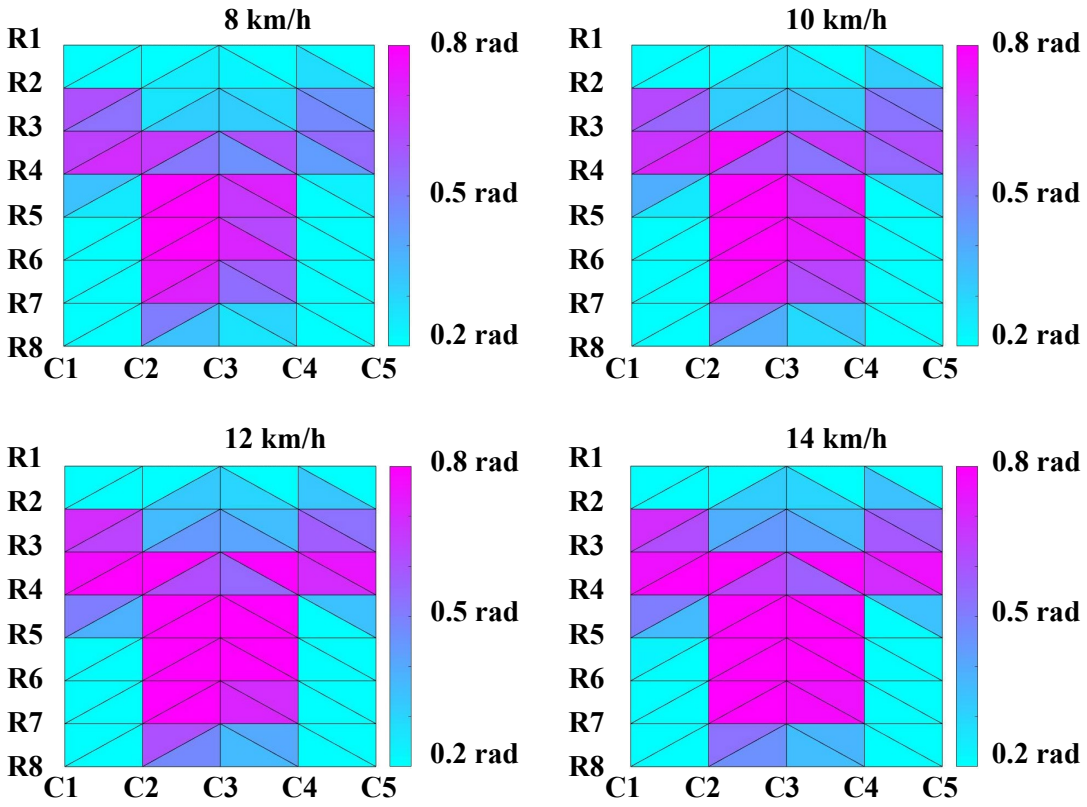

Figure 2.8 Variation in the direction of normal vector for each area in the frontal plane

Table 2.2 The minimum and maximum value of the SD of the normal vectors directed in the (a) transverse, (b) sagittal, and (c) frontal planes.

(a) Transverse plane

	SD (rad)		SD (deg)	
Condition	min	max	min	max
8 km/h	0.01	0.28	1	16
10 km/h	0.01	0.28	1	16
12 km/h	0.02	0.24	1	14
14 km/h	0.02	0.31	1	18

(b) Sagittal plane

	SD (rad)		SD (deg)	
Condition	min	max	min	max
8 km/h	0.02	0.11	2	6
10 km/h	0.02	0.10	1	6
12 km/h	0.02	0.11	1	6
14 km/h	0.03	0.11	1	6

(c) Frontal plane

	SD (rad)		SD (deg)	
Condition	min	max	min	max
8 km/h	0.03	1.33	2	76
10 km/h	0.03	1.35	1	78
12 km/h	0.04	1.36	2	78
14 km/h	0.03	1.34	2	77

2.4. *Discussion*

The purpose of this study was to quantify the trunk deformation occurring during dynamic movements. Thus, significant interactions between the location and speed were obtained via the CVs of the horizontal and vertical lengths. Additionally, significant main effects of the area and running speed were detected on the SD of the normal vectors in the sagittal plane, along with the significant interactions in the transverse and frontal planes. These results implied a complex deformation of the trunk during running.

Significant interactions between the translational and angular deformation were observed according to specific trunk location and running speed, affecting the magnitude of trunk deformation. As an increase in running speed indicates that the whole-body movements become more dynamic, the results of this study indicate that the pattern of trunk deformation will become more complex as the body movements become more dynamic. This suggests that the importance of trunk movement will increase as the analyzed movements become more dynamic. These findings conform with those of previous studies that showed that the trunk exhibited multi-segmental movements during gait, and that the magnitude of these movements increased with the gait velocity (Feipel et al., 2001). Therefore, these findings suggest that the trunk exhibits a significant amount of position- and plane-specific deformations, and that these deformations increase as the dynamics of the movements increase. Thus, they also indicate the importance of considering the contribution of the trunk when assessing human dynamic motion.

The visualization of trunk deformation obtained in this study can help to inclusively understand how the trunk moves during running from a kinematic viewpoint. The changes in the direction of the divided areas in the transverse, sagittal, and frontal planes result from the axial rotation, flexion-extension, and lateral bending movements of the trunk, respectively. Thus, the observation that the largest angular deformations in the transverse plane found in the upper regions of the trunk (Figure

2.6) implies that there exist different patterns of deformation in the upper and lower parts of the trunk, likely because of the twisting between them (Feipel et al., 2001; Syczewska et al., 1999). These findings suggest that the trunk twists significantly between its upper and lower parts during running, and that the methodology used in this study is applicable to quantify complex trunk deformations, including twisting movements.

The methodology used in this study can also be helpful when assessing trunk dynamics in patients who exhibit a certain geometric deformity of the trunk during locomotion resulting from scoliosis, lordosis, or excessive deformation to compensate for muscle weakness in the lower extremities. Although these diseases have been clinically assessed by observing the imbalance and left–right asymmetry of trunk posture in the static condition, there is limited knowledge regarding their effects on movements in the dynamic condition. This is because clinicians typically employ simple visual analysis or quantitative measurements collected by radiographic or three-dimensional scanner evaluation, which can only be undertaken in the static condition. Accordingly, the results of this study demonstrate that the applied methodology can detect a significant amount of trunk deformation in healthy individuals that represent the multi-segmental motion of the trunk during human locomotion. Therefore, the method proposed in this study can be useful in the assessment of trunk deformity in the dynamic condition, thus providing effective basal data when evaluating patients during locomotion.

In conclusion, translational and angular trunk deformations were quantified during the dynamic movements associated with human running. The findings indicated that the trunk exhibited a significant amount of deformation, primarily induced by twisting movements between its upper and lower parts; the magnitude of these movements was position-specific and dependent on the running speed. These findings can be useful in constructing an optimal multi-segmental trunk model to represent the complex and flexible trunk movements that occur during the dynamic movements

associated with human locomotion.

Chapter 3: *Quantitative evaluation of linked rigid-body representation of the trunk*

3.1. *Introduction*

The number of rigid-body segments used to represent the trunk model significantly affects the resultant trunk kinematics occurring during dynamic movements (Leardini et al., 2009; Leardini et al., 2011). Different linked rigid-body representations of the trunk, which had adopted several rigid-body segments, resulted in varying patterns of range of motion and angular displacement for each segment during the dynamic movements (Crosbie et al., 1997b; Frigo et al., 2003; Leardini et al., 2009; Leardini et al., 2011; Mahallati et al., 2016; Preuss and Popovic, 2010; Schinkel-Ivy and Drake, 2015). Thus, the quantitative assessment of various linked rigid-body representations having different numbers of segments is valuable in determining the optimal number of rigid-body segments required for accurately analyzing trunk dynamics.

Therefore, the purpose of this study was to quantitatively assess the effects of trunk deformability on the resultant kinematics of multi-segmental trunk models having varying numbers of rigid-body segments. The trunk was modeled with one, two, three, and six linked rigid-body representations. In addition, the differences in the three-dimensional kinematics observed between the actual and modeled data were assessed in static and dynamic movement conditions.

3.2. *Methods*

3.2.1. *Participants*

Ten male collegiate students participated in this study (mean age: 22.6 ± 1.5 y, mean height: 1.70 ± 0.05 m, mean body mass: 64.6 ± 6.0 kg). All participants reviewed and signed an informed consent form, and the study was approved by the Institutional Review Board at Ritsumeikan

University Biwako-Kusatsu Campus, Japan.

3.2.2. *Measurement protocol*

The three-dimensional kinematics data recorded under static and dynamic movement conditions were examined in this study. For the static trials, the participants were asked to move their trunk in each plane of motion to their physical limit (i.e., trunk lateral bending to the left and right sides, axial rotation to the left and right sides, thorax flexion, and thorax extension), and hold that posture for 5 s. This protocol was performed to assess the adequacy of the linked rigid-body representations in describing the actual posture of the trunk at the maximum range of motion. For the dynamic trials, the participants were asked to walk barefoot along a 5 m walkway at a self-selected speed. This protocol was adopted to assess to what extent the linked rigid-body representations in describing the actual multi-segmental trunk movement during dynamic motion.

3.2.3. *Data collection*

A 24-camera motion capture system (MAC3D, Motion Analysis Corporation, CA, USA) captured the entire body motion. Three-dimensional position data were obtained at 250 Hz and were then low-pass filtered at 8 Hz using a fourth-order digital Butterworth filter. Moreover, the motion capture system offered submillimeter accuracy, and its residual systematic error was less than 0.5 mm at the instant of calibration. Seventy reflective markers were placed on the back (Figure 3.1-a) and front (Figure 3.1-b) of the trunk at regular intervals to define 48 triangular areas on each side. The markers were placed at the level of the seventh cervical vertebra (C7), third thoracic vertebra (T3), sixth thoracic vertebra (T6), ninth thoracic vertebra (T9), twelfth thoracic vertebra (T12), third lumber vertebra (L3), and first sacral vertebra (S1). The markers placed on the back and front sides of the trunk were defined as B- and F-markers, respectively. The trunk was divided into seven rows (from

B- or F-Row 1 to B- or F-Row 7) and five columns (from B- or F-Column 1 to B- or F-Column 5). Additional markers were placed at the PSIS and ASIS to define the pelvic frame of reference (Leardini et al., 2011).

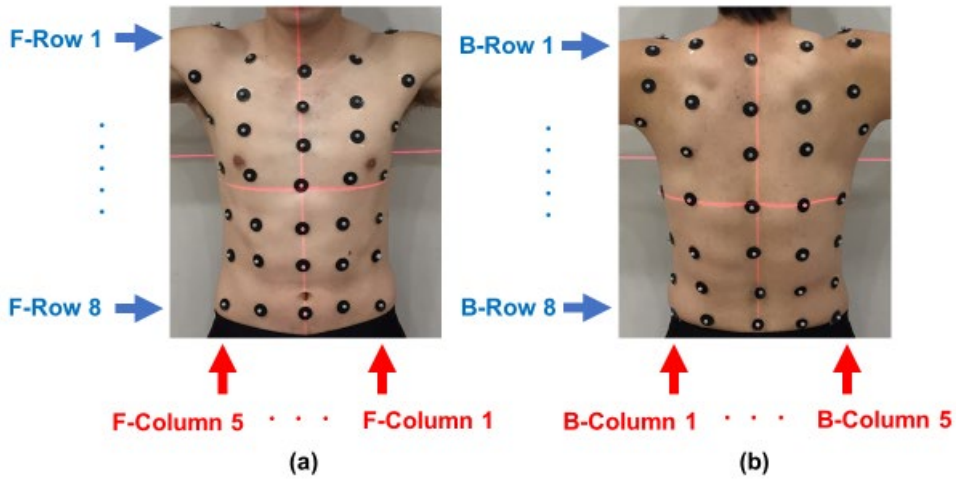

Figure 3.1 Placement of the markers.

Seventy reflective markers were placed on the back (a) and front (b) sides of the trunk at the levels of the seventh cervical vertebra, third thoracic vertebra, sixth thoracic vertebra, ninth thoracic vertebra, twelfth thoracic vertebra, third lumber vertebra (L3), and first sacral vertebra, at regular intervals.

3.2.4. *Data analysis*

The trunk was modeled with one (M1), two (M2), three (M3), and six (M6) linked rigid-body segments to quantitatively assess the adequacy of the linked rigid-body representations in describing the actual complex movements of the trunk (Figure **3.2**). The trunk was divided by the number of segments in each model, and the endpoints of each segment were determined by the vertebral

landmarks on the spine (M1: C7–S1; M2: C7–T9, and T9–S1; M3: C7–T6, T6–T12, and T12–S1; M6: C7–T3, T3–T6, T6–T9, T9–T12, and T12–S1). In addition, a local frame of reference was defined for each rigid-body segment. The origin of the local coordinate system was set at the averaged position of the markers on the lower base of each segment (Figure 3.2). The vertical axis (z-axis) was defined from the origin to the averaged position of the markers placed on the upper base of each segment. The anterior–posterior axis (x-axis) was defined as the line perpendicular to the plane defined by the z-axis and the line connecting the origin and the averaged position of the column 1 markers placed on the front and back sides, pointing in the anterior direction. The medial–lateral axis (y-axis) was defined as the line perpendicular to both the z- and x-axes, directed leftward. Furthermore, two adjacent segments of the trunk were linked with a ball joint, and thereby M1, M2, M3, and M6 individually had six, nine, twelve, and twenty-one degrees of freedom, respectively. The position data were determined with respect to the local coordinate system defined for each rigid-body segment.

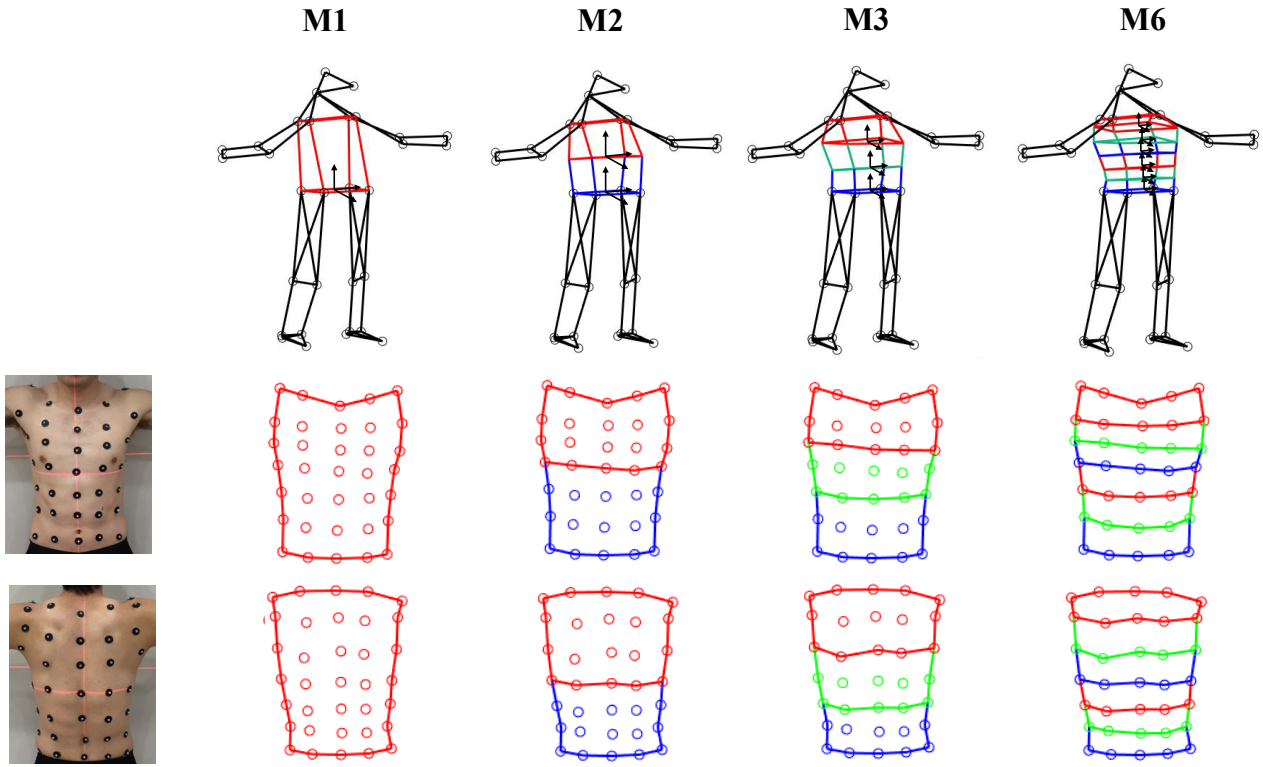

Figure 3.2 Linked rigid-body representations used in this study.

The trunk was modeled as one, two, three, or six linked rigid-body representations. The trunk was evenly divided into one, two, three, or six rigid-body segments based on anatomical landmarks.

The positional error—indicated by the three-dimensional positional difference between the actual and modeled data—was calculated to quantify the accuracy of these models describing the actual trunk kinematics. A simultaneous transformation matrix (STM) from the local to global coordinate system was determined for each rigid-body segment. The rotation matrix of the STM was determined using a Y–X–Z Euler-angle sequence. Thereafter, the distances between the points of the actual and modeled data were calculated to quantify the positional error in each movement condition. The perpendicular distance from the center of the triangular area defined by the actual data to the triangular plane defined by the modeled data was calculated. Further, a nonlinear optimization analysis (fmincon in the MATLAB optimization toolbox; Figure 3.3) was used to obtain a set of parameters for the STM to minimize the averaged perpendicular distance for all pairs of the actual and modeled data. Subsequently, this minimized distance was used as the positional error for each model to assess the adequacy of each linked rigid-body representation in describing the actual trunk position.

The total angular displacement for each model was calculated to determine the accuracy of each model in representing the actual multi-segmental trunk movements. The joint angles between two adjacent segments were calculated based on the STM parameters derived using nonlinear optimization analysis. The angles about the Y, X, and Z axes were obtained as angles of lateral bending (LB_x), axial rotation (AR_z), thorax flexion (TE_y), and thorax extension (TF_y) between two adjacent rigid-body segments. The sum of the absolute values of angular displacement for each segment (i.e., the total angular displacement) was used as the measure of variation in the resultant multi-segmental trunk kinematics for each linked rigid-body representation.

For the static trials, the positional error and total angular displacement for each subject were averaged over 5 s. The total angular displacement was calculated only for each plane of motion (LB_x for lateral bending, AR_ z for axial rotation, TE_y for thorax extension, and TF_y for thorax flexion). Moreover, the position error and total angular displacement for lateral bending and axial rotation were

averaged over the left and right sides because these conditions were performed on the left and right sides. For the dynamic trials, the maximum values of the positional error and total angular displacement were used for each representation during a gait cycle. A gait cycle was defined on the instant of heel strike detected from the vertical velocity component of the midfoot (O'Connor et al., 2007). All data processing was performed using the MATLAB software (MathWorks, Natick, MA, USA).

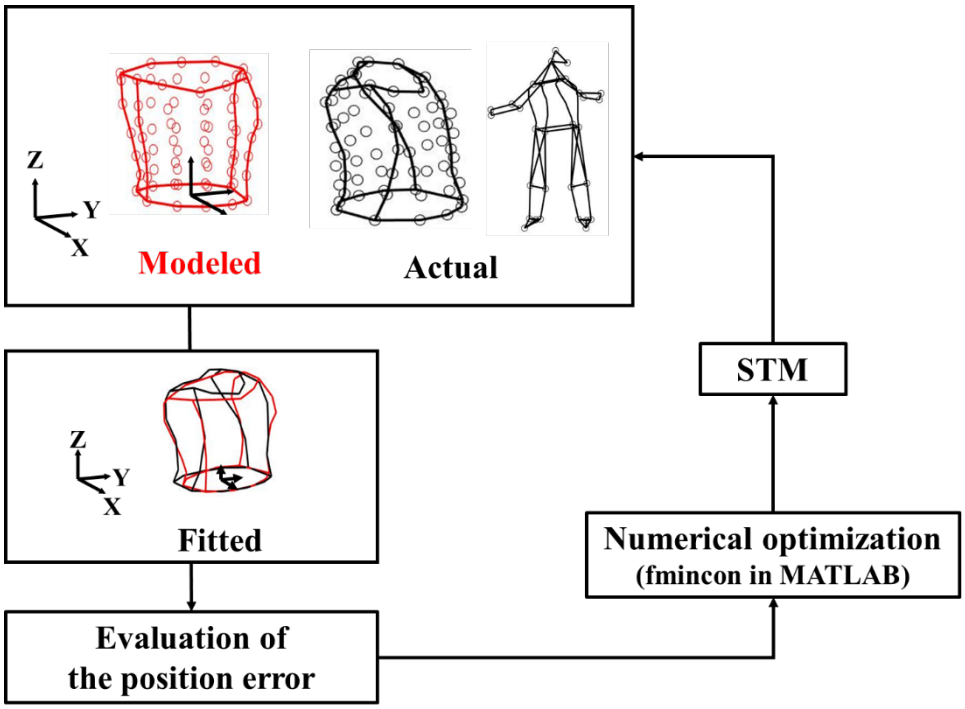

Figure 3.3 Outline of a nonlinear optimization analysis.

A set of parameters for STM to minimize the position error was found via a nonlinear optimization analysis.

3.2.5. *Statistical analysis*

A two-way repeated-measure ANOVA test investigated the main effects and interactions on the position error for the static trials. The four models (M1, M2, M3, and M4) and conditions (static trials:

lateral bending, axial rotation, thorax flexion, and thorax extension) were used as factors of analysis. For the dynamic trials, a one-way repeated-measure ANOVA was used to investigate the main effects of the model on both the position error and the total angular displacement. Statistical analyses were performed using SPSS (Chicago, IL, USA), and the significance level was set at $p<0.05$.

3.3. *Results*

3.3.1. *Positional error and total angular displacement in static trials*

As the number of segments increased in the model, the positional error reduced from 12 to 5 mm, 8 to 4 mm, 7 to 5 mm, and 6 to 4 mm for the lateral bending, axial rotation, thorax flexion, and thorax extension conditions, respectively (Table 3.1a). Moreover, a significant interaction was observed between the model and postural condition on the positional error ($p = 0.001$). Furthermore, significant simple effects were of the model ($p < 0.001$) and the postural condition ($p = 0.002$) were found on the positional error for each postural condition. Overall, the positional error decreased as the number of rigid bodies increased.

Likewise, as the number of segments increased in the model, the total angular displacement increased from 45° to 55°, 68° to 82°, 72° to 97°, and 24° to 48° for the lateral bending (LB_x), axial rotation (AR_z), anteflexion (TF_y), and retroflexion (TE_y) conditions, respectively (Table 3.1b). In addition, significant main effects of the model were found on the total angular displacement for lateral bending ($p < 0.001$), axial rotation ($p = 0.004$), thorax flexion ($p < 0.001$), and thorax extension ($p < 0.001$) conditions.

3.3.2. *Positional error and total angular displacement in dynamic trials*

During walking, the positional error ranged from 7 to 11 mm (Table 3.2a). Besides, a significant main effect of the model was observed on the position error ($p < 0.001$), where the position error

decreased with the increasing number of segments used for the model.

The total angular displacement during walking ranged from 5° to 10°, 10° to 16°, 3° to 8°, and 1° to 3° for LB_x, AR_ z, TE_y, and TF_y, respectively (Table 3.2b). In addition, it was observed that the model had a significant effect on the total angular displacement for LB_x ($p < 0.001$), AR_z ($p < 0.001$), TE_y ($p < 0.001$), and TF_y ($p < 0.001$).

Table 3.1 Positional error and total angular displacement in static trials

(a) Positional error in static trials (mm)

	M1		M2		M3		M6	
Condition	Mean	SD	Mean	SD	Mean	SD	Mean	SD
Lateral bending	12	3	8	2	6	1	5	1
Axial rotation	8	2	6	1	5	1	4	1
Thorax flexion	7	3	6	2	5	2	5	1
Thorax extension	6	2	4	1	4	1	4	1

(b) Total angular displacement in static trials (°)

	M1		M2		M3		M6	
Condition	Mean	SD	Mean	SD	Mean	SD	Mean	SD
Lateral bending (LB_x)	45	14	50	15	51	15	55	14
Axial rotation (AR_z)	68	14	77	17	79	17	82	19
Thorax flexion (TE_y)	72	16	78	17	84	19	97	23
Thorax extension (TF_y)	24	19	35	24	39	22	48	24

※ LB_x, AR_z, TF_y and TE_y indicate the total angular displacement about the x-axis, z-axis, y-axis, and y-axis, respectively. Only the angle on the plane of primary motion for each postural condition was calculated (i.e., LB_x for lateral bending, AR_z for axial rotation, TF_y for thorax flexion, and TE_y for thorax extension)

Table 3.2 Positional error and total angular displacement in dynamic trials

(a) Positional error in dynamic trials (mm)

	M1		M2		M3		M6	
Condition	Mean	SD	Mean	SD	Mean	SD	Mean	SD
Walking	11	2	8	2	7	2	7	2

(b) Total angular displacement (°)

	M1		M2		M3		M6	
Angle	Mean	SD	Mean	SD	Mean	SD	Mean	SD
LB_x	5	1	6	2	7	2	10	3
AR_z	10	3	10	3	12	4	16	5
TE_y	3	1	4	1	5	1	8	2
TF_y	1	1	2	1	2	2	3	1

※ LB_x, AR_z, TF_y and TE_y indicate the total angular displacement during walking about the x-axis (lateral bending), z-axis (axial rotation), y-axis (thorax flexion), and y-axis (thorax extension), respectively.

3.4. *Discussion*

The purpose of this study was to quantitatively assess the effects of trunk deformability on the resultant kinematics for various numbers of rigid-body segments used in the trunk model. The positional error was used to assess the difference in three-dimensional positions observed between the actual and modeled data for each model in the static and dynamic trials. The total angular displacement of the trunk segments was used to examine the accuracy of each model in representing the actual multi-segmental trunk movement in both the trials. The positional error significantly decreased as the number of rigid bodies increased in both the trials. In contrast, the total angular displacement significantly increased as the number of rigid-body segments increased in both the trials. These findings suggest that the number of rigid-body segments used to model the trunk could significantly affect the resultant trunk kinematics, and a small number of linked rigid-body representations would underestimate the actual trunk deformation occurring during dynamic movements.

The simple effect of the model found on the positional error indicated that the model estimates significantly improved as the number of rigid bodies increased. The results of this study are in agreement with those of previous studies that reported a decrease in the resultant differences of spine kinematics with an increasing number of rigid-body segments in the trunk model (Breloff and Chou, 2015; Preuss and Popovic, 2010). These findings suggest that the resultant errors in the trunk kinematics would decrease as the number of segments in the model increased, even considering trunk deformability. In addition, the significant interaction (model × condition) found on the positional error suggested that the improvement of model estimates was influenced not only by the model used but also by the postural condition. Therefore, the number of rigid-body segments used in the trunk model should be considered depending upon the movement of interest and the accuracy required for the analysis. Accordingly, the quantified values of positional error demonstrated in this study would be

useful in determining the optimal number of linked rigid-body segments for complex trunk deformation analysis.

In contrast to the decreased positional error observed above, the total angular displacement significantly increased as the number of segments in the model increased. This result indicated that the smaller number of linked rigid-body representations underestimated the extent of actual multi-segmental trunk movements. Moreover, the twisting movement of each segment appeared to be underestimated when using a small number of segments, as each segment of the trunk significantly has been observed to rotate during dynamic movement (Preuss and Popovic, 2010). This underestimation was the result of the variation in the angular displacements about each joint of the model with the limited number of rigid-bodies used to describe the deformed geometry of the trunk. Such underestimations significantly affect the resultant trunk kinetics through the associated differences in the kinematic parameters when assessing body dynamics using the Newton–Euler equations of motion. Specifically, the joint angular acceleration derived from each model will be different when different models describe different values of angular displacement about the same joint during a given time, and this discrepancy will affect the calculation of joint torque in the trunk during walking. Therefore, these findings suggested that the number of rigid-body segments used to model the trunk significantly affected the resultant trunk kinetics as well as the kinematics.

A multi-segmental model provides a better representation of the trunk, as demonstrated by the reduction of position errors resulting from a greater number of segments used in the trunk model. However, this study further demonstrated that such position errors did not monotonously decrease with the increasing number of segments. For instance, the degree of improvement observed when the trunk was divided into two segments (up to 4 mm) was significantly higher than that observed when the trunk was divided into more than two segments (up to 2 mm). Therefore, two rigid-body segment representations of the trunk may be sufficient to describe the gross trunk movements. Further studies

should evaluate the quality and usability of a model using quantitative measures, such as goodness-of-fit indices, which would help us determine the “best approximating” model for the analysis of trunk movements.

In conclusion, the effects of trunk deformability on the resultant kinematics were quantitatively assessed based on the positional error and total angular displacement of trunk models with different numbers of rigid-body segments. The findings of this study suggest that the number of rigid-body segments used to model the trunk will significantly affect the resultant trunk kinematics; therefore, the number of rigid-body segments used to model the trunk should be considered according to the required accuracy. Additionally, the findings of this study suggest that at least two linked-rigid body representations should be used to describe gross trunk movements because significant improvement in the position error was observed when the trunk was divided into two segments, but limited improvement was observed when the number of rigid-body segments was increased further. Therefore, the quantified positional error values demonstrated in this study will be useful in determining the optimal number of linked rigid-body segments for the trunk model.

Chapter 4: *Determination of the optimal number of linked rigid-bodies of the trunk during walking based on Akaike's information criterion*

4.1. *Introduction*

A multi-segmental rigid-body model provides a better representation of the trunk than a single rigid-body model in terms of goodness-of-fit. Thus, a larger number of segments are generally applied to assess the detailed multi-segmental movements of the trunk during human locomotion (Breloff and Chou, 2017; Leardini et al., 2011; Preuss and Popovic, 2010). However, the simplicity of the model has to be optimized in relation to the fitness of the data, because higher DOFs tend to complicate the model and impairs its ability to be generalized by being too specific for a particular dataset of participants (Hicks et al., 2015). Moreover, the computational complexity of the analysis increases with higher DOFs (Hicks et al., 2015; Zhang, 2001). Although the goodness-of-fit benefits from increased model complexity, undue model complexity and participant-specificity should be avoided for a more generalizable model selection. Therefore, the optimal model complexity needs to be determined by optimizing the considerations of goodness-of-fit and generalizability.

In context, Akaike's information criterion (AIC) can address this optimization and can be used for determining the optimal model complexity. AIC is a composite measure consisting the sum of two terms: the maximized value of the likelihood function for the estimated model and a function of DOF that declines with additional parameters, thus penalizing increases in model complexity (Akaike, 1973, 1974). Therefore, the AIC not only rewards goodness-of-fit but also includes a penalty directed by a function on the number of estimated parameters. Thus, the AIC could be used as a means for optimal model selection that balances goodness-of-fit and generalizability.

The current study aimed to determine the optimal number of rigid-body segments in the trunk

model for dynamic conditions (walking) by optimizing the goodness-of-fit and the generalizability of the model using AIC. The trunk was modeled with varying numbers of rigid-body segments, and the relative quality assessed by AIC during walking was compared among the models for optimal model selection.

4.2. *Methods*

4.2.1. *Participants*

Ten male college students (mean age: 22.6 ± 1.5 y, height: 1.70 ± 0.05 m, body mass: 64.6 ± 6.0 kg) participated in this study. All participants reviewed and signed an informed consent form, and the study was approved by the Institutional Review Board at Ritsumeikan University, Biwako-Kusatsu Campus, Japan.

4.2.2. *Data collection*

The participants were instructed to walk on a 20 m circuit walkway continuously for five times, keeping their own preferred speed. Three-dimensional positional data of the trunk along a 5 m straight section of the walkway (from 2.5 to 7.5 m section of the runway) was recorded on the third lap of each trial using a 24-camera motion capture system at 250 Hz (MAC3D, Motion Analysis Corporation, California, USA). Seventy reflective markers (seven rows and five columns) were placed on the back (Figure 4.1a) and front (Figure 4.1b) of the trunk at equidistant intervals. The markers were placed at the levels of C7, T3, T6, T9, T12, L3, and S1 to detect the multi-segmental movements and geometrical deformation of the trunk during walking and running because of the anatomical structure (Breloff and Chou, 2015; Breloff and Chou, 2017). Additional markers were placed on the heel and toe (metatarsal head II) for detecting the heel strike (O'Connor et al., 2007).

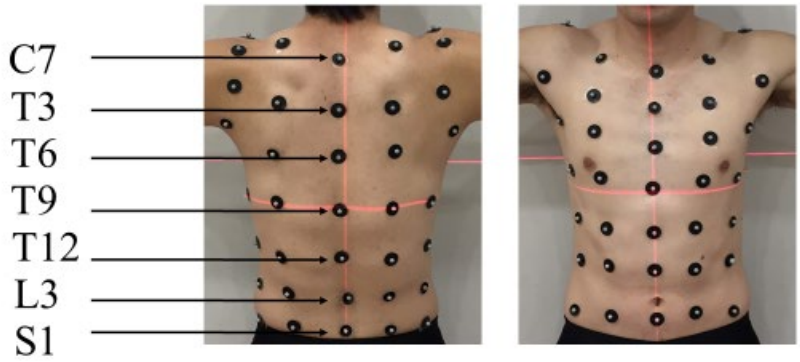

Figure 4.1 Placement of markers.

Seventy reflective markers were placed on (a) the back and (b) front sides of the trunk at the levels of the seventh cervical vertebra (C7), third thoracic vertebra (T3), sixth thoracic vertebra (T6), ninth thoracic vertebra (T9), twelfth thoracic vertebra (T12), third lumber vertebra (L3), and first sacral vertebra (S1), at equidistant intervals.

4.2.3. *Data analysis*

The trunk was modeled with one (M1), two (M2), three (M3), and six (M6) linked rigid-body segments that were defined by the level of vertebral landmarks based on the study in Chapter 3 (Kudo et al., 2018) (M1: C7–S1; M2: C7–T9 and T9–S1; M3: C7–T6, T6–T12, and T12–S1; M6: C7–T3, T3–T6, T6–T9, T9–T12, and T12–S1). The same number of reflective markers was present in each segment to eliminate the bias of the number of positional data when quantifying the positional error between the empirically obtained and modeled data using the AIC. Each set of two adjacent segments was linked by a ball joint; therefore, M1, M2, M3, and M6 had six, nine, twelve, and twenty-one DOFs,

respectively. Moreover, a local coordinate system was defined for each rigid-body segment based on our previous study (Kudo et al., 2018). The positional data of the markers were transformed from global to each local coordinate system using an STM.

A set of parameters was determined at each frame of the STM by using a nonlinear optimization algorithm (fmincon in the MATLAB optimization toolbox; Figure 4.2) to minimize the sum of squares of the Euclidian distance for all pairs of the empirical and modeled data. The distances for all pairs of the empirical and modeled data (positional errors: PEs) during one complete stride cycle were used to quantitatively assess the relative quality of each model.

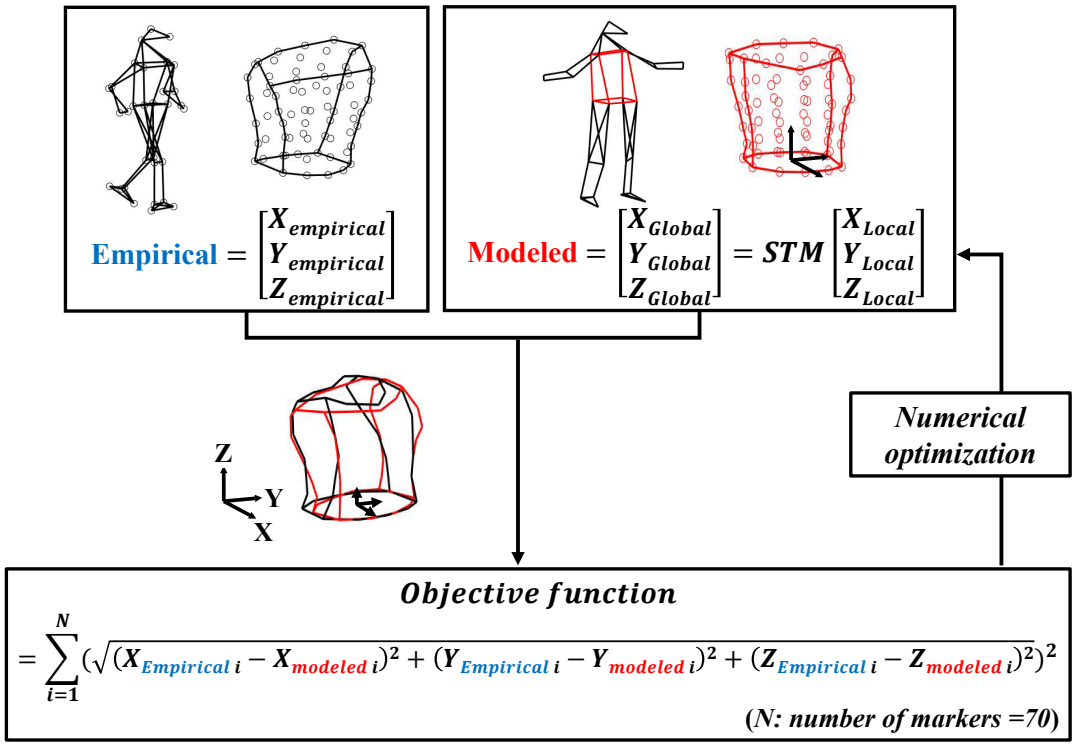

Figure 4.2 Outline of a nonlinear optimization analysis for M2 as an example.

A set of parameters for STM of each rigid body to minimize the sum of squares of the Euclidian distance for all pairs of the empirical and modeled data were found with a nonlinear optimization analysis.

In this study, the bias-corrected AIC (AICc) was used to assess the relative quality of the model, which was proposed to resolve the selection tendency of AIC toward models having a larger number of parameters (Sugiura, 2007). The AICc value of each model was calculated as follows:

$$\text{AICc value} = \text{AIC value} + \frac{2DOF(DOF+1)}{N - DOF - 1}$$

(Equation 4.1)

where *N* and *DOF* indicate the number of reflective markers placed on the trunk (i.e., 70 in this study) and the DOF for each model, respectively. The AICc is essentially the AIC with an extra penalty term for the DOF. The AIC value of each model was calculated using the following equation (Akaike, 1974):

$$\text{AIC value} = -2 \times (\text{MLL}) + 2 \times \text{DOF}$$

(Equation 4.2)

where MLL indicates the maximized logarithmic likelihood as a measure of goodness-of-fit. The MLL of each rigid-body model was estimated by defining the likelihood function for calculating the conditional probability of observing the PEs, given a normal probability distribution of the PEs and the distribution parameters (average value and standard deviation of PEs). The AIC value decreases as the MLL (i.e., goodness-of-fit of the model) increases and the DOF (i.e., complexity of the model) decreases. The maximized logarithmic likelihood was calculated as follows:

$$\text{MLL} = -\frac{1}{2\sigma^2}\sum_{i=1}^{N}(\text{PE}_i)^2 - \frac{N}{2}\log 2\pi\sigma^2$$

(Equation 4.3)

where the PE and σ^2 indicate the distance for a pair of the empirical and modeled data and the variance of the PEs, respectively. For each model, the MLL was calculated based on the frame in which the sum of the PEs for M1 reached its maximum during the stride. The model with the smallest AICc value was considered as the optimal model, indicating that the goodness-of-fit and generalizability of the identified model were better balanced in comparison to the other models.

4.2.4. *Statistical analysis*

In this study, non-parametric tests were used because the Shapiro–Wilk normality test revealed that the obtained data were not distributed normally. In addition, Friedman's test was performed to determine the presence of significant differences in the AICc values for various models. Thereafter, a Wilcoxon signed-rank test was used to facilitate multiple comparisons between the models, and the calculated p-values were adjusted with a Bonferroni–Holm correction. All statistical analyses were performed using the SPSS software package (Chicago, IL, USA). The significance level was set at $p = 0.05$.

4.3. *Results*

A significant main effect of the model was observed on the AICc values ($p < 0.001$). Furthermore, post-hoc multiple comparisons demonstrated that the AICc values of M2 and M3 were significantly smaller than those of M1 and M6 (Figure 4.3). Therefore, no significant differences were found in the AICc values of M2 and M3 and that between M1 and M6. The AICc values (mean ± SD) were 1743.5 ± 103.7, 1673.7 ± 113.7, 1673.3 ± 117.9, and 1710.8 ± 126.8 for M1, M2, M3, and M6, respectively.

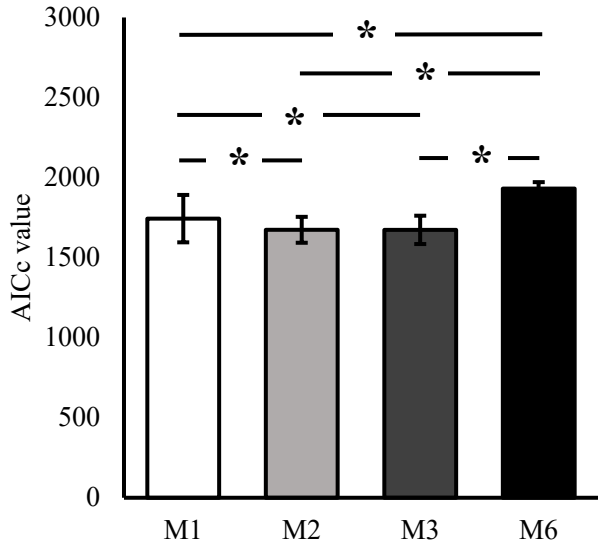

Figure 4.3 AICc values during walking.

A significant main effect of the model was observed on the AICc value ($p < 0.001$). The AICc values (mean ± SD) were 1743.5 ± 103.7, 1673.7 ± 113.7, 1673.3 ± 117.9, and 1710.8 ± 126.8, for M1, M2, M3, and M6, respectively.

4.4. *Discussion*

This study aimed to determine the optimal number of rigid-body segments in terms of goodness-of-fit and generalizability using the AICc. The model with the smallest AICc value was considered the optimal model, indicating that the goodness-of-fit and generalizability of the model were better balanced as compared to the other models. The AICc values of M2 and M3 were found to be considerably smaller than those of M1 or M6, but no significant difference was observed between the AICc values of M2 and M3. These findings suggested that a model with a larger DOF would not always be the optimal model in terms of goodness-of-fit and generalizability when representing the trunk in walking condition.

The significantly larger AICc value of the M1 model resulted from its lower goodness-of-fit

compared to that of the M2 and M3 models. Several previous studies have reported that a model with a small number of segments underestimates the actual multi-segmental movements of the trunk (Kudo et al., 2018; Leardini et al., 2009; Preuss and Popovic, 2010), which implies that the goodness-of-fit of a simpler model is lower than that of multi-segmental models. Thus, these results indicated that a two- or three-linked rigid-body model would provide more accurate results for walking as compared to that of a single rigid-body model in terms of goodness-of-fit.

In contrast, the significantly larger AICc value of M6 compared with those of M2 and M3 resulted from its complexity during walking. An increase in the number of DOFs increases the complexity of the multi-segmental rigid-body models, resulting in a more appropriate goodness-of-fit; however, the computational demand will also increase with the number of segments, resulting in decreased computational efficiency (Zhang, 2001). Specifically, because the number of equations of motion used to analyze the dynamics of the linked rigid-body model is associated with the number of DOFs, M6 (21 DOFs) requires an approximately twofold computational cost for analysis compared to M2 (9 DOFs) and M3 (12 DOFs). Moreover, the generalizability of the model decreases as the number of DOFs increase. Therefore, the two- and three-link rigid-body models are more generalizable and economical for the analysis of trunk movement during walking than the six-link model because both computational efficiency and generalizability decrease with increasing model complexity.

It would also be valuable to understand what type of trunk movements can be detected or simplified when modeling the trunk using M2 or M3, compared with M1 or M6, to determine the number of rigid bodies required to achieve the desired analysis accuracy. Accordingly, the joint angular displacements of each model fitted to the actual data of the trunk during the stride cycle (from the right heel contact to ipsilateral heel contact) was calculated (Appendix A) to evaluate the effect of the number of rigid-bodies on the kinematics measured during walking. These data indicated that a significant amount of twisting movement about each joint was detected when the trunk was modeled

using multiple segments in contrast to a single rigid-body. Additionally, the range of motion for each joint was smaller as the number of rigid bodies in the trunk model increased. The data also demonstrated that a larger range of axial rotation was exhibited by each joint during walking relative to the lateral bending and flexion-extension movements. This implies that the twisting movement about the longitudinal axis of the trunk can be simplified by modeling the trunk using two or three linked rigid-bodies during walking. Therefore, the quantified values of such kinematic information can also be useful in determining the number of linked rigid-body segments required to achieve the desired trunk analysis accuracy.

In conclusion, the AICc values of the two- and three-linked rigid-body models were found to be significantly smaller than those of one- or six-segment models for the walking motion. This result indicated that both the two- and three-linked rigid-body models would represent trunk movements better than the one- and six-linked rigid-body representations during walking. Therefore, the findings of the current study could be useful in determining the optimal number of rigid-body representations to analyze multi-segmental trunk movements during walking.

Chapter 5: *Musculoskeletal modeling of the human body considering the multi-segmental structure of the trunk*

5.1. *Overview of musculoskeletal computer simulation system in this study*

The neuromusculoskeletal computer simulation system used in this dissertation includes a skeletal, muscular, and an external environment interaction model (i.e., foot/ground interaction, Figure 5.1). Inputs of the entire system were time-independent neural stimulation profiles of each muscle (STIM in Figure 5.1) that passed through a first-order process to result in activation of the contractile element (CE) in the Hill-type muscle model. The musculoskeletal model was enacted upon forces developed by the series elastic element (F_{SEE}), ground reaction forces (GRF), and passive moments about each joint (M_{pass}). This neuromusculoskeletal computer simulation system was implemented using the commercial package MotionGenesis (Motion Genesis LLC, Stanford, CA, USA) linked with C-language code. The process for neuromusculoskeletal modeling of the human body was closely adopted from the modeling methodology reported by Nagano et al. (Nagano, 2003; Nagano and Gerritsen, 2001; Nagano et al., 2005a; Nagano et al., 2005c). Detailed information of each model is described in the following section.

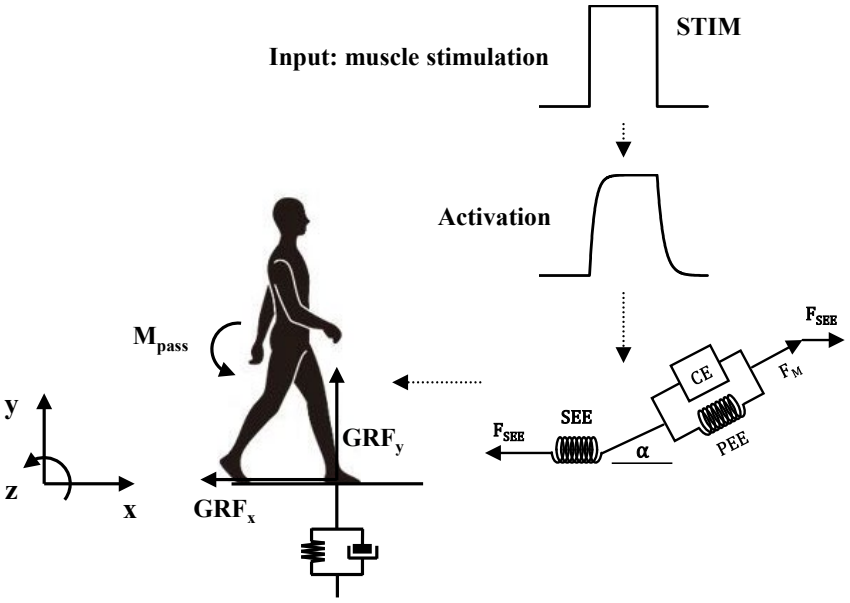

Figure 5.1 Illustration of the system of musculoskeletal computer simulation.

The neuromusculoskeletal computer simulation system used in this study includes a model of skeleton, a model of muscle, and a model of external environment interaction (i.e., foot/ground interaction).

5.2. *Skeletal model*

5.2.1. *Linked rigid-body segment model*

The skeleton of the human body was modeled with eighteen rigid-body segments: head, thorax, abdomen, pelvis, right and left—hands, upper and lower arms, upper and lower legs, and hind and fore feet, all interconnected with joints (Figure 5.2). The equations of motion for the skeletal model were obtained using the MotionGenesis multibody software package. A full description of the skeletal model coded to be processed with MotionGenesis can be found in Nagano et al. (2005c). The body height and mass of the model were set to 1.741 m and 72.8 kg, respectively. In addition, the anthropological parameter values (length, mass, position of the mass center, and moment of inertia of segments) were derived from de Leva (1996).

The total degree of freedom (DOF) of the model was 24, where the DOF of the pelvis was 6 (3 translations and 3 rotations), that of the thoracic joint was 3 (flexion/extension, right/left lateral bending, torsional rotation), the lumbar joint had 3 (flexion/extension, right/left lateral bending, torsional rotation), hip joints had 3 (flexion / extension, abduction / adduction, internal / external rotation), and each knee, ankle, and subtalar joints had 1 (flexion/extension, dorsi flexion/plantar flexion, and inversion/eversion). All other joints (the neck, shoulder, elbow, wrist, and metatarsal joints) were constrained.

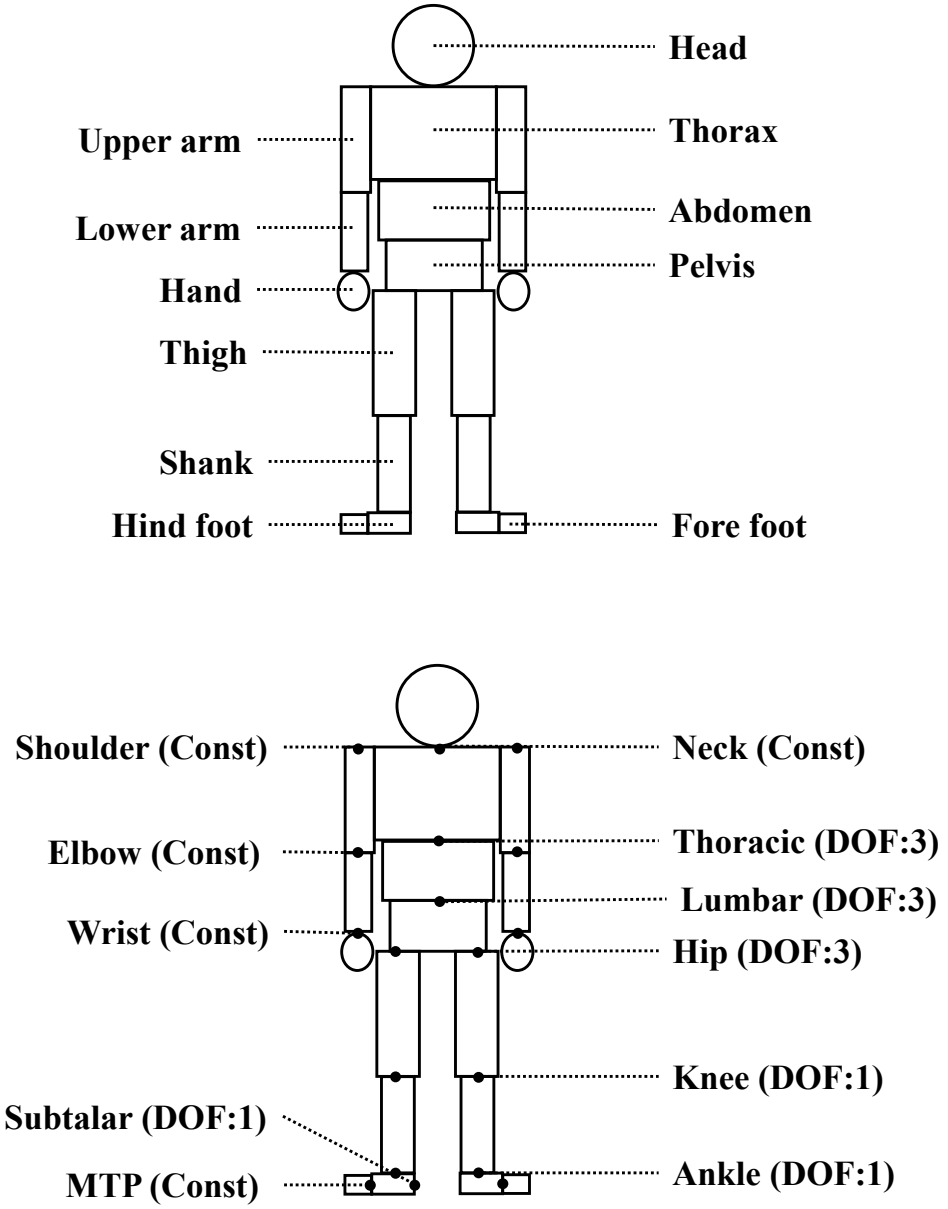

Figure 5.2 Linked rigid-body model constructed in this dissertation.

The skeleton of the human body was modeled with 18 rigid body segments in total: head, thorax, abdomen, pelvis, right and left upper arms, right and left lower arms, right and left hands, right and left lower arms, right and left lower legs, right and left hind feet, and right and left fore feet, these segments were interconnected with joints.

Owing to the tilt (Delp, 1990), the subtalar joint axis of the skeletal model originates as the heel, with a direction vector of:

$$\vec{V}_{subt} = \begin{bmatrix} 0.791 \\ 0.600 \\ -0.120 \end{bmatrix}$$

(Equation 5.1)

for the right foot and

$$\vec{V}_{subt} = \begin{bmatrix} 0.791 \\ 0.600 \\ 0.120 \end{bmatrix}$$

(Equation 5.2)

for the left foot (Delp, 1990) (Figure 5.3).

Thus, the direction vectors of the subtalar joint axis were adopted from Delp (1990).

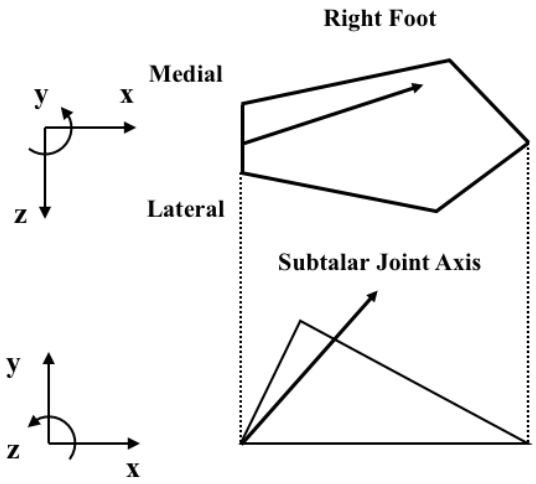

Figure 5.3 Illustration of the subtalar joint axis

5.2.2. *Passive joint moments*

Passive joint moments (M_{pass}) that exist in the trunk and the lower limb joints (representing ligaments and other structures around the joints) were implemented as described by Anderson (1999) and Anderson and Pandy (1999). The passive moments were computed as follows:

$$M_{pass_j} = k_{0_j} + k_{1_j} \exp\left(k_{2_j}(q_j - \theta_j)\right) + k_{3_j} \exp\left(k_{4_j}(q_j - \phi_j)\right)$$

(Equation 5.3)

where q_j is the joint angle in degrees for the j^{th} joint. The values of the constants k_0, k_1, k_2, k_3, θ, and φ for the joint in the lower extremities was adopted from (Anderson, 1999). The musculoskeletal model developed by Anderson (1990) includes only one rigid-body trunk segment and represents the motion with about the lumbar joint, whereas the model developed in this dissertation distinctly represented the trunk as two linked rigid bodies connected by the lumbar as well as the thoracic joints. Therefore, the values of these constants for the lumbar and thoracic joints were adjusted to correspond to half of the ranges of each joint motion reported by Anderson (1990). The values of the constants are listed in Appendix C.

5.3. *Muscle model*

5.3.1. *Outline of muscle model*

The muscle–tendon tissue dynamics were modeled with activation and contraction dynamics (Figure 5.4). Activation dynamics corresponds to the transformation of the neural excitation to activate the contractile element and the muscle contraction dynamics corresponds to the transformation of activation to muscle force. The force-producing characteristics of a muscle–tendon model depend on the maximum isometric strength of the muscle (F_{max}), the corresponding optimal fiber length (L_{CEopt})

and pennation angle (α), slack length of the tendon (L_{slack}), and percentage of first twitch fibers (%FT: type IIa and IIb).

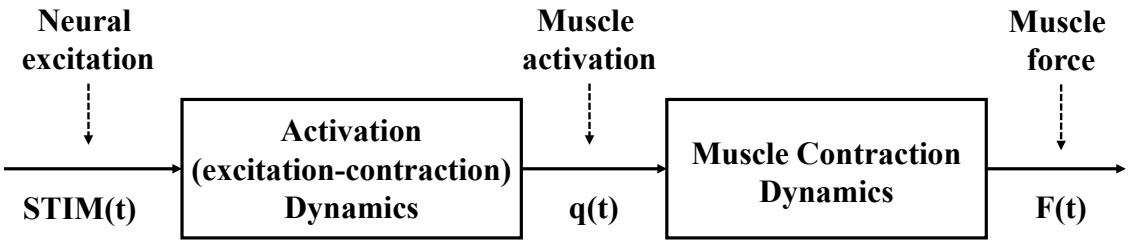

Figure 5.4 Dynamics of neuro-muscular system

The dynamics of muscle-tendon tissue are modeled as activation dynamics and contraction dynamics.

5.3.2. *Implemented muscles*

Ninety Hill-type muscle-tendon models (25 in each lower extremity and 20 in each right and left side of the trunk) were implemented into the skeletal model according to the model proposed by (Raabe and Chaudhari, 2016) (Figure 5.5). The muscle-tendon models implemented on the trunk were classified according to the main muscle group:

- **Erector spinae:** m. iliocostalis lumborum pars lumborum (ILIOCLUMB_LUMB), lower part of m. iliocostalis lumborum pars thorasis (ILIOCLUMB_THOR1), upper part of m. iliocostalis lumborum pars thorasis (ILIOCLUMB_THOR2), m. longissimus thoracis pars lumborum (LONGISTHOR_LUMB), m. lower part of longissimus thoracis pars thoracis (LONGISTHOR_THOR1), upper part of m. longissimus thoracis pars thoracis (LONGISTHOR_THOR2), lower rib part of m. longissimus thoracis pars thoracis (LONGISTHOR_THOR_RIB1), upper rib part of m. longissimus thoracis pars thoracis

(LONGISTHOR_THOR_RIB1)

- **Abdominal muscles:** m. rectus abdominis (RECABD), anterior part of m. internal oblique (INTOB 1), m. middle part of internal oblique INTOB 2), posterior part of m. internal oblique (INTOB3), anterior part of m. external oblique (EXTOB1), middle part of m. external oblique (EXTOB 2), posterior part of m. external oblique (EXTOB3)
- **Quadratus lumborum:** posterior part of m. quadratus lumborum (QUADLUMB_POST), middle part of m. quadratus lumborum (QUADLUMB_MID), anterior part of m. quadratus lumborum (QUADLUMB_ANT)
- **Multifidus** (MULFID)

The muscle–tendon models implemented in the lower extremities were classified according to their primary function:

- **Bi-articular lumbar flexor and hip flexor:** m. psoas major (PSOASM)
- **Mono-articular hip flexor:** m. iliacus (ILIA)
- **Mono-articular hip extensor:** m. gluteus maximus (GMAXI)
- **Mono-articular hip abductors:** m. gluteus medius (GMEDI) and m. gluteus minimus (GMINI)
- **Mono-articular hip adductors:** m. adductor longus (ADDLO), m. adductor magnus (ADDMA) and m. adductor brevis (ADDBR)
- **Mono-articular hip external rotators:** m. piriformis (PIRI) and m. quadratus femoris (QUAD)
- **Bi-articular hip flexor and knee extensor:** m. rectus femoris (RECTF)
- **Bi-articular hip extensors and knee flexors:** m. biceps femoris caput longum (BIFEL),

m. semimembranosus (SEMM), and m. semitendinosus (SEMT)

- **Mono-articular knee extensors:** m. vastus lateralis (VASL), m. vastus intermedialis (VASI) and m. vastus medialis (VASM)
- **Mono-articular knee flexors:** m. biceps femoris caput brevis (BIFES)
- **Bi-articular knee flexors and ankle plantar flexors:** m. gastrocnemius medialis (GASM) and m. gastrocnemius lateralis (GASL)
- **Mono-articular ankle dorsi flexor:** m. tibialis anterior (TIBAN)
- **Mono-articular ankle plantar flexors:** m. soleus (SOLEU), m. tibialis posterior (TIBPOS), m. peroneus longus (PERL), m. peroneus brevis (PERLB), and m. flexor hallucis longus (FHAL)

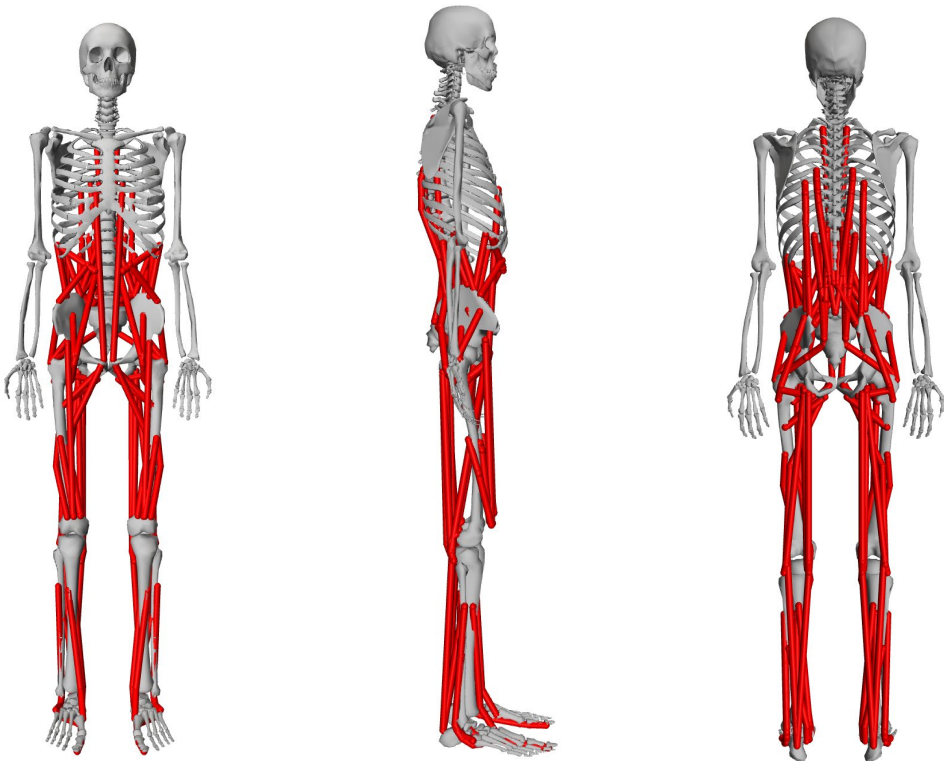

Figure 5.5 Musculoskeletal model used in this dissertation.

Ninety Hill-type type muscle-tendon model (25 in each lower extremity and 20 in each right and left side of the trunk) were implemented into the skeletal model according to the model proposed by Raabe and Chaudhari (2016).

The original model proposed by Raabe and Chaudhari (2016) has numerous (324) musculotendon actuators; however, some separated portions of a muscle were lumped into a single muscle for computational efficiency in this study. For the muscles in the lower extremity, ones having a physiological cross-sectional area (PCSA) < 14 cm^2 were lumped into a single muscle according to previous studies (Friederich and Brand, 1990; Nagano et al., 2005b). For the muscles of the trunk, the separated portion of a muscle was manually lumped, while maintaining the original torque–angle curve of the lumbar joint under the movement conditions of lateral flexion, axial rotation, flexion, and extension. To validate this simplification, the torque–angle curves derived from the original and current models are plotted in Figure 5.6–Figure 5.9. These torque–angle curves were qualitatively similar to each other. Moreover, the validation of the original model could not be adopted because it does not consider the torque about the thoracic joint. Furthermore, the value of the origin, insertion, and via-points of each muscle were adopted from Christophy et al. (2012), (Raabe and Chaudhari, 2016), and Delp (1990) (Appendix F).

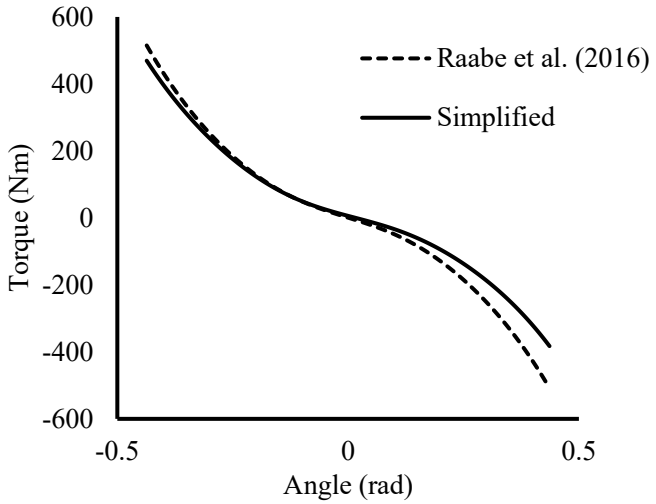

Figure 5.6 Torque–angle curves about the lumbar joint for lateral bending motion derived from the original and current model.

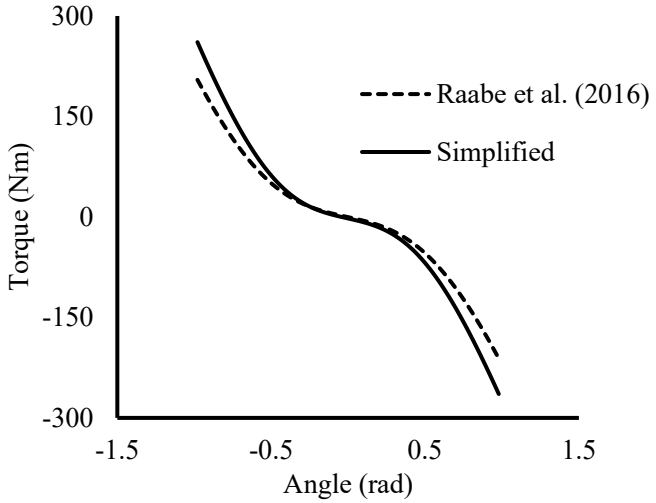

Figure 5.7 Torque–angle curves about the lumbar joint for axial rotation motion derived from the original and current model.

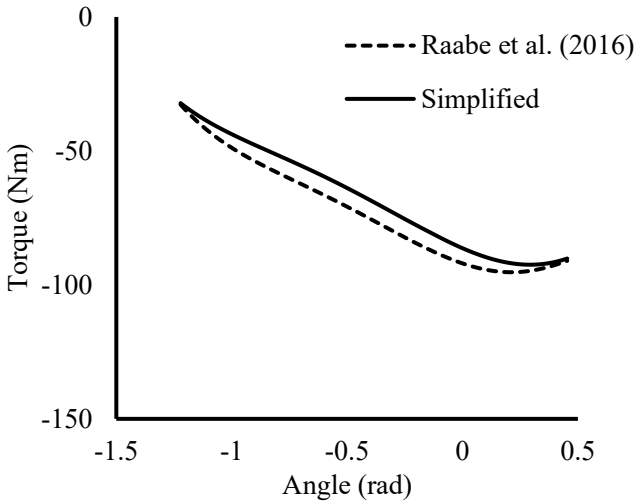

Figure 5.8 Torque–angle curves about the lumbar joint for flexion motion derived from the original and current model.

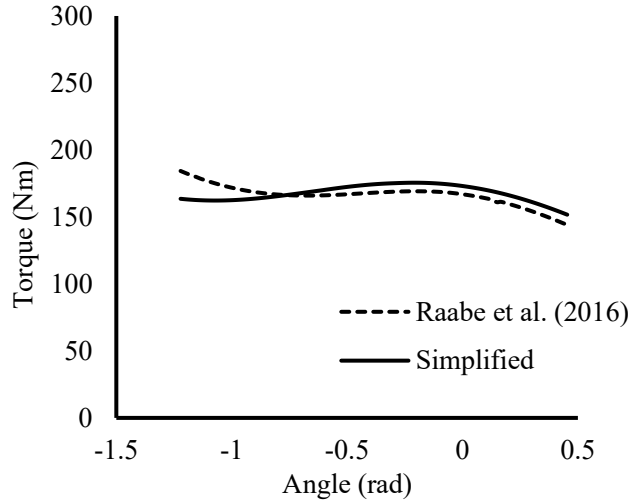

Figure 5.9 Torque–angle curves about the lumbar joint for extension motion derived from the original and current model.

5.3.3. *Musculoskeletal parameters*

The maximal isometric contractile force (F_{max}) of each muscle in the musculoskeletal model was determined as follows:

$$F_{max} = K \times PCSA \quad \text{(Equation 5.4)}$$

where K and PCSA are the specific tension and physiological cross-sectional area for each muscle, respectively. The value of *K* was set to 46 N/cm^2 (Christophy et al., 2012). The PCSA data of the muscles in lower extremity, which were obtained from the specimen as 1.83 m and 91 kg (Friederich and Brand, 1990), were scaled to the value of 1.74 m and 73 kg for the current musculoskeletal model used in this study. The original values of F_{max} were adopted from Raabe et al. (2016) without scaling, because the values of F_{max} were determined from several different PCSA values for each trunk muscle of the subjects (Bogduk et al., 1992; Delp et al., 2001; Macintosh and Bogduk, 1986).

The percentage of fast-twitch fiber (%FT) for the muscles in the lower extremity and trunk was adopted from (Johnson et al., 1973).

All other values of musculoskeletal parameters ($L_{CEopt,}$ α, $L_{slack,}$) were based on data reported by (Delp, 1990) and (Raabe and Chaudhari, 2016). The values of each muscle parameter used in this dissertation are listed in Appendix B.

5.3.4. *Activation dynamics*

The activation dynamics of the contractile element of the muscle was modeled with a first-order ordinary differential equation (ODE) to represent the neuromuscular delay between neural stimulation input of a muscle (STIM: $0 \leqq STIM \leqq 1$) and its active state (q) as described in (He et al., 1991;

Nagano and Gerritsen, 2001) (Figure 5.10). The muscle activation input was specified by three factors: onset time, offset time, and magnitude. The relationship between neural stimulation (STIM) and the active state of the muscle (q) is represented by the following formula:

$$\dot{q} = \big(\mathrm{STIM}(t) - q(t)\big) \cdot (t1 \cdot \mathrm{STIM}(t) + t2)$$

(Equation 5.5)

where

$$t1 = \frac{1}{T_{act}} - t2, \qquad t2 = \frac{1}{T_{deact}}$$

T_{act} and T_{deact} were time constants for muscle activation and de-activation, respectively. The values for T_{act} = 0.055 s and T_{deact} = 0.065 s were considered according to Winters and Stark (1988) and Nagano and Gerritsen (2001). The time-integrated value on the left side of this equation, which represents the rate of change of the active state of the muscle with respect to time, was used for computing the muscle contraction dynamics.

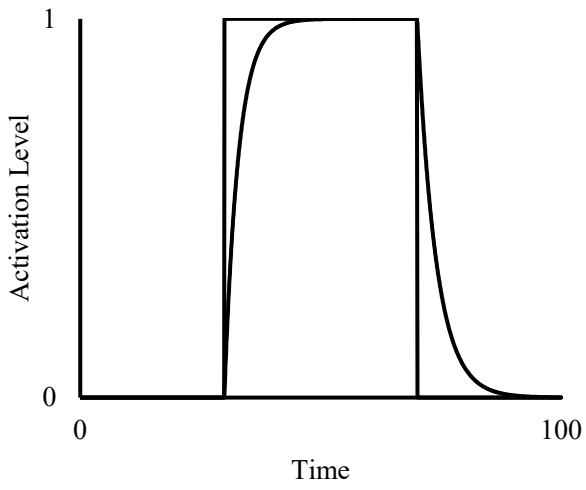

Figure 5.10 Muscle excitation dynamics.

5.3.5. *Muscle contraction dynamics*

A muscle–tendon complex was represented by a Hill-type muscle model (Hill, 1938) composed of a contractile element (CE), a parallel elastic element (PEE), and a series elastic element (SEE), serially connected with a pennation angle (Figure 5.11). Besides, models of CE force–length and force–velocity relations were reported by (Cole et al., 1996; Nagano and Gerritsen, 2001; van Soest and Bobbert, 1993). As the force in the CE was represented as a function of CE-length and CE-velocity, the contractile dynamics were described with one additional ODE per muscle.

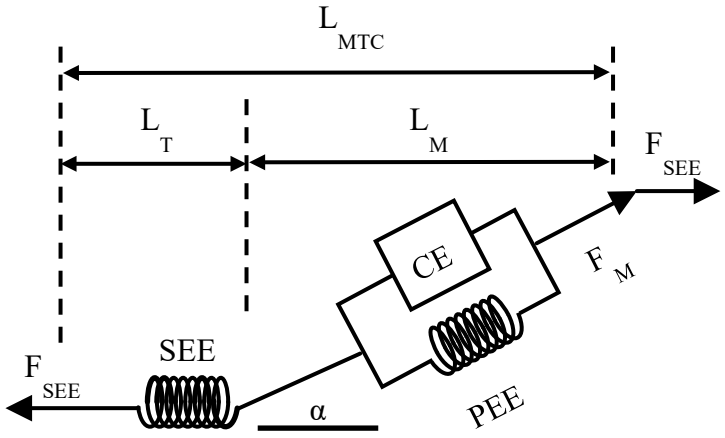

Figure 5.11 A Model of Muscle-Tendon Complex

5.3.5.1. *Force – length relationship of contractile element and parallel elastic element*

The resultant force developed by a muscle is represented as the sum of forces generated actively and passively according to the principle of force–length relationship of CE and PEE (Figure 5.12). The force relative to the maximal isometric force produced isometrically by a CE is represented by Equation 4.6 as the active isometric force (F_{isom}):

$$F_{isom} = c \cdot \left(\frac{L_{CE}}{L_{CEopt}}\right)^2 - 2c \cdot \left(\frac{L_{CE}}{L_{CEopt}}\right) + c + 1$$

(Equation 5.6)

where

$$c = -\frac{1}{(width)^2}$$

L_{CEopt}: optimal contractile element length, L_{CE}: contractile element length; width: half the maximal-

length range of active force production relative to L_{CEopt} (55%), derived using a parabolic approximation of the theoretical force–sarcomere–length relation for humans (Allinger et al., 1996). The force–length relationship of PEE is described as follows:

$$F_{PEE} = F_{max} \cdot \left(\frac{L_{CE} - L_{CEopt}}{0.47 \cdot L_{CEopt}} \right)^3$$

(Equation 5.7)

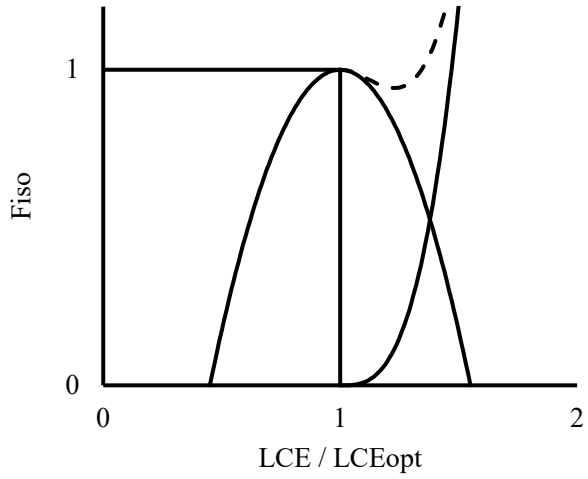

Figure 5.12 Force-length relationship of contractile element and parallel elastic element.

5.3.5.2. *Force – velocity relationship of contractile element*

In addition to the force–length relationship, the magnitude of the active force developed by the muscle is influenced by the rate of change of muscle fiber length (Figure 5.13). When the muscle contracts concentrically, the force–velocity relationship can be described as follows:

$$V_{CE} = -FACTOR \cdot L_{CEopt} \cdot \left(\frac{(F_{isom} + A_{rel}) \cdot B_{rel}}{\frac{F_{CE}}{F_{max} \cdot q} + A_{rel}} - B_{rel} \right)$$

(Equation 5.8)

where

$$FACTOR = \min(1, 3.33 \cdot q)$$

Arel based on whole muscle fiber type composition was descripted as follows (Umberger et al., 2003; Winters and Stark, 1988):

$$Arel = 0.1 + 0.4\ (\%FT/100)$$

where %FT is the percentage of first-twitch fibers (type IIa and IIb) in each muscle. The B_{rel} constant can be represented as follows:

$$B_{rel} = A_{rel} \cdot V_{CEmax}$$

where V_{CEmax} is the maximum shortening velocity of the muscle considered as 12 ms^{-1} according to (Umberger et al., 2003).

The force–velocity relationship of CE can be described as follows:

$$V_{CE} = -L_{CEopt} \cdot \left(\frac{c1}{\frac{F_{CE}}{F_{max} \cdot q} + c2} - c3 \right)$$

(Equation 5.9)

where c1, c2, and c3 specify the shape of the eccentric force–velocity relation:

$$c2 = = F_{isom} \cdot F_{asympt}$$

$$c1 = \frac{FACTOR \cdot B_{rel} \cdot (F_{isom} + c2)^2}{(F_{isom} + A_{rel}) \cdot Slopefactor}$$

$$c3 = \frac{c1}{(F_{isom} + c2)}$$

where F_{asympt} is the asymptotic maximal force value in the eccentric phase (relative to F_{max}) and Slopefactor is the ratio between eccentric and concentric derivatives.

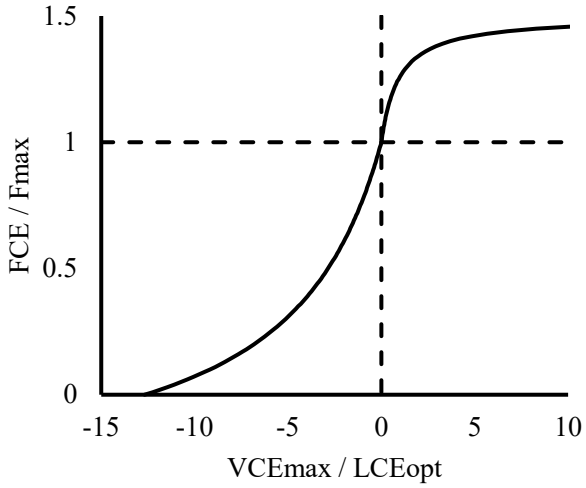

Figure 5.13 Force-velocity relationship

5.3.6. *Force – length relationship of series elastic element*

The series elastic element was modeled as a nonlinear spring (Figure 5.14):

If $\Delta L_{SEE} = L_{SEE} - L_{slack} > 0$,

$$F_{SEE} = F_{max} \cdot \left(\frac{\Delta L_{SEE}}{u \cdot L_{slack}} \right)^2$$

(Equation 5.10)

where ΔL_{SEE}, L_{slack}, and u are the length of SEE, slack length of SEE, and relative elongation of the SEE at maximal isometric force, respectively. The relationship between the contractile element force (F_{CE}) and the series elastic element force (F_{SEE}) can be described as

$$F_{CE} = \frac{F_{SEE}}{\cos \alpha}$$

(Equation 5.11)

where α is the pennation angle. The quadratic stiffness of the SEE was defined such that the strain of the SEE-length (ΔL_{SEE}) was 4% of the L_{slack} when the contractile element force (F_{CE}) was equal to the maximal isometric muscle force (i.e., $F_{CE} = F_{max}$).

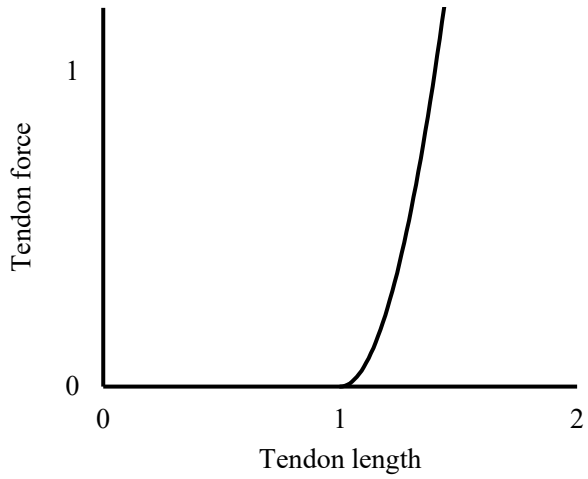

Figure 5.14 Force-length relationship of series elastic element.

5.4. *Ground reaction force model*

The ground reaction force was modeled by a nonlinear viscoelastic element adopted from (Anderson, 1999):

$$\mathrm{GRF_y} = \alpha_1 \exp\left(-\alpha_2(y-\beta_1)\right) - \frac{\alpha_3 \cdot \dot{y}}{1+\alpha_4 \exp\left(\alpha_5(y-\beta_2)\right)}$$

(Equation 5.12)

where GRF_y is the vertical component of the ground reaction force, and y is the vertical position (floor = 0.0 m) of the foot/ground contact point (Figure 5.15). The parameter values were adopted from Nagano et al. (2005b): $\alpha_1 = 1.039$ N; $\alpha_2 = 491.804$ m^{-1}; $\alpha_3 = 963.321$ Nm^{-1}; $\alpha_4 = 44.715$ (no units); $\alpha_5 = 706.924$ m^{-1}; $\beta_1 = 0.857 \times 10^{-3}$ m; and $\beta_2 = -2.325 \times 10^{-3}$ m. The anterior–posterior (x) and medio–lateral (z) components of the ground reaction force were described by a Coulomb (dry) friction model with a friction coefficient of 1.0 (Gerritsen et al., 1995):

$$GRF_x = -1.0 \cdot GRF_y \cdot \frac{\dot{x}}{|\dot{x}|}$$

(Equation 5.13)

$$GRF_z = -1.0 \cdot GRF_y \cdot \frac{\dot{z}}{|\dot{z}|}$$

(Equation 5.14)

where GRF_x and GRF_z are the anterior–posterior and medio–lateral components of the reaction force, respectively; x and z are the anterior–posterior and medio–lateral positions of the foot/ground contact point, respectively. For numerical reasons, this relationship was approximated by a continuous function with a slope of 3000 Nsm^{-1} at $\dot{x} = 0$ ms^{-1} and $\dot{z} = 0$ ms^{-1}, respectively.

Five contact points on each foot (2 on the heel, 2 on the metatarsophalangeal joint, and 1 on the toe) were modeled (Figure 5.16).

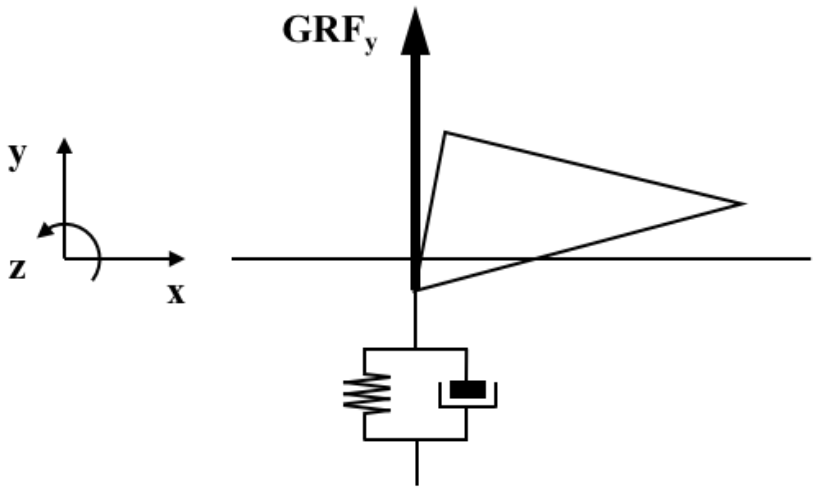

Figure 5.15 Illustration of the ground reaction force model.

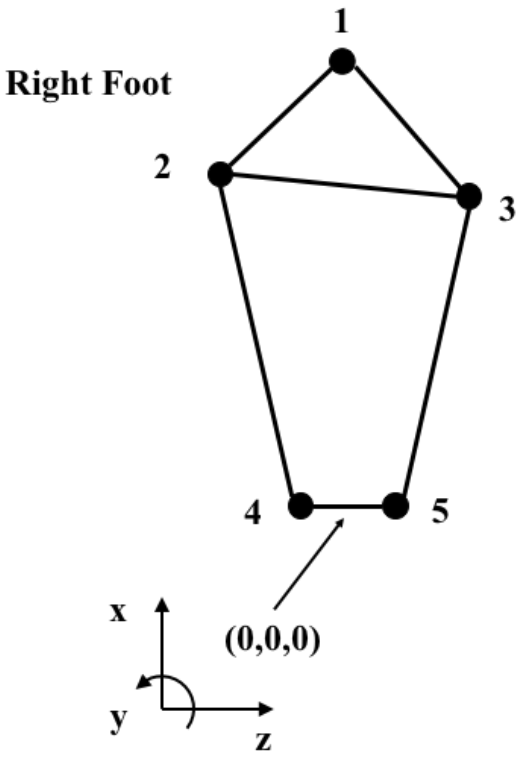

Foot/Ground contact points

	x	y	z
1	0.168	0	0.000
2	0.126	0	-0.024
3	0.108	0	0.022
4	0.000	0	-0.011
5	0.000	0	0.011

Figure 5.16 Illustration of the foot/ground contact points.

Chapter 6: *Walking simulation and assessment of the musculoskeletal computer simulation system*

6.1. *Introduction*

Locomotion (i.e., walking) is one of the most common activities in daily life, and an understanding how our neuromusculoskeletal system controls the whole-body could be helpful in designing an effective intervention for addressing the impairments of human locomotion and extending healthy life expectancy. From this point of view, the neuromusculoskeletal control of the trunk could affect the stability and mobility of the whole-body during walking motion, as the mass of the trunk accounts for approximately half of the total body mass (de Leva, 1996). However, although several researches have reported on the musculoskeletal contribution of the lower and upper extremities to control of human walking (Lin et al., 2014; Pandy et al., 2010), sufficient information for the trunk is not available. Specifically, a framework to analyze human dynamic movements considering the musculoskeletal contribution of the trunk has not been clarified. Therefore, the lack of knowledge regarding the biomechanics of the trunk has been a major barrier in understanding how we control our whole-body to achieve walking.

In this regard, a neuromusculoskeletal computer simulation system that is applicable for both inverse and forward dynamics simulation has been constructed and described in chapters 4 and 5 to help researchers assess the neuromusculoskeletal contribution of the trunk in human locomotion. However, the validity of this musculoskeletal computer simulation system when simulating human movement is yet not be confirmed. To investigate the neuromusculoskeletal contribution of the trunk to the control of human locomotion, the validity of the kinematic and kinetic data derived from the computer simulation system needs to be assessed. Therefore, this study aimed to generate human walking motion using the designed neuromusculoskeletal computer simulation system and to assess

the validity of the simulated data derived from the simulation system through comparison with kinematic and kinetic data of human walking motion derived from both the inverse and forward dynamics approaches.

6.2. *Methods*

The validity of the simulated data was assessed by comparing it with the experimental data. More specifically, the joint angular displacements and the net muscle torque of the lumbar and thoracic joints simulated by the model were compared with those of the experimental data, as kinematic and kinetic measures, respectively.

6.2.1. *Walking simulation with musculoskeletal model*

The only inputs to the neuromusculoskeletal model to simulate walking motion were 90 muscle activation profiles, each specified by three values: onset time (T_{on}), offset time (T_{off}), and amplitude of stimulation (STIM). The muscle stimulation profiles in the right leg and right side of the trunk were assumed to be identical to, but 50% out of phase with, the profiles in the left side. The optimal muscle stimulation profiles to generate the walking motion were determined by using numerical optimization. The goal of the numerical optimization was to minimize an objective function comprising four separate terms: (1) the difference between the simulated posture at the end of the step and a typical upright posture described by segment Euler angles, (2) the whole-body energy expenditure per meter traveled, (3) the sum of the maximum and minimum values of head acceleration obtained during a step, and (4) the sum of the angular displacement of the head during a step. Details on each term are provided in the following sections.

Three steps of the walking motion (i.e., 150% of a gait cycle) were simulated in this study. The duration for the simulation was set according to the spaciotemporal characteristics observed from the

experimental data. The averaged step length and averaged COM velocity during one stride over ten participants were 1.30 m and 1.17 m/s, respectively. Therefore, the duration of one step was estimated to be 1.30 m / 1.17 ms^{-1} / 2 steps (i.e., one stride) = 0.56 s, and thus the duration of simulation for three step walking was calculated as 0.56 s $\times$ 3 steps = 1.68 s.

6.2.1.1. *Evaluation of kinematics*

The initial and target postures at the end of the step, except for the vertical displacement of the pelvis and the subtalar joint angle, were based on averaged values of kinematic data from the experiment. The simulation was initialized at the right toe-off. The differences in the segment Euler angles (3 Euler angles for each of the thorax segment, abdomen segment, pelvis segment, right and left thigh segments, right and left shank segments, right and left hind foot segments, and right and left fore foot segments = 33) between the initial (i.e., target) posture and the simulated posture as the instant of the subsequent toe-off were calculated as follows:

$$\mathbf{RMS_{ang}} = \sqrt{\frac{\sum_{\mathbf{i=1}}^{\mathbf{33}}(\Delta\boldsymbol{\theta})^{\mathbf{2}}}{\mathbf{33}}}$$

(Equation 6.1)

where the $\Delta\theta$ are the difference in the 33 Euler angles.

6.2.1.2. *Evaluation of whole-body energy consumption*

Energy expenditure is an important factor in human locomotion. Previous simulation studies have shown that minimization of the cost of walking a unit distance does in fact lead to realistic simulations of human walking (Anderson and Pandy, 2001a; Nagano et al., 2005b). Therefore, the objective

function was formulated to produce an economical walking pattern. Whole body energy expenditure per meter traveled during walking (WBE_{travel}: J / (kg·m)) was calculated as the sum of three components: 1) mechanical work produced by all muscle contractile elements: muscle power integrated over time, 2) heat produced by all muscle contractile elements: the sum of the activation heat, the maintenance heat, and the additional heat due to contractile element shortening and lengthening, and 3) an estimate of heat produced by all body tissues not accounted for by the modeled muscles. A detailed mathematical description of the muscle energy expenditure model may be found in a preceding study (Nagano, 2001; Umberger et al., 2003).

6.2.1.3. *Evaluation of head acceleration*

It is assumed that the central nerve and vestibular system manages to keep the trunk erect and ensures severely attenuated head accelerations during walking (Thorstensson et al., 1984; Winter, 1995). Therefore, the square root of the sum of the squares of the maximum and minimum value of head acceleration for the anterior-posterior direction was calculated as follows:

$$\mathrm{RSS}_{\mathrm{headacc}} = \sqrt{(\mathrm{H}_{\mathrm{accmax}})^2 + (\mathrm{H}_{\mathrm{accmin}})^2}$$

(Equation 6.2)

where H_{accmax} and H_{accmin} are the maximum and minimum value of head acceleration for the anterior-posterior direction during a step, respectively.

6.2.1.4. *Evaluation of angular displacement of the head*

Ensuring clear vision while minimizing the angular displacement of the head during locomotion is also an important task in postural control. Therefore, to evaluate the angular displacement of the

head during a step, the sum of the three-dimensional angular displacement of the head relative to the global reference frame was calculated as follow:

$$S_{headangdisp} = H_{angdispX} + H_{angdispY} + H_{angdispZ}$$

(Equation 6.3)

where $H_{angdispX}$, $H_{angdispY}$, and $H_{angdispZ}$ are the angular displacement of the head about each axis of the global reference frame during a step.

6.2.1.5. *Optimization settings*

The RMSang value, whole body energy consumption per meter traveled (WBEmeter: section 5.2.2.2.), and head acceleration value ($RSS_{headacc}$) were added using the following weight factors:

$$\text{Objective function} = C_1 \cdot RMS_{ang} + C_2 \cdot WBE_{meter} + C_3 \cdot RSS_{headacc} + C_4 \cdot S_{headangdisp}$$

(Equation 6.4)

where

$$C_1 = 1.0,\ C_2 = 0.1\ C_3 = 0.02, \text{and}\ C_4 = 0.1$$

Muscle activation profiles that reduced the objective function value were searched with the algorithm of Bremermann (1970). The resolution of Ton and Toff was set to 0.001 s, the resolution of ACT was set to 0.001 (1.0 = maximum activation), and the resolution of the walking performance was set to 0.001. The optimization process was terminated when walking performance did not increase for 500 consecutive iterations.

For the kinematic data, the joint angular displacement about the lumbar and thoracic joint were

calculated from the optimized walking data. More specifically, the joint angular displacement for each joint was calculated as the angle of the upper part of segment relative to the lower part of segment (i.e., lumbar joint: angle of abdomen relative to the pelvis, thoracic joint: angle of thorax relative to the abdomen). For the kinetic data, net muscle torque about the lumbar and thoracic joint were calculated by using cross product of both muscle force and the corresponding moment arm. The muscle torque about lumbar and thoracic joint were represented in the reference frames on the pelvis and abdomen segment, respectively.

Because the simulated walking data at the instant of initiation and termination might be significantly affected by the initial condition and the objective function, respectively, the kinematic and kinetic data in only the second step (i.e., from the instant of left toe-off to the instant of right toe-off) were used for the analysis. The simulated kinematic and kinetic data were reversed along the axis of time to ensure that they conformed to the experimental data, which included the kinematic and kinetic data from the right toe-off to the left toe-off. The simulated data were then normalized to percentage of the step (see Section 6.2.2.1). The instant of toe-off was determined using the total ground reaction force applied on the five contact points of the foot segment (threshold: 5% of total body mass).

6.2.2. *Human experiments*

6.2.2.1. *Experimental protocol*

Ten male college student （age: 22.7 ± 0.9 y, height: 1.72 ± 0.05 m, body mass: 67.4 ± 6.0 kg）participated in this experiment. They were instructed to continuously walk on a 20 m circuit walkway for five times, keeping their own preferred speed. The three-dimensional positional data of the trunk and ground reaction force along a 5 m straight section of the walkway (from 2.5. to 7.5 m section of the walkway) were recorded during the third lap of each trial using a 24-camera motion

capture system at 250 Hz (MAC3D, Motion Analysis Corporation, California, USA) and two force plates at 1250 Hz (Tec Gihan, TF-4060-B, Japan). A total of 38 reflective markers were placed on both the left and right sides of the participant's body at the following locations to measure the three-dimensional positions of the segments: the top head, front head, rear head, 7th cervical vertebra, suprasternal, acromion, lateral and medial elbow, lateral and medial wrist, mid-spine at 10th rib level, 10th rib, anterior superior iliac spine, posterior superior iliac spine, lateral and medial femoral epicondyles, spyrion, lateral malleolus, calcaneus, 1st and 5th metatarsal heads, and 2nd toe tip (Figure 6.1). The entire body of the participants was modeled with eighteen rigid-body segments as constructed in Chapter 5.

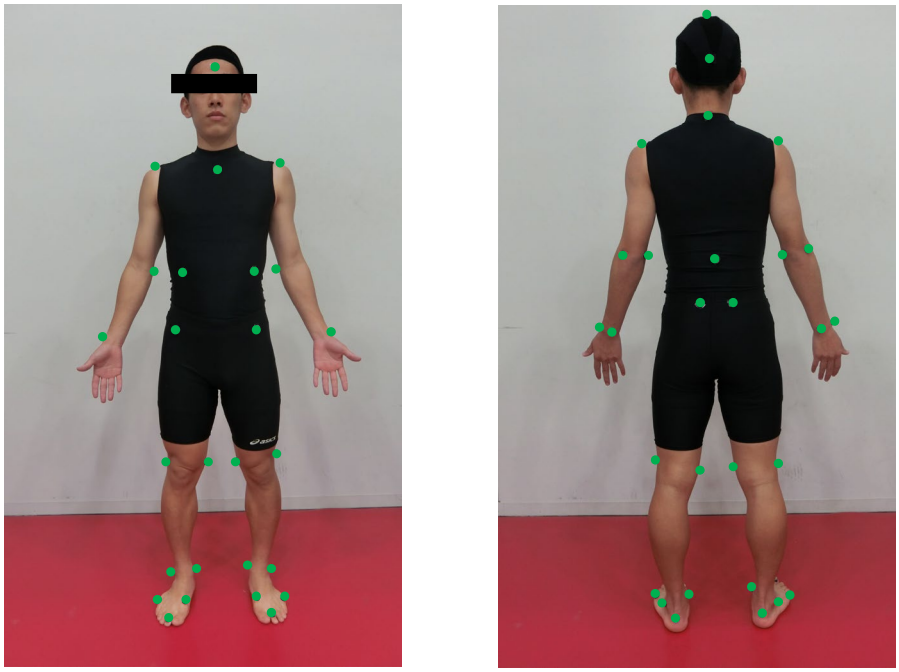

Figure 6.1 Placement of markers.

6.2.2.2. *Inverse dynamics analysis*

An inverse dynamics approach was applied to calculate the joint angular displacement and joint

torques about the lumbar and thoracic joints using the Newton–Euler equations of motion. In addition, anthropometric estimates of mass, center of mass (COM), and radius of gyration in each plane of rotation were calculated for each segment using the parameters reported in previous studies (Dumas et al., 2007a; Dumas et al., 2007b; Dumas et al., 2015). Furthermore, the joint angular displacement for each joint was calculated as the angle between the upper and the lower part of the segment (i.e., lumbar joint: angle of abdomen relative to the pelvis, thoracic joint: angle of thorax relative to the abdomen). The joint torques about the lumbar and thoracic joints were represented in the reference frames on the pelvis and abdomen segments, respectively. The averaged value and standard deviation (SD) data for ten participants for both joint angle and joint torque were calculated to compare and validate the simulated data.

The data during a stride from the right toe-off to the next left toe-off were analyzed, and the data were normalized to the percentage of the step. The instant of toe-off was determined using the total ground reaction force applied on the five contact points of the foot segment (threshold: 5% of total body mass).

6.2.3. *Data analysis*

The simulated joint angular displacements and the experimental joint angular displacement averaged over ten participants were compared to assess the validity of the simulated kinematic data derived from the simulation system. For the kinematic data, the simulated net muscle torque and the experimental joint torque averaged over ten participants were compared to assess the validity of the kinetic data derived from the simulation system.

6.3. *Results*

Three-step walking motion was successfully generated using the neuromusculoskeletal

computer simulation system established in this study (Figure 6.2). The root mean square of the differences between the Euler angles for all the segments (RMSang), which has the largest weight in the objective function (Equation 6.3), were less than 7°. The numerical optimization process always resulted in smooth and natural-looking kinematics. The whole-body energy consumption per meter traveled was estimated to be 8. 5 J / kg /m.

Similar trends were found in the profile of the kinematics and kinetics of the lumbar and thoracic joint between the simulated and experimented data, although there also existed discrepancies. For kinematic data, the simulated joint angular displacements during walking motion about both the lumbar and thoracic joints (red line in Figure 6.3-4) were in the mean +/- 2 SD range of the experimental data (blue line in Figure 6.3-4). However, larger flexion angle was found in the simulated data during a step of walking compared with the experimented data. For kinetic data, the simulated net muscle torque about both the lumbar and thoracic joints during the second step (red line in Figure 6.5-6) were partially outside the mean +/- 2 SD range of the experimental data (blue line in Figure 6.5-6), although the profiles of the net muscle torque simulated using the model were similar to those of the experimental data.

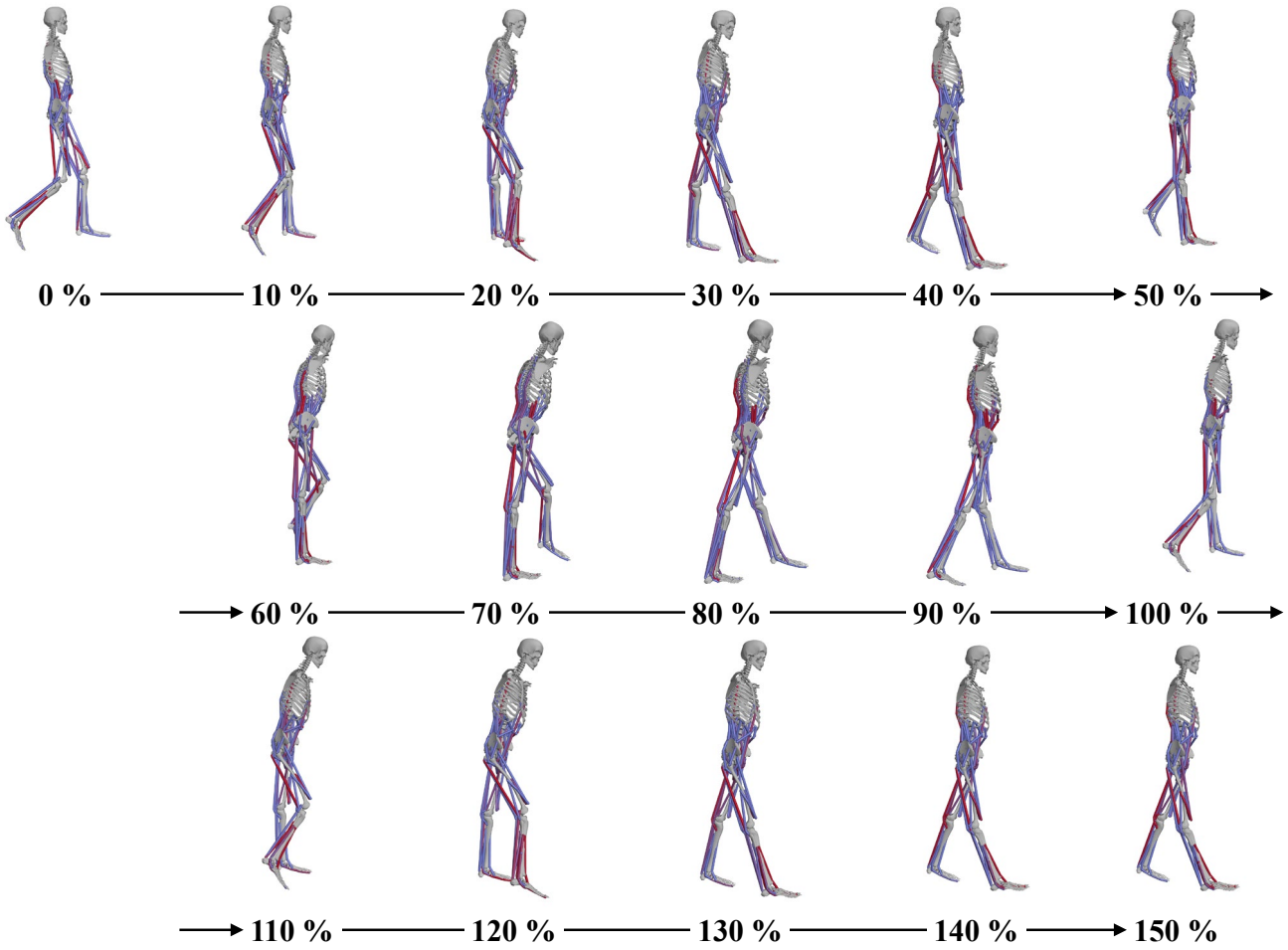

Figure 6.2 Snapshots of cyclic three-step walking movement generated by musculoskeletal model developed in this study

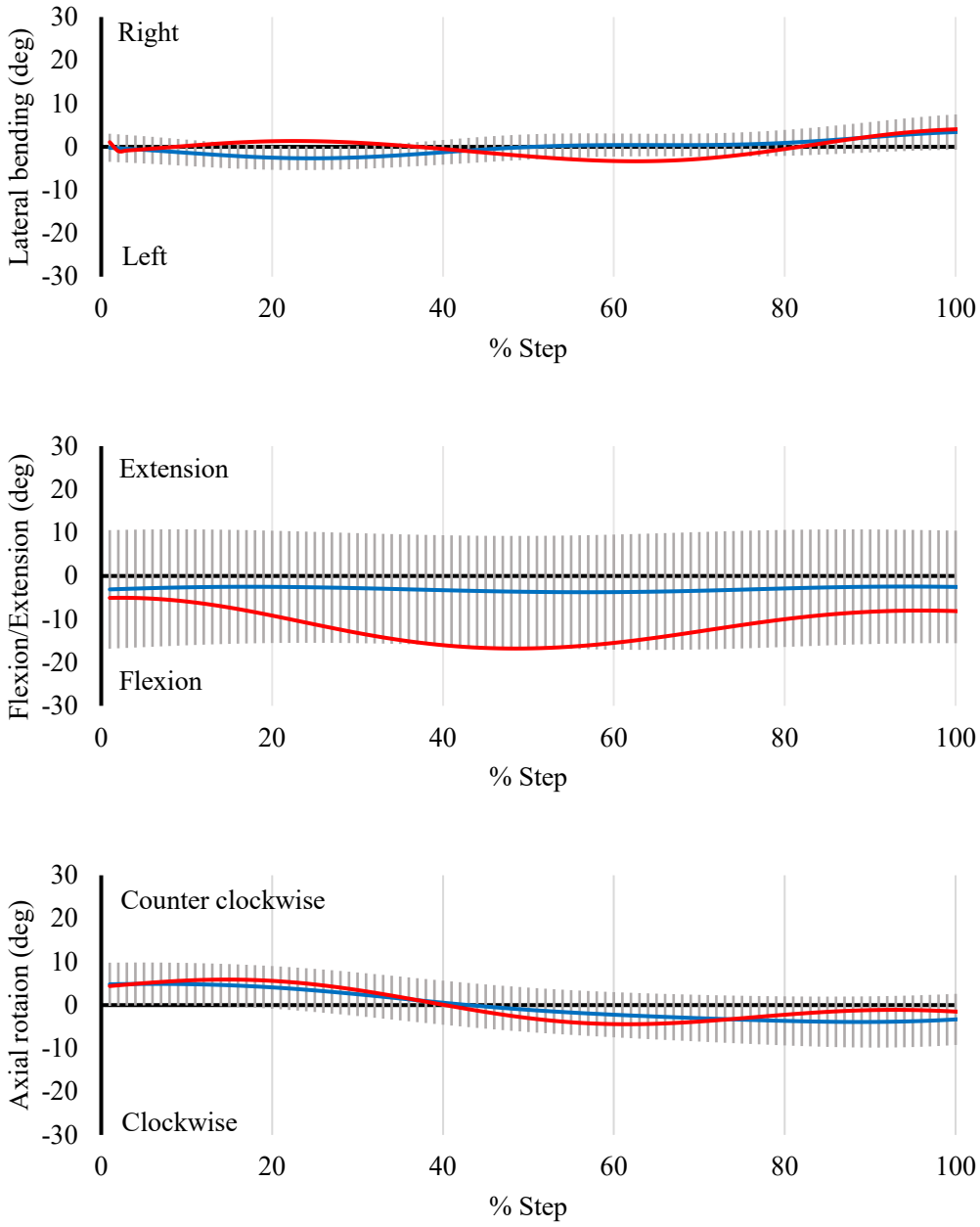

Figure 6.3 Lumbar joint angle

The red and blue lines indicate the simulated and experimental data, respectively.

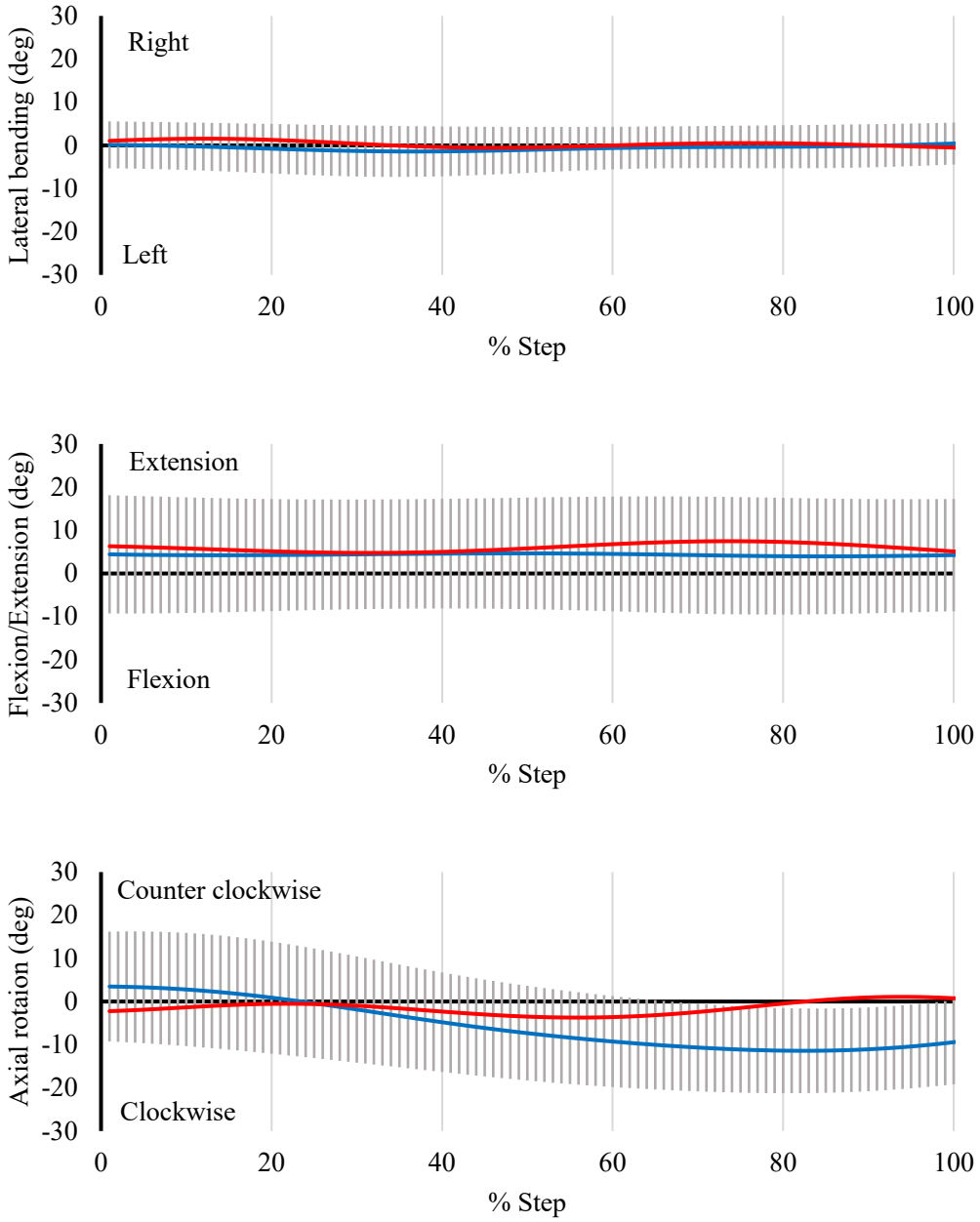

Figure 6.4 Thoracic joint angle

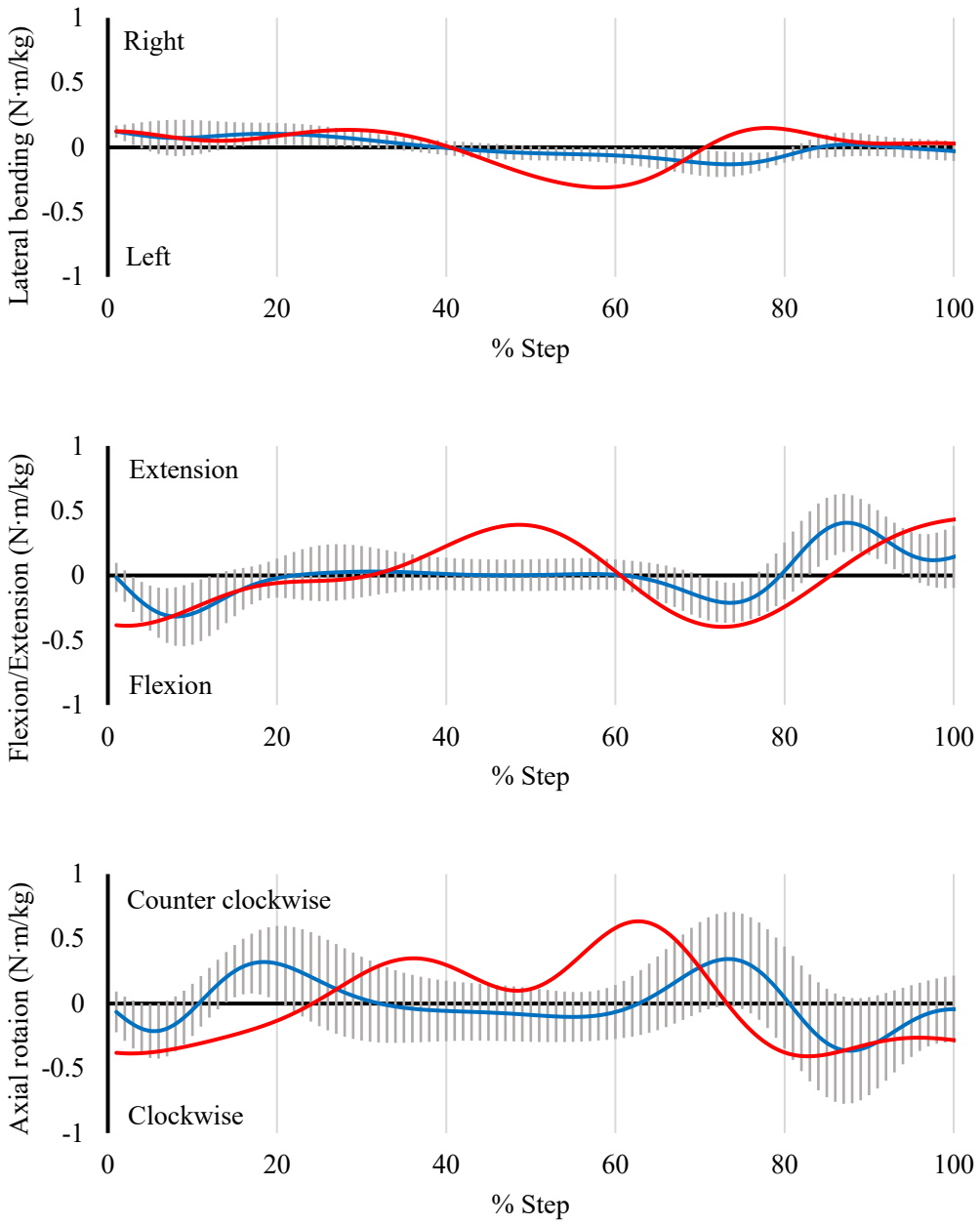

Figure 6.5 Net muscle torque about the lumbar joint torque

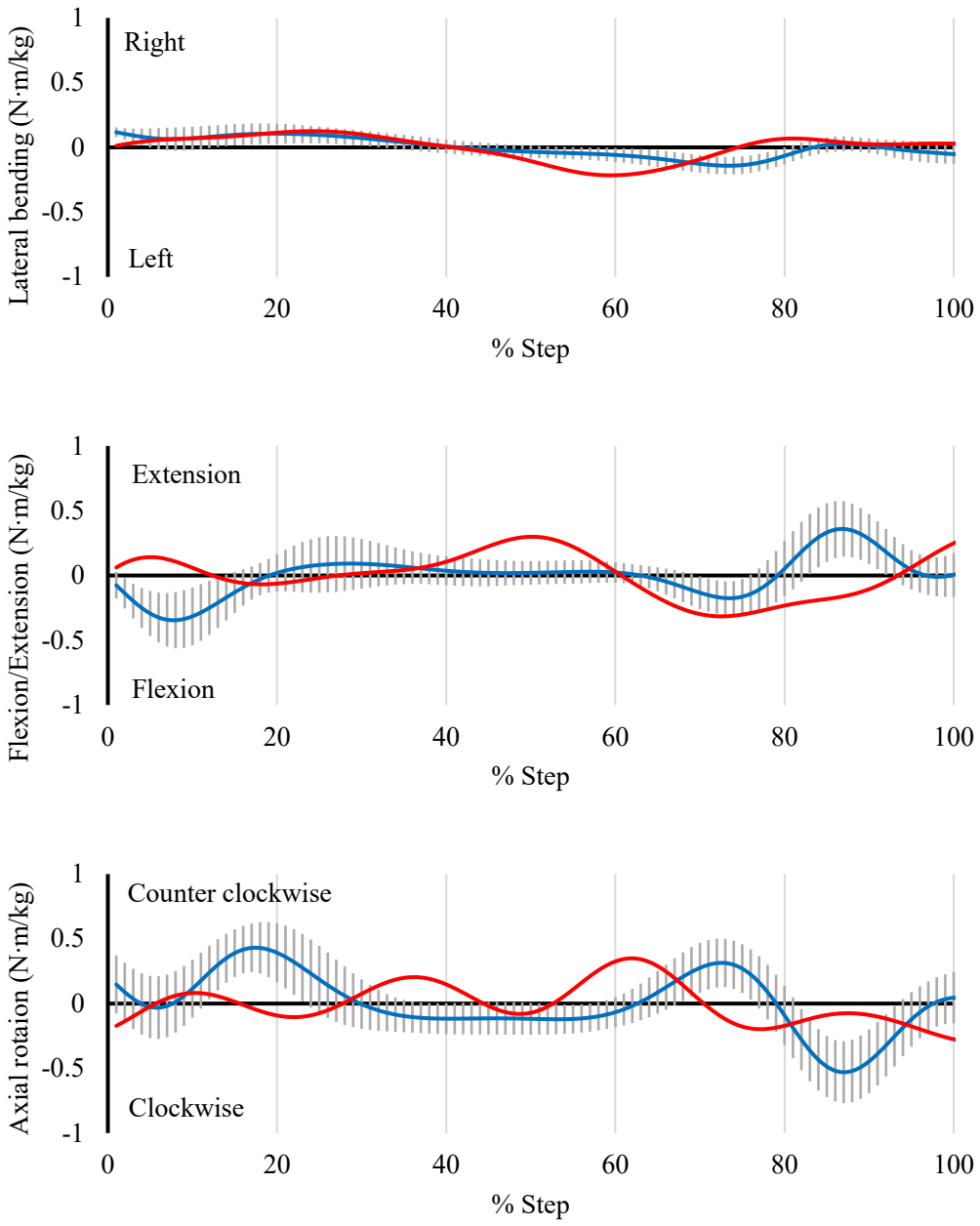

Figure 6.6 Net muscle torque about the thoracic joint

6.4. *Discussion*

This study generated the human walking motion, including the lower extremities and multi-segmental structure of the trunk, using the neuromusculoskeletal computer simulation system presented in Chapter 5. Additionally, the validity of the designed system was assessed by comparing the simulated kinematic and kinetic data of the trunk during walking with the corresponding experimental data. A cyclic three-step walking movement was successfully generated using the proposed computer simulation system. The value of RMS_{ang}, which has the largest weight in the objective function, was 7° and was comparable with that obtained in previous studies (Anderson, 1999; Nagano et al., 2005b). Additionally, the estimated WBE_{travel} (8.5 J / kg /m) complied with the values (7.7 J / kg /m) predicted by Nagano et al. (2005b) using the musculoskeletal model of the human lower extremity. These results imply that when generating human walking motion, the proposed simulation system would have comparable quality to that of previously established neuromusculoskeletal computer simulation systems. However, partial discrepancies on the profiles of the kinematics and kinetics data describing the lumbar and thoracic joint during walking motion was found between the simulated and experimental data. Furthermore, the estimated WBE_{travel} (8.5 J / kg /m) was significantly larger than that obtained by an experiment (2.4 J / kg /m) conducted in a previous study (Das Gupta et al., 2019). Therefore, these findings suggest that the quality of the proposed simulation system is comparable with that of previously established simulations, but there remains a discrepancy between the predicted and observed values of the kinematic, kinetics, and energy expenditure.

The optimized values of RMS_{ang} and WBE_{travel} obtained by the proposed neuromusculoskeletal computer simulation system were similar to those obtained in previous studies (Anderson and Pandy, 2001a; Nagano et al., 2005b), indicating that the simulation system established in this study could provide comparable data. Indeed, RMS_{ang} and WBE_{travel} are often used as valid measures of walking performance when generating human walking motion using neuromusculoskeletal simulation systems.

Accordingly, the finding that the estimated RMS_{ang} (7°) and WBE_{travel} (8.5 J / kg /m) conformed with the values (9° and 7.7 J / kg /m) predicted by Nagano et al. (2005b) indicates that the proposed simulation system considering the multi-segmental structure of the trunk would provide comparable quality to previously established neuromusculoskeletal computer simulation systems when used to generate human walking motion. Therefore, the successful generation of multiple walking steps via the forward simulation analysis proposed in this study provides important insights into the neuromusculoskeletal contribution of the trunk to the walking motion.

The discrepancies between the kinematic and kinetic data obtained using the proposed simulation system and that observed in the experimental data indicate that the proposed simulation system is subject to several limitations. A possible reason for this discrepancy is that the stimulation profiles used as the input for the muscles when simulating human walking using the proposed system were substantially simplified compared with the actual condition. In particular, the muscle activation dynamics modeled in the proposed simulation system were represented by three values: onset time (T_{on}), offset time (T_{off}), and amplitude of stimulation (STIM). However, this cannot effectively provide flexible control of muscle activation when simulating natural human walking. Therefore, further improvement is required to more accurately quantify the kinematic and kinetic data of human walking using proposed simulation system, particularly in terms of the muscle activation dynamics.

The oversimplification of the muscle stimulation dynamics implemented in the proposed simulation system approximately tripled the whole-body energy expenditure per distance traveled compared with the observed energy expenditure. This excessive simulated energy expenditure was in fact similar to that of poststroke patients (Reisman et al., 2009). Thus, the condition reflected by a small number of simulation nodes could be recognized as similar to the impairment of flexible control over the neural system, which results in unnecessary muscle activation in both the proposed simulation system and patients with impaired motor control systems. Therefore, these findings suggest that the

pattern of muscle stimulation significantly affects the walking efficiency and coordination of the human body during walking, implying that the influence of the neural control on human walking could be effectively assessed using the proposed neuromusculoskeletal simulation system.

In conclusion, cyclic walking motion on level ground was simulated using the theory of forward dynamics in this study, providing comparable quality to previously established methods. However, there remains a discrepancy between the predicted and observed values of the kinematic, kinetics, and energy expenditure. Therefore, this study demonstrated that cyclic walking motion on level ground was simulated with comparable quality to previously established methods, but further improvement is required to represent the actual kinematic, kinetic, and energetic data.

Chapter 7: *Summary and general discussion*

The goal of this dissertation was to establish a framework for analyzing human body movement considering the musculoskeletal contribution of the trunk. The five defined aims in this dissertation are as follows:

(1) To quantify the geometric deformation of the trunk during human locomotion.

(2) To quantify the effects of trunk deformability on the resultant kinematics of trunk models having varying number of rigid-body segments.

(3) To determine the optimal number of linked rigid-bodies representing trunk movements during walking.

(4) To establish a neuromusculoskeletal computer simulation system considering the multi-segmental structure of the trunk.

(5) To simulate human walking motion and assess the validation of the neuromusculoskeletal computer simulation system constructed in this study.

Thus, five studies described in chapters 2, 3, 4, 5, and 6 addressed the questions 1, 2, 3, 4, and 5, respectively. The main findings and limitations of these studies are discussed below.

7.1. *Summary and main findings of individual studies*

7.1.1. *Quantitative assessment of trunk deformation during running*

The study in Chapter 2 quantitatively assessed trunk deformation during running. Ten male participants ran at four different speeds: 8, 10, 12, and 14 km/h. Forty reflective markers were placed on the backs of these individuals to define 56 small triangular areas, and three-dimensional kinematic

data were recorded with a motion capture system. The CV of the horizontal and vertical lengths between two adjacent markers and the SD of the normal vectors of the triangular areas were calculated as measures for translational and angular deformation, respectively. Relatively, up to about 14% of CV and 78% of SD appeared as the measure of translational and angular deformation, respectively. These results implied that the trunk underwent a significant amount of position-specific deformation. These findings were useful in the construction of an optimal trunk segment model representing complex and flexible trunk movements during human locomotion.

7.1.2. *Quantitative evaluation of linked rigid-body representation of the trunk*

The study in Chapter 3 quantitatively assessed the effects of deformability on the resultant trunk kinematics for models having numerous rigid-body segments. The trunk was modeled as a single rigid-body segment or as two-, three-, and six-linked rigid-body segments to represent the both static and dynamic conditions; a non-linear optimization analysis was performed to minimize the differences between the actual and modeled position data. Furthermore, positional errors were evaluated to assess the difference in three-dimensional positions between the actual and modeled data for each model. Besides, the total angular displacement was evaluated to examine the accuracy of each model in describing the actual multi-segmental trunk movements. The positional error between the modeled and actual kinematic data of the trunk was up to 12mm and 11 mm when the trunk was simplified as a single segment, but the error decreased to 5 mm and 7 mm when the trunk was modeled with six segments during the static and dynamic trials. On the contrary, the total angular displacement increased as the number of rigid-body segments increased. These results implied that a small number of linked rigid-body representations underestimated the actual multi-segmental trunk movements during human movement.

7.1.3. *Determination of the optimal number of linked rigid-bodies of the trunk*

The study in Chapter 4 determined the optimal number of rigid-body segments using AIC to appropriately represent walking conditions. The AIC is a measure for optimal model selection that balances goodness-of-fit and generalizability. Moreover, a nonlinear optimization algorithm was used to fit the empirically obtained kinematic data with one-, two-, three-, and six-linked rigid-body models representing the trunk during walking. The relative quality of these models was assessed using their AICc values. For walking trials, the AICc values of the two- and three-linked rigid-body models were significantly smaller than those of one- or six-segment models. This result suggested that both the two- and three-linked rigid-body models would be better than the one- and six-linked rigid-body representations for analyzing trunk movements during walking in terms of the balance between the goodness-of-fit and generalizability of the model.

7.1.4. *Musculoskeletal modeling of the human body considering the multi-segmental structure of the trunk*

The musculoskeletal model implemented 90 Hill-type muscle–tendon models (25 in each lower extremity and 20 in each right and left sides of the trunk) was constructed in the study presented in Chapter 4. This musculoskeletal computer simulation system was implemented using MotionGenesis (OnLine Dynamics, Stanford, CA, USA), a commercial package linked with C-language code that could describe the muscle activation and contraction dynamics, musculoskeletal interaction, and foot/ground interaction. The skeleton of this musculoskeletal model was modeled with 18 rigid-body segments, including 2 linked rigid bodies of the trunk proposed in Chapter 3 (i.e., abdomen and thorax segments), the head, pelvis, and four extremities segments. A muscle–tendon complex was represented by a Hill-type muscle model, comprising a contractile element (CE), parallel elastic element (PEE), and a series elastic element (SEE) serially connected with a pennation angle. In addition, the ground

reaction force was modeled by a nonlinear viscoelastic element.

7.1.5. *Walking simulation and assessment of the musculoskeletal computer simulation system*

Normal walking motion on level ground was simulated using the theory of forward dynamics. The kinematic and kinetic data of walking motion simulated using the proposed method were compared with those derived using an inverse dynamics approach to assess the validity of the musculoskeletal model constructed in this research. The results of this study demonstrated that similar trends were found in the profile of the kinematics and kinetics of the lumbar and thoracic joint between the simulated and experimented data, although there also existed discrepancies. Therefore, this study demonstrated that cyclic walking motion on level ground was simulated with comparable quality to previously established methods, but further improvement is required to represent the actual kinematic, kinetic, and energetic data.

7.2. *Limitations of individual studies*

7.2.1. *Quantitative assessment of trunk deformation during human locomotion*

A larger angular deformation appeared in the frontal plane, because the vector component used to calculate the angular deformation in the frontal plane appeared to be more sensitive to small directional changes in comparison to other components. The angular deformation in the frontal plane was calculated based on the component of the normal vector projected on the frontal plane, which was very small relative to the components on the other two planes (less than 1% of the magnitude of the normal vector), because the back surface of the trunk mainly lies on the frontal plane. Thus, a small directional change of the normal vector could appear as a large angular movement on the frontal plane with this methodology. Therefore, the validity and repeatability of this methodology for the analysis of trunk deformation during dynamic movements other than running needs to be evaluated through

further studies.

7.2.2. *Quantitative Evaluation of Linked Rigid-Body representation of the trunk*

The total angular displacement calculated in this study could be affected by the choice of STM rotation sequence. As our postural conditions involve three different planes of motion, different choices of rotational sequence may affect the resultant angles. However, the statistical significance was not affected in changing the rotation sequence to X–Y–Z from Y–X–Z, where a significant main effect of the model was found for all the conditions (lateral bending: $p < 0.001$; axial rotation: $p = 0.004$; anteflexion: $p < 0.001$; retroflexion: $p < 0.001$; walking: $p < 0.001$). Thus, the choice of rotation sequence did not appear to affect the findings of the current study.

7.2.3. *Determination of the optimal number of linked rigid-bodies of the trunk*

The demographics of the participants were limited to non-disabled male college young adults only, and the sample size was relatively small. The reason for recruiting only male participants was the difficulty in standardizing marker placements on the front of the trunk for female participants. Thus, the current findings may not be applicable to other populations, because the kinematics of the trunk during walking vary between different sexes and ages depending upon several kinds of pathological conditions (Crosbie et al., 1997a; Gimmon et al., 2015; Seay et al., 2011). Therefore, further studies are needed to determine the applicability of the current results on other populations. Moreover, the walking speeds were not controlled in this study, and the complexity of the multi-segmental movement of the trunk increased with the gait velocity (Feipel et al., 2001; Kudo et al., 2017). Therefore, the results demonstrated in this study, where no significant differences were found in the AICc values between the two- and three-linked rigid-body models in walking trials, might have been affected by the variability in trunk movements owing to differences in the gait speed among the

participants. Furthermore, note that the trunk was evenly divided into multiple segments in this study, but the divisions were not based on the anatomical structure (e.g., thoracic and lumbar regions). As the AIC value was the determining variable used to assess the relative quality of the models of the experiment, other models with different segmentations might yield different results, even with the same number of segments. Additionally, a model with a different number of rigid bodies might also yield different results. Therefore, further studies should investigate the effect of different segmentation approaches for the trunk on the resulting AIC values obtained to determine the optimal segmentation for kinematic analysis.

7.2.4. *Walking simulation and assessment of the musculoskeletal computer simulation system*

As discussed in Chapter 6, the oversimplification of the muscle stimulation dynamics implemented in the proposed simulation system would affect the results of simulated kinematic and kinetic data during walking motion. The muscle activation dynamics modeled in the proposed simulation system were represented by three values: onset time (T_{on}), offset time (T_{off}), and amplitude of stimulation (STIM), and this cannot effectively provide flexible control of muscle activation when simulating natural human walking. Actually, the discrepancies on the measures of kinematics, kinetics and energetics during walking motion was found between simulated and experimented data in this study. Therefore, further improvement is required to more accurately quantify the kinematic and kinetic data of human walking using proposed simulation system, particularly in terms of the muscle activation dynamics.

The upper extremities of the musculoskeletal model used in this study were constrained by the thorax segment, which might have also affected the results of this study. In fact, the movements of the upper extremities significantly affect the angular momentum of the center of the total mass of the human body about the vertical axis (Hamner and Delp, 2013), as well as the energy expenditure during

locomotion (Umberger, 2008). Thus, a more detailed model should be constructed, considering the motion of the upper extremities, to address the aforementioned limitation. Furthermore, the muscle activation profile of the trunk was not validated using the experimental data (i.e., electromyography), which is another limitation of this study. Therefore, further studies are needed to evaluate the validity of trunk muscle activation.

7.3. *General discussion*

7.3.1. *Contributions of this dissertation*

This study successfully established a framework to analyze dynamic movements of the human body considering the musculoskeletal contribution of the trunk, which has not been clarified in the past. The main contributions of this study are as follows:

- The optimal number of linked rigid bodies of the trunk for representing its multi-segmental motion during walking was determined through a quantitative measurement.

  The most significant contribution in this study is that the optimal number of linked rigid-body segments to represent the multi-segmental movement of the trunk during human locomotion was determined through a quantitative model assessment (Chapter 4). Although the number of rigid-body segments to model the trunk has been recognized as a crucial factor for describing the multi-segmental trunk motion during human locomotion in the past, a concrete methodology or quantitative method for model evaluation, which can determine the "best approximating" model for analysis of trunk movement, had not been developed. In this regard, this study introduces a novel method to assess the quality of a model considering the trade-off between goodness-of-fit and generalizability.

  This study quantitatively assessed the effects of trunk deformability on the resultant

trunk kinematics when the trunk is modeled with different numbers of rigid-body segments, based on the position error between the model prediction and the actual data (Chapter 3). The results are useful for determining the appropriate number of linked rigid-body segments of the trunk depending on the required accuracy for analysis of human movement. Since the model should originally be constructed depending on the required accuracy for a specific study, first, it is important to understand how accurately linked rigid-body representations with different numbers of segments can describe actual trunk movements. However, few previous studies had addressed this requirement. Therefore, the findings of this study can be helpful for determining the optimal number of rigid bodies to represent the multi-segmental motion of the trunk during locomotion, depending on the required accuracy for a study.

- A neuromusculoskeletal computer simulation system independent of the specifications of commercial packages was constructed.

  In this study, human walking movement was generated considering the multi-segmental movement and neuromuscular contribution of the trunk (Chapter 6), which had not been achieved in the past. The movement was generated using a neuromusculoskeletal computer simulation system independent of the specification of commercial packages. This system is effective for freely adjusting simulation parameters depending on the study aims. Therefore, the proposed simulation system can help researchers and clinicians acquire a more detailed understanding of the effect of the musculoskeletal contribution to the control of human movements.

  The proposed simulation system (Chapter 5), which was coded using the C programming language, also reduces the time required for simulation processes involving multiple computers in parallel. In fact, in this study, the process for optimizing muscle

activation profiles to generate walking motion was executed with a total of four computers in parallel. Moreover, this system is also adaptive to execute neuromuscular computer simulation using parallel supercomputers, this could substantially reduce the central processing unit time required for the calculation processes. Therefore, the proposed simulation system is also useful in terms of computational efficiency.

The aforementioned contributions can enable biomechanical analysis of human movements based on the musculoskeletal systems of the lower extremities and the trunk, which are traditionally adapted for the whole body.

7.3.2. *Advantages of proposed model from the viewpoint of kinematics, kinetics, and neuromuscular physiology*

Throughout this dissertation, the optimal musculoskeletal model considering the multi-segmental motion of the trunk has been discussed from the viewpoint of the geometrical deformation of the trunk. Accordingly, it was determined that models of the trunk using two or three linked rigid-bodies were optimal in terms of their goodness-of-fit and generalizability when analyzing multi-segmental motion during human locomotion. The human walking motion was thus simulated using a musculoskeletal model based on a two-link rigid-body model. These achievements extend the conventional knowledge—which to date has been limited to the neuromusculoskeletal control of the lower and upper limbs during human walking—to the control of the entire body, including the trunk.

Although the knowledge obtained from this research describing the effects of the number of rigid bodies on the geometrical deformability of the model can be useful for trunk model selection, understanding the effects of the number of rigid bodies on the kinematics, kinetics, and neuromuscular physiology of the trunk would also be important when selecting an optimal model to assess the multi-

segmental movements of the trunk. Therefore, following subsections discuss the advantages of using the musculoskeletal model proposed in this study from the viewpoints of kinematics, kinetics, and neuromuscular physiology.

7.3.2.1. *Kinematics*

The results of the studies detailed in this dissertation suggested that models of the trunk consisting of two or three linked rigid-bodies optimally represented its multi-segmental motion. Additionally, the two-link rigid-body model of the trunk was adopted in the musculoskeletal model to simulate walking motion using the theory of forward dynamics. However, the merit of using this model when assessing the kinematics of the trunk has not yet been determined. Therefore, the kinematic measures derived from the single rigid-body model (M1; often used in previous studies) and two linked rigid-bodies model (M2; proposed as the optimal model in this dissertation) were compared to discuss the effect of the number of linked rigid-bodies on the kinematic data describing the trunk.

The angular displacement about the lumbar joint during walking derived from M1 and M2 were compared using the data set obtained from the study discussed in Chapter 6. The results indicated that the range of motion (ROM) of the lumbar joint derived from M1 was larger than that derived from M2 for all planes of motion (Figure **7**.**1**). Additionally, the difference in the ROM of the lumbar joint in the transverse plane was remarkably larger than those in any other planes. These results indicate that the single rigid-body model of the trunk overestimated the lumbar joint ROM when assessing trunk motion during locomotion. Thus, the number of rigid-body segments used to model the trunk during human locomotion would primarily affect the representation of axial rotation about the lumbar joint. These findings accordingly suggest that the proposed model, which divides the trunk into two linked rigid-body segments, would help to prevent the overestimation of lumbar joint angle. This advantage notably affects the representation of axial rotation during human locomotion.

A significant amount of thoracic joint angular displacement was found during walking when using M2, and this was remarkable in both the sagittal and transverse planes (Figure 7.1). This implies that the motions about the thoracic and lumbar joints are among the major features representing trunk motion during walking. This implication agrees with the findings of a previous study, indicating that significant twisting movements between the upper and lower parts of the trunk were found in the sagittal and transverse planes during walking (Frigo et al., 2003). Therefore, a linked rigid-body model with a large number of segments would have an advantage in describing the multi-segmental motion of the trunk in the sagittal and transverse planes.

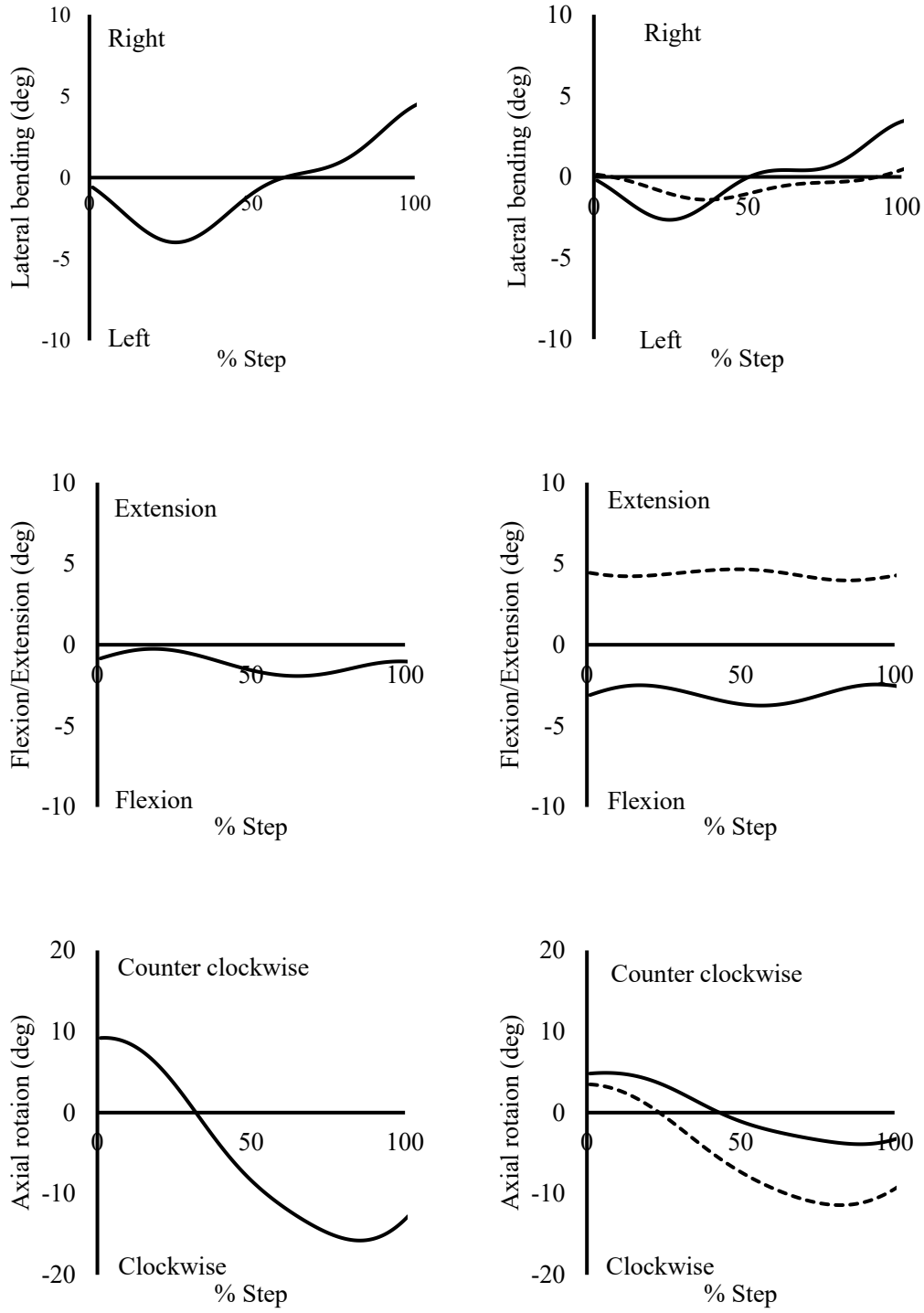

Figure 7.1 Angular displacement about the lumbar (solid line) and thoracic (dashed line) joints during one step of walking derived from M1 (left side column of this figure) and M2 (right side column of this figure).

7.3.2.2. *Kinetics*

Although little has been reported on the kinetic behavior of the trunk during human locomotion, the research detailed in this dissertation was able to describe the kinetics by establishing a linked rigid-body model considering the multi-segmental structure of the trunk. For instance, Chapter 6 reported the torques about the lumbar and thoracic joints during walking in healthy individuals using the inverse dynamics approach. These torques were small during walking (blue lines in Figure **6.5** Figure **6.6**) relative to those in the joints in the lower extremity, which are the primary mobilizers used to generate the walking motion (Winter and Robertson, 1978). This implies that the muscles in the trunk do not actively generate force to develop torque about these joints during healthy walking, compared to those in the lower extremity. These findings provide important evidence describing a feature of trunk kinetics during walking in healthy individuals.

The evidence describing the kinetic behavior of the trunk during walking reported in this dissertation could also serve as effective basal data for evaluating the kinetics of abnormal walking in patients with various neuromuscular diseases, such as those manifested by the Duchenne or Trendelenburg gait (Schmid et al., 2013). Differences between the kinematics of the trunk during walking for healthy individuals and patients with neuromuscular diseases have previously been reported (Böhm et al., 2013; Krautwurst et al., 2013; Salami et al., 2017). Understanding the concrete reason for these differences would be significant for designing effective interventions to improve associated abnormalities in human walking. Additionally, given that an increased range of multi-segmental motion of the trunk is viewed as a compensatory mechanism for abnormal walking in patients with neuromuscular diseases (Schmid et al., 2013), a model is required to optimally describe the multi-segmental motion of the trunk during walking when assessing such abnormality. Therefore, the linked rigid-body model proposed in this dissertation by considering the multi-segmental motion of the trunk could also be useful in assessing and detecting the cause of abnormal walking.

7.3.2.3. *Neuromuscular physiology*

One of the primary novelties of the research detailed in this dissertation is the establishment of a system to integrate the neuromuscular data of the trunk (e.g., muscle activation, muscle force, etc.) with the rigid-body motion of the trunk during human locomotion. Though several previous studies have separately assessed the kinematic/kinetic data (Callaghan et al., 1999; Cappozzo, 1981, 1983; Crosbie et al., 1997b; Frigo et al., 2003) and the electromyographical pattern of muscle activities (Anders et al., 2007; Saunders et al., 2004; Thorstensson et al., 1982; Waters et al., 1973; Waters and Morris, 1972), they could not effectively provide evidence to clarify a concrete causal relationship between the neuromuscular system of the trunk and the stability and mobility of the body during human locomotion. Additionally, the inability to measure the muscle forces exhibited during human movements was a major limitation in previous experimental studies. In this regard, the neuromusculoskeletal model including the muscles of the lower extremities and trunk developed in this study can help to investigate the causal relationship between the neuromuscular system and the skeletal motion of the trunk during human locomotion.

The profiles of individual muscle activations and forces in the trunk during walking (Appendix D and E) demonstrate the significant activation of particular trunk muscles, even though only small amounts of torque were found about the lumbar and thoracic joint during walking. For instance, the activation profiles indicated that the m. iliocostalis lumborum par lumborum (ILIOCLUMB_LUMB), m. longissimus thoracis pars lumborum (LONGISTHOR_LUMB), and anterior part of m. external oblique (EXTOB1) were relatively active during walking compared to the other muscles (Appendix D). This suggests that individual muscles cooperatively activate to maintain the angular momentum of the trunk during normal walking, constituting a concrete example of the integration of neuromuscular data with the rigid-body motion of the trunk during human locomotion. Therefore, the neuromusculoskeletal simulation system established in this research can potentially provide new

insight into the neuromusculoskeletal contribution to generate human locomotion by extending the scope of analysis from the lower extremity to the entire body, including the trunk.

7.3.3. *Possibilities of the proposed neuromusculoskeletal model*

As discussed in Chapter 1, the proposed model is anticipated to be useful in the clinical field. In particular, an increased trunk motion, known as the Duchenne or Trendelenburg gait, is widely viewed as a compensatory mechanism for hip abductor muscle weakness during human locomotion (Böhm et al., 2013; Schmid et al., 2013). These excessive trunk movements have also been shown to result in an increased cost of locomotion (Salami et al., 2017) and may contribute to the development of back pain. Although the trunk accomplishes such functions to compensate for the impairments of the neuromusculoskeletal system of the lower extremities, the neuromusculoskeletal mechanism employed by the trunk to do so is unknown due to the lack of knowledge required to model and optimally assess the musculoskeletal contribution of the trunk. Therefore, the proposed model, which enables the assessment of the neuromusculoskeletal activity of the trunk, allows the causal relationship between the neuromusculoskeletal activity and compensatory mechanisms of the trunk during human locomotion to be examined using both inverse and forward dynamics theories.

7.3.4. *Future work*

Considering the recent strained situation in the medical field, the difficulty for medical professionals to directly diagnose the risk of health impairment caused by falling is expected to continue for providing an effective intervention. From this perspective, it would be desirable to establish a system that enables researchers or healthcare professionals to remotely measure and assess their patients' activities on a daily basis.

In this respect, the neuromusculoskeletal computer simulation system poses a great potential to

provide noninvasive means for studying human movements and predicting the motion of our musculoskeletal system during variation of muscle properties. This is an advantage of remotely assessing human dynamic movements and the effects of the intervention on its impairments. Consequently, the findings of this dissertation would contribute toward expanding the scope of analyses from the motion of four extremities to the whole-body motion, considering the effects of force developed by the trunk muscles. Additionally, as the technology and methodology for easy capturing and assessment of human motion have been exponentially advancing in the recent years with the use of marker-less devices, wearable sensors, and artificial neural network systems (Nagano et al. (2017), further advancements of "remote exercise intervention system" could be expected from the combination of these technologies and the musculoskeletal computer system.

Considering the outstanding progress of technologies for human motion analysis that enable researchers to easily capture and provide more detailed information describing human motions, biomechanists should consider how this information can be effectively generalized. A model with a larger goodness-of-fit is not always acceptable, as a tradeoff exists between the fitness and generalizability of a complex model. Although the goodness-of-fit improves with increased model complexity, undue complexity and overfitting of the data should also be avoided to ensure a more generalizable model. The method proposed in this dissertation for modeling trunk movements—considering the optimization of general analytical issues—has the potential to serve as an effective approach to comprehensively understand the contribution of the musculoskeletal system to human dynamic movements, as opposed to the conventional method for modeling human dynamic movements as accurately and intricately as possible.

7.4. *Conclusion*

This dissertation has demonstrated the value of a musculoskeletal computer simulation system for analyzing the neuromusculoskeletal contribution toward the multi-segmental motion of the trunk for controlling human locomotion. In particular, both two- and three-linked rigid-body models would be optimal for analyzing trunk movements during walking, in terms of both goodness-of-fit and generalizability. These achievements extend the conventional knowledge—which to date has been limited to the neuromusculoskeletal control of the lower and upper limbs during human walking—to the control of the entire body, including the trunk. Finally, the musculoskeletal computer simulation system presented in this study can be expected to further contribute toward a better understanding of the biomechanics of our neuromusculoskeletal system for designing an effective intervention to improve the physical activities and a healthy life-expectancy of humans.

References

Akaike, H., 1973. Information theory and an extension of the maximum likelihood principle. Proceedings of the 2nd International Symposium on Information Theory, 267-281.

Akaike, H., 1974. A new look at the statistical model identification. IEEE transactions on automatic control 19, 716-723.

Allinger, T.L., Herzog, W., Epstein, M., 1996. Force-length properties in stable skeletal muscle fibers--theoretical considerations. J Biomech 29, 1235-1240.

Anders, C., Wagner, H., Puta, C., Grassme, R., Petrovitch, A., Scholle, H.C., 2007. Trunk muscle activation patterns during walking at different speeds. J Electromyogr Kinesiol 17, 245-252.

Anderson, F.C., 1999. A dynamic optimization solution for a complete cycle of normal gait. Dissertation, The University of Texas at Austin, USA.

Anderson, F.C., Pandy, M.G., 1999. A Dynamic Optimization Solution for Vertical Jumping in Three Dimensions. Comput Methods Biomech Biomed Engin 2, 201-231.

Anderson, F.C., Pandy, M.G., 2001a. Dynamic optimization of human walking. J Biomech Eng 123, 381-390.

Anderson, F.C., Pandy, M.G., 2001b. Static and dynamic optimization solutions for gait are practically equivalent. J Biomech 34, 153-161.

Anderson, F.C., Pandy, M.G., 2003. Individual muscle contributions to support in normal walking. Gait & Posture 17, 159-169.

Arvin, M., van Dieen, J.H., Bruijn, S.M., 2016. Effects of constrained trunk movement on frontal plane gait kinematics. J Biomech 49, 3085-3089.

Bayoglu, R., Galibarov, P.E., Verdonschot, N., Koopman, B., Homminga, J., 2019. Twente Spine Model: A thorough investigation of the spinal loads in a complete and coherent musculoskeletal model of the human spine. Med Eng Phys 68, 35-45.

Bayoglu, R., Geeraedts, L., Groenen, K.H.J., Verdonschot, N., Koopman, B., Homminga, J., 2017a. Twente spine model: A complete and coherent dataset for musculo-skeletal modeling of the lumbar region of the human spine. J Biomech 53, 111-119.

Bayoglu, R., Geeraedts, L., Groenen, K.H.J., Verdonschot, N., Koopman, B., Homminga, J., 2017b. Twente spine model: A complete and coherent dataset for musculo-skeletal modeling of the thoracic and cervical regions of the human spine. J Biomech 58, 52-63.

Bazrgari, B., Nussbaum, M.A., Madigan, M.L., Shirazi-Adl, A., 2011. Soft tissue wobbling affects trunk dynamic response in sudden perturbations. J Biomech 44, 547-551.

Bogduk, N., Macintosh, J.E., Pearcy, M.J., 1992. A universal model of the lumbar back muscles in the upright position. Spine (Phila Pa 1976) 17, 897-913.

Böhm, H., Dussa, C.U., Multerer, C., Döderlein, L., 2013. Pathological trunk motion during walking in children with Amyoplasia: Is it caused by muscular weakness or joint contractures? Research in Developmental Disabilities 34, 4286-4292.

Breloff, P., S., Chou, L., 2015. A multi-segmented approach to the quantification of trunk movement during gait. Journal of Musculoskeletal Research 18, 1-11.

Breloff, S.P., Chou, L.S., 2017. Multi-Segmented Trunk Motion of Healthy Non-Elderly Adults in Different Decades of Life. Biomed Eng (Singapore) 29.

Bremermann, H., 1970. A method of unconstrained global optimization. Mathematical Biosciences 9, 1-15.

Callaghan, J.P., Patla, A.E., McGill, S.M., 1999. Low back three-dimensional joint forces, kinematics, and kinetics during walking. Clin Biomech (Bristol, Avon) 14, 203-216.

Campos, M.H., de Paula, M.C., Depra, P.P., Brenzikofer, R., 2015. The geometric curvature of the spine of runners during maximal incremental effort test. J Biomech 48, 969-975.

Cappozzo, A., 1981. Analysis of the Linear Displacement of the Head and Trunk during Walking at

Different Speeds. Journal of Biomechanics 14, 411-425.

Cappozzo, A., 1983. The forces and couples in the human trunk during level walking. J Biomech 16, 265-277.

Christophy, M., Faruk Senan, N.A., Lotz, J.C., O'Reilly, O.M., 2012. A musculoskeletal model for the lumbar spine. Biomech Model Mechanobiol 11, 19-34.

Cole, G.K., vandenBogert, A.J., Herzog, W., Gerritsen, K.G.M., 1996. Modelling of force production in skeletal muscle undergoing stretch. Journal of Biomechanics 29, 1091-1104.

Crosbie, J., Vachalathiti, R., Smith, R., 1997a. Age, gender and speed effects on spinal kinematics during walking. Gait & Posture 5, 13-20.

Crosbie, J., Vachalathiti, R., Smith, R., 1997b. Patterns of spinal motion during walking. Gait & Posture 5, 6-12.

Das Gupta, S., Bobbert, M.F., Kistemaker, D.A., 2019. The Metabolic Cost of Walking in healthy young and older adults - A Systematic Review and Meta Analysis. Sci Rep 9, 9956.

de Leva, P., 1996. Adjustments to Zatsiorsky-Seluyanov's segment inertia parameters. J Biomech 29, 1223-1230.

de Zee, M., Hansen, L., Wong, C., Rasmussen, J., Simonsen, E.B., 2007. A generic detailed rigid-body lumbar spine model. J Biomech 40, 1219-1227.

Delp, S.L., 1990. Surgery simulation : a computer graphics system to analyze and design musculoskeletal reconstructions of the lower limb. Dissertation, Stanford University, USA.

Delp, S.L., Anderson, F.C., Arnold, A.S., Loan, P., Habib, A., John, C.T., Guendelman, E., Thelen, D.G., 2007. OpenSim: open-source software to create and analyze dynamic simulations of movement. IEEE Trans Biomed Eng 54, 1940-1950.

Delp, S.L., Loan, J.P., 1995. A graphics-based software system to develop and analyze models of musculoskeletal structures. Comput Biol Med 25, 21-34.

Delp, S.L., Suryanarayanan, S., Murray, W.M., Uhlir, J., Triolo, R.J., 2001. Architecture of the rectus abdominis, quadratus lumborum, and erector spinae. J Biomech 34, 371-375.

Dumas, R., Cheze, L., Verriest, J.P., 2007a. Adjustments to McConville et al. and Young et al. body segment inertial parameters. J Biomech 40, 543-553.

Dumas, R., Chèze, L., Verriest, J.P., 2007b. Corrigendum to "Adjustments to McConville et al. and Young et al. body segment inertial parameters" [J. Biomech. 40 (2007) 543–553]. Journal of Biomechanics 40, 1651-1652.

Dumas, R., Robert, T., Cheze, L., Verriest, J.-P., 2015. Thorax and abdomen body segment inertial parameters adjusted from McConville et al. and Young et al. International Biomechanics 2, 113-118.

Feipel, V., De Mesmaeker, T., Klein, P., Rooze, M., 2001. Three-dimensional kinematics of the lumbar spine during treadmill walking at different speeds. Eur Spine J 10, 16-22.

Friederich, J.A., Brand, R.A., 1990. Muscle fiber architecture in the human lower limb. J Biomech 23, 91-95.

Frigo, C., Carabalona, R., Dalla Mura, M., Negrini, S., 2003. The upper body segmental movements during walking by young females. Clinical Biomechanics 18, 419-425.

Gerritsen, K.G., van den Bogert, A.J., Hulliger, M., Zernicke, R.F., 1998. Intrinsic muscle properties facilitate locomotor control - a computer simulation study. Motor Control 2, 206-220.

Gerritsen, K.G., van den Bogert, A.J., Nigg, B.M., 1995. Direct dynamics simulation of the impact phase in heel-toe running. J Biomech 28, 661-668.

Gimmon, Y., Riemer, R., Rashed, H., Shapiro, A., Debi, R., Kurz, I., Melzer, I., 2015. Age-related differences in pelvic and trunk motion and gait adaptability at different walking speeds. J Electromyogr Kinesiol 25, 791-799.

Hamner, S.R., Delp, S.L., 2013. Muscle contributions to fore-aft and vertical body mass center

accelerations over a range of running speeds. J Biomech 46, 780-787.

He, J.P., Levine, W.S., Loeb, G.E., 1991. Feedback Gains for Correcting Small Perturbations to Standing Posture. Ieee Transactions on Automatic Control 36, 322-332.

Hicks, J.L., Uchida, T.K., Seth, A., Rajagopal, A., Delp, S.L., 2015. Is my model good enough? Best practices for verification and validation of musculoskeletal models and simulations of movement. J Biomech Eng 137, 020905.

Hill, A.V., 1938. The heat of shortening and the dynamic constants of muscle. Proc R Soc Ser B-Bio 126, 136-195.

Hurt, C.P., Rosenblatt, N., Crenshaw, J.R., Grabiner, M.D., 2010. Variation in trunk kinematics influences variation in step width during treadmill walking by older and younger adults. Gait Posture 31, 461-464.

Johnson, M.A., Polgar, J., Weightman, D., Appleton, D., 1973. Data on the distribution of fibre types in thirty-six human muscles. An autopsy study. J Neurol Sci 18, 111-129.

Krautwurst, B.K., Wolf, S.I., Heitzmann, D.W.W., Gantz, S., Braatz, F., Dreher, T., 2013. The influence of hip abductor weakness on frontal plane motion of the trunk and pelvis in patients with cerebral palsy. Research in Developmental Disabilities 34, 1198-1203.

Kudo, S., Fujimoto, M., Isaka, T., Nagano, A., 2017. Quantitative assessment of trunk deformation during running. J Biomech 59, 116-121.

Kudo, S., Fujimoto, M., Sato, T., Nagano, A., 2018. Quantitative evaluation of linked rigid-body representations of the trunk. Gait Posture 63, 119-123.

Leardini, A., Biagi, F., Belvedere, C., Benedetti, M.G., 2009. Quantitative comparison of current models for trunk motion in human movement analysis. Clin Biomech (Bristol, Avon) 24, 542-550.

Leardini, A., Biagi, F., Merlo, A., Belvedere, C., Benedetti, M.G., 2011. Multi-segment trunk

kinematics during locomotion and elementary exercises. Clin Biomech (Bristol, Avon) 26, 562-571.

Lin, Y.C., Gfoehler, M., Pandy, M.G., 2014. Quantitative evaluation of the major determinants of human gait. J Biomech 47, 1324-1331.

Macintosh, J.E., Bogduk, N., 1986. The biomechanics of the lumbar multifidus. Clin Biomech (Bristol, Avon) 1, 205-213.

MacKinnon, C.D., Winter, D.A., 1993. Control of whole body balance in the frontal plane during human walking. J Biomech 26, 633-644.

Mahallati, S., Rouhani, H., Preuss, R., Masani, K., Popovic, M.R., 2016. Multisegment Kinematics of the Spinal Column: Soft Tissue Artifacts Assessment. J Biomech Eng 138.

Nagano, A., 2001. A computer simulation study on the potential locomotor patterns of Australopithecus afarensis (A.L. 288-1). Dissertation, Arizona State University, USA.

Nagano, A., 2003. Modeling of the Hill-type musculotendon complex and its application to computer simulation. Japanese Journal of Biomechanics in Sports and Exercise 7, 225-237.

Nagano, A., Fujimoto, M., Kudo, S., Akaguma, R., 2017. An image-processing based technique to obtain instantaneous horizontal walking and running speed. Gait Posture 51, 7-9.

Nagano, A., Gerritsen, K.G.M., 2001. Effects of neuromuscular strength training on vertical jumping performance - A computer simulation study. J Appl Biomech 17, 113-128.

Nagano, A., Komura, T., Yoshioka, S., Fukashiro, S., 2005a. Contribution of non-extensor muscles of the leg to maximal-effort countermovement jumping. Biomed Eng Online 4, 52.

Nagano, A., Umberger, B.R., Marzke, M.W., Gerritsen, K.G., 2005b. Neuromusculoskeletal computer modeling and simulation of upright, straight-legged, bipedal locomotion of Australopithecus afarensis (A.L. 288-1). Am J Phys Anthropol 126, 2-13.

Nagano, A., Yoshioka, S., Komura, T., Himeno, R., Fukashiro, S., 2005c. A three-dimensional linked

segment model of the human whole body. International Journal of Sports and Health Science.

Needham, R., Naemi, R., Healy, A., Chockalingam, N., 2016. Multi-segment kinematic model to assess three-dimensional movement of the spine and back during gait. Prosthet Orthot Int 40, 624-635.

O'Connor, C.M., Thorpe, S.K., O'Malley, M.J., Vaughan, C.L., 2007. Automatic detection of gait events using kinematic data. Gait Posture 25, 469-474.

Pandy, M.G., Lin, Y.C., Kim, H.J., 2010. Muscle coordination of mediolateral balance in normal walking. J Biomech 43, 2055-2064.

Preuss, R.A., Popovic, M.R., 2010. Three-dimensional spine kinematics during multidirectional, target-directed trunk movement in sitting. J Electromyogr Kinesiol 20, 823-832.

Raabe, M.E., Chaudhari, A.M.W., 2016. An investigation of jogging biomechanics using the full-body lumbar spine model: Model development and validation. J Biomech 49, 1238-1243.

Rajagopal, A., Dembia, C.L., DeMers, M.S., Delp, D.D., Hicks, J.L., Delp, S.L., 2016. Full-Body Musculoskeletal Model for Muscle-Driven Simulation of Human Gait. IEEE Trans Biomed Eng 63, 2068-2079.

Reisman, D.S., Rudolph, K.S., Farquhar, W.B., 2009. Influence of speed on walking economy poststroke. Neurorehabil Neural Repair 23, 529-534.

Salami, F., Niklasch, M., Krautwurst, B.K., Dreher, T., Wolf, S.I., 2017. What is the price for the Duchenne gait pattern in patients with cerebral palsy? Gait Posture 58, 453-456.

Saunders, S.W., Rath, D., Hodges, P.W., 2004. Postural and respiratory activation of the trunk muscles changes with mode and speed of locomotion. Gait Posture 20, 280-290.

Schinkel-Ivy, A., Drake, J.D., 2015. Which motion segments are required to sufficiently characterize the kinematic behavior of the trunk? J Electromyogr Kinesiol 25, 239-246.

Schmid, S., Schweizer, K., Romkes, J., Lorenzetti, S., Brunner, R., 2013. Secondary gait deviations in

patients with and without neurological involvement: a systematic review. Gait Posture 37, 480-493.

Seay, J.F., Van Emmerik, R.E., Hamill, J., 2011. Low back pain status affects pelvis-trunk coordination and variability during walking and running. Clin Biomech (Bristol, Avon) 26, 572-578.

Stokes, V.P., Andersson, C., Forssberg, H., 1989. Rotational and translational movement features of the pelvis and thorax during adult human locomotion. J Biomech 22, 43-50.

Sugiura, N., 2007. Further analysts of the data by akaike' s information criterion and the finite corrections. Communications in Statistics - Theory and Methods 7, 13-26.

Swinnen, E., Baeyens, J.P., Pintens, S., Buyl, R., Goossens, M., Meeusen, R., Kerckhofs, E., 2013. Walking more slowly than with normal velocity: The influence on trunk and pelvis kinematics in young and older healthy persons. Clin Biomech (Bristol, Avon) 28, 800-806.

Syczewska, M., Oberg, T., Karlsson, D., 1999. Segmental movements of the spine during treadmill walking with normal speed. Clinical Biomechanics 14, 384-388.

Thorstensson, A., Carlson, H., Zomlefer, M.R., Nilsson, J., 1982. Lumbar back muscle activity in relation to trunk movements during locomotion in man. Acta Physiol Scand 116, 13-20.

Thorstensson, A., Nilsson, J., Carlson, H., Zomlefer, M.R., 1984. Trunk movements in human locomotion. Acta Physiol Scand 121, 9-22.

Umberger, B.R., 2008. Effects of suppressing arm swing on kinematics, kinetics, and energetics of human walking. J Biomech 41, 2575-2580.

Umberger, B.R., Gerritsen, K.G., Martin, P.E., 2003. A model of human muscle energy expenditure. Comput Methods Biomech Biomed Engin 6, 99-111.

van Soest, A.J., Bobbert, M.F., 1993. The contribution of muscle properties in the control of explosive movements. Biol Cybern 69, 195-204.

Vogt, L., Banzer, W., 1999. Measurement of lumbar spine kinematics in incline treadmill walking.

Gait Posture 9, 18-23.

Waters, R.L., Morris, J., Perry, J., 1973. Translational motion of the head and trunk during normal walking. J Biomech 6, 167-172.

Waters, R.L., Morris, J.M., 1972. Electrical activity of muscles of the trunk during walking. J Anat 111, 191-199.

Winter, D., A, 1995. Human balance and posture cotrol during standing ans walking. Gait and Posture 3, 193-214.

Winter, D.A., Robertson, D.G., 1978. Joint torque and energy patterns in normal gait. Biol Cybern 29, 137-142.

Winters, J.M., Stark, L., 1988. Estimated mechanical properties of synergistic muscles involved in movements of a variety of human joints. J Biomech 21, 1027-1041.

Yamaguchi, G.T., Zajac, F.E., 1990. Restoring unassisted natural gait to paraplegics via functional neuromuscular stimulation: a computer simulation study. IEEE Trans Biomed Eng 37, 886-902.

Zhang, X., 2001. Biomechanical realism versus algorithmic efficiency: A trade-off in human motion simulation modeling. SAE Technical Paper.

Appendix A: Joint angular displacements of each model fitted to the actual data of the trunk during the walking

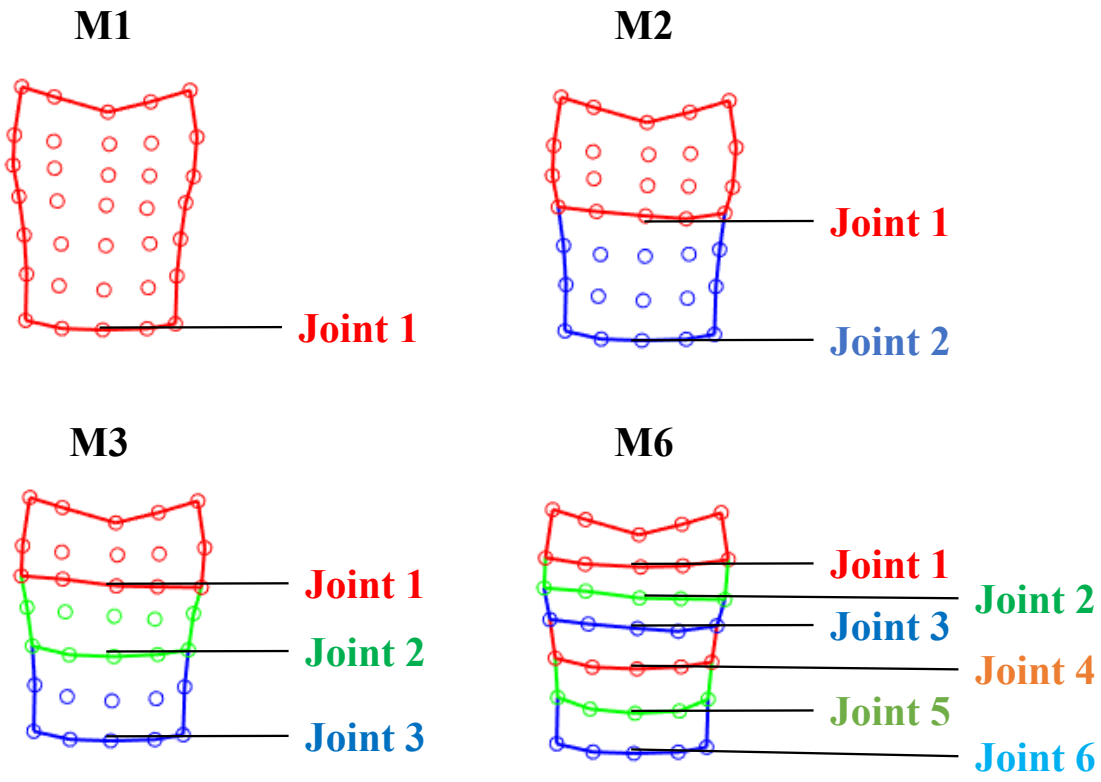

Figure: Joints of each model used in the study in Chapter 4. Text colors in this figure correspond to the colors of the data in following figures.

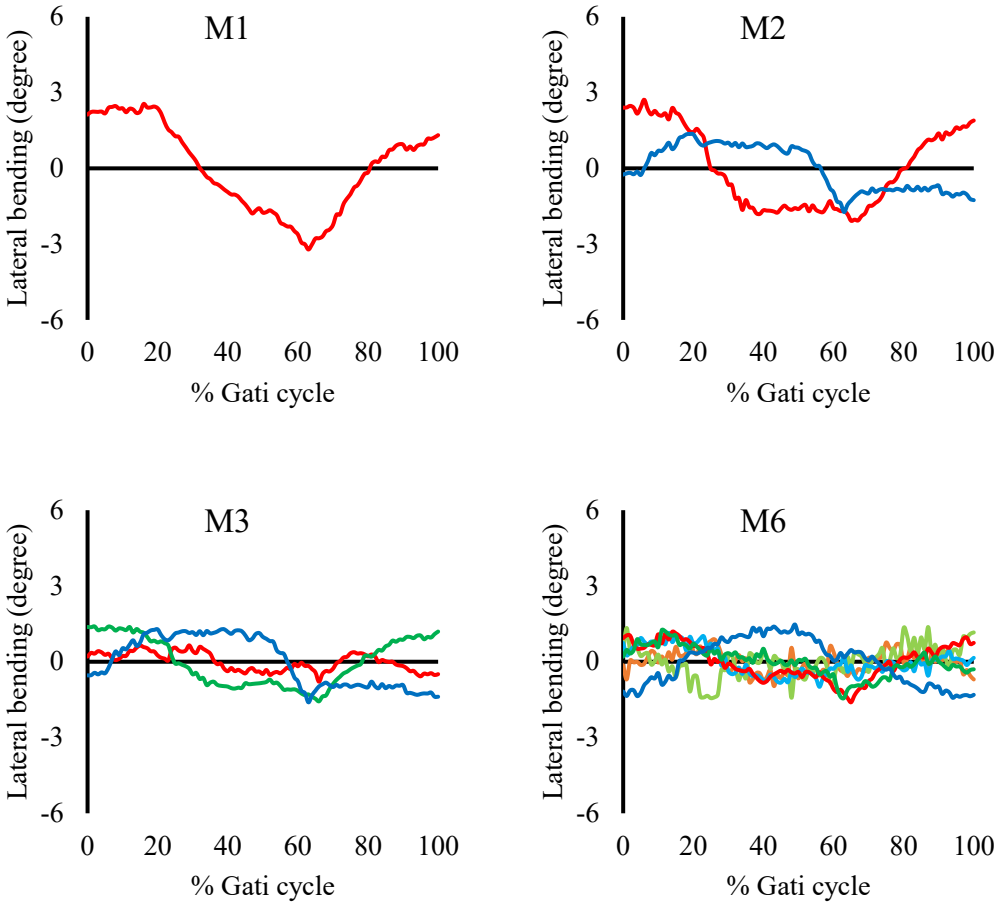

Figure: Angular displacement in the frontal plane about the joints of the trunk derived from M1, M2, M3, and M6 through the optimization analysis.

※Note that these data do not demonstrate smooth curves as the optimizations were performed on a frame-by-frame basis to determine the posture of each rigid-body in the analyzed models.

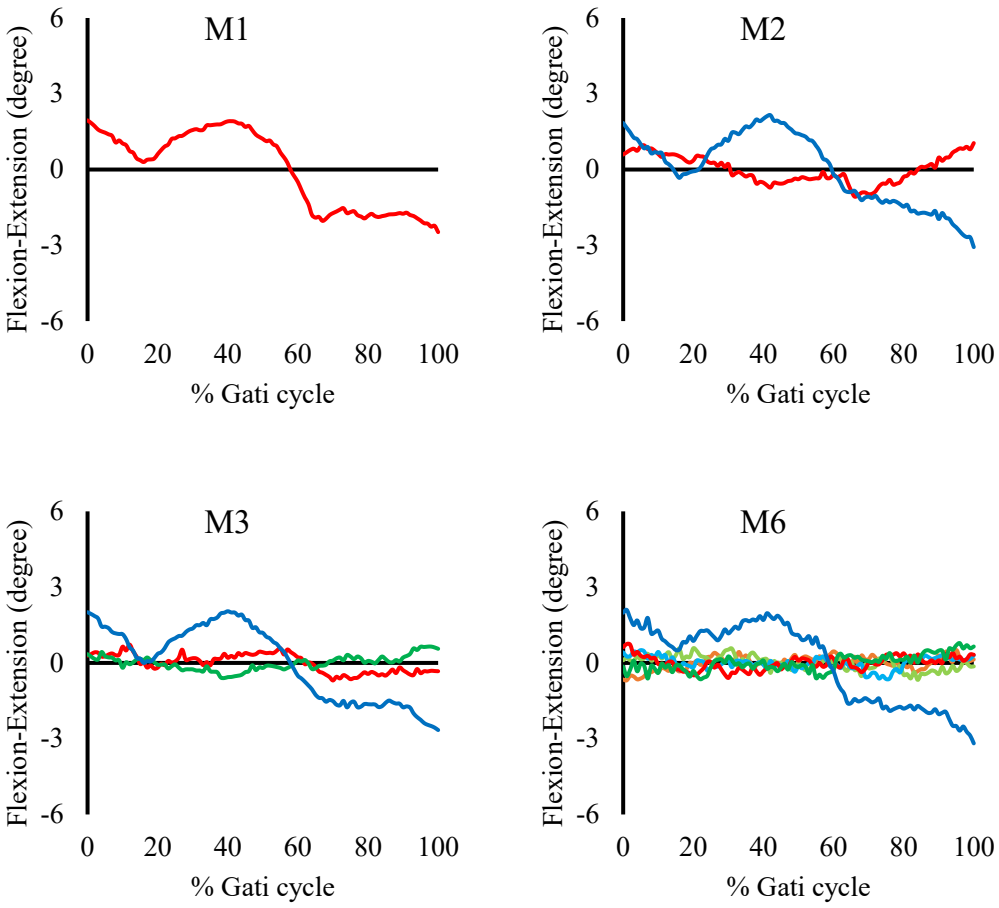

Figure: Angular displacement in the sagittal plane about the joints of the trunk derived from M1, M2, M3, and M6 through the optimization analysis.

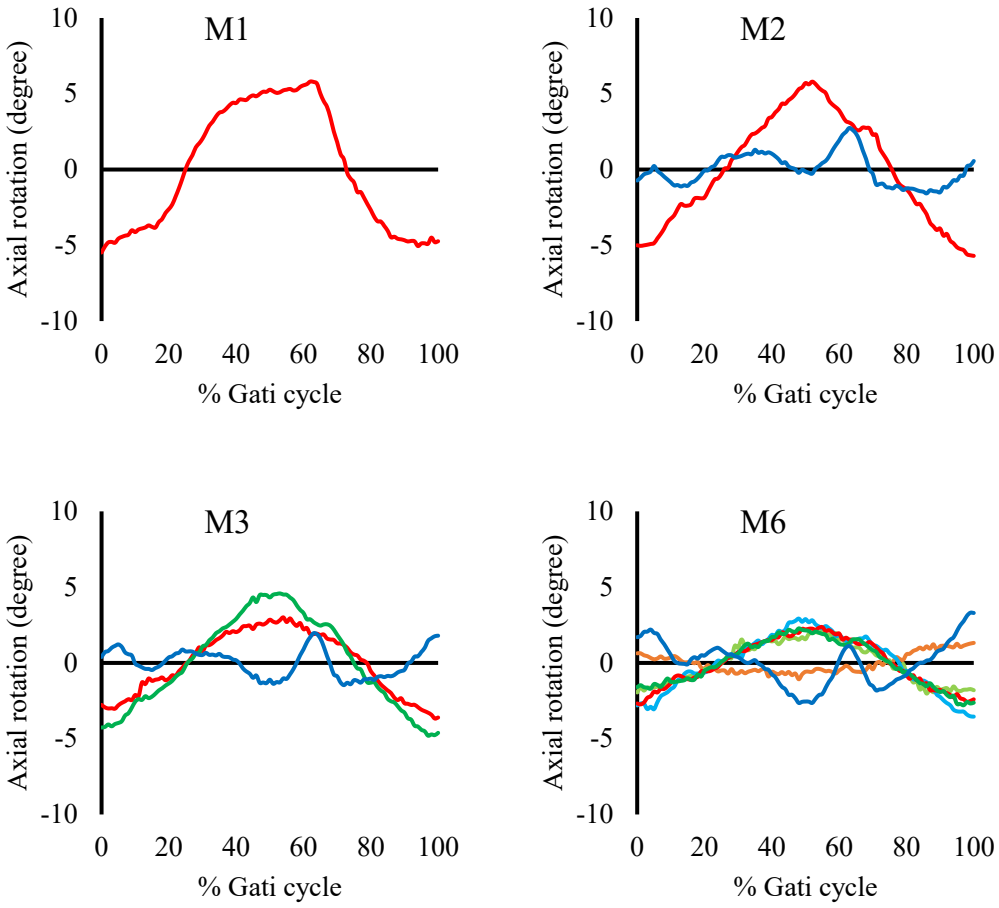

Figure: Angular displacement in the transverse plane about the joints of the trunk derived from M1, M2, M3, and M6 through the optimization analysis.

Appendix B: Parameter values of muscle model

Name	F_{max} (N)	L_{CEopt} (m)	L_{slack} (m)	α (deg)	*Mass* (kg)	*FT* (%)
RECABD	260.82	0.30	0.08	0.00	0.18	54
ILIOCLUMB_LUMB	566.64	0.02	0.04	13.80	0.02	34
ILIOCLUMB_THOR1	375.97	0.07	0.04	12.60	0.04	38
ILIOCLUMB_THOR2	113.69	0.15	0.15	13.80	0.02	38
LONTHOR_LUMB	446.68	0.05	0.00	12.60	0.03	34
LONTHOR_THOR1	365.23	0.10	0.15	12.60	0.05	38
LONTHOR_THOR2	196.04	0.11	12.60	12.60	0.02	38
LONTHOR_THOR_RIB1	365.23	0.10	0.13	12.60	0.04	38
LONTHOR_THOR_RIB2	68.93	0.14	0.18	12.60	0.01	38
QUADLUMBM_POST	115.46	0.04	0.03	7.40	0.01	34
QUADLUMBM_MID	29.90	0.06	0.03	7.40	0.00	34
QUADLUMBM_ANT	46.46	0.10	0.05	7.40	0.01	34
MULFID	488.06	0.08	0.02	0.00	0.08	34
EXTOB1	516.63	0.04	0.05	0.00	0.04	54
EXTOB2	155.84	0.05	0.05	0.00	0.01	54
EXTOB3	226.63	0.06	0.06	0.00	0.02	54
INTOB1	426.17	0.05	0.08	0.00	0.03	54
INTOB2	337.58	0.07	0.05	0.00	0.03	54
INTOB3	138.93	0.05	0.04	0.00	0.01	54
PSOASM	1113.11	0.16	0.06	10.70	0.21	50
ILIA	1357.37	0.10	10.00	7.00	0.21	50
GMAXI	2359.05	0.14	12.50	5.00	0.77	50
GMEDI	2421.11	0.05	7.80	8.00	0.37	50
GMINI	1044.93	0.04	5.10	1.00	0.12	50
ADDLO	881.64	0.14	11.00	6.00	0.28	35
ADDMA	2359.05	0.09	6.00	5.00	0.60	45
ADDBR	446.83	0.13	2.00	0.00	0.14	55

PIRI	796.69	0.03	11.50	10.00	0.05	50
QUAD	1065.10	0.05	2.40	0.00	0.12	50
RECTF	1666.31	0.08	43.20	5.00	0.32	55
BIFEL	1060.45	0.11	34.10	0.00	0.27	35
SEMM	1797.02	0.08	35.90	15.00	0.33	50
SEMT	902.58	0.20	26.20	5.00	0.42	50
VASL	2498.30	0.08	33.60	5.00	0.48	55
VASI	3180.57	0.09	31.50	3.00	0.64	50
VASM	2593.72	0.09	30.50	5.00	0.53	50
BIFES	315.73	0.17	10.00	23.00	0.13	35
GASM	1962.65	0.05	40.80	17.00	0.20	45
GASL	554.66	0.06	38.50	8.00	0.08	45
TIBAN	654.73	0.10	22.30	5.00	0.15	30
SOLEU	7238.91	0.03	26.80	25.00	0.50	25
TIBPOS	1018.95	0.03	31.00	12.00	0.07	45
PERL	956.11	0.05	34.50	10.00	0.11	40
PERLB	760.62	0.05	16.10	5.00	0.09	55
FHAL	718.34	0.04	38.00	10.00	0.07	50

Appendix C: Parameter values of passive joint torque

	k_0	k_1	k_2	k_3	k_4	$\boldsymbol{\theta}$	$\boldsymbol{\phi}$
Thoracic FE	0	-0.35	61.44	0.25	-40.72	0.085	-0.175
Thoracic LB	0	-0.25	40.72	0.25	-40.72	0.085	-0.085
Thoracic AR	0	-0.25	40.72	0.25	-40.72	0.085	-0.085
Lumbar FE	0	-0.35	61.44	0.25	-40.72	0.085	-0.175
Lumbar LB	0	-0.25	40.72	0.25	-40.72	0.085	-0.085
Lumbar AR	0	-0.25	40.72	0.25	-40.72	0.085	-0.085
Hip FE	0	-2.44	5.05	1.51	-21.88	1.81	-0.47
Hip AA	0	-0.03	14.94	0.03	-14.94	0.5	-0.5
Hip IE	0	-0.03	14.94	0.03	-14.94	0.92	-0.92
Knee FE	0	-6.09	33.94	11.03	-11.33	0.13	-2.4
Ankle DP	0	-2.03	38.11	0.18	-42.12	0.52	-0.74
Subtalar IE	0	-60.21	16.32	60.21	-16.32	0.65	-0.65

※ FE: Flexion and extension. LB: Lateral bending. AR: Axial rotation. AA: Abduction and adduction. IE: Internal and external rotation. DP: Dorsi flexion and planter flexion.

Appendix D: Muscle activity profiles of the trunk muscles during walking

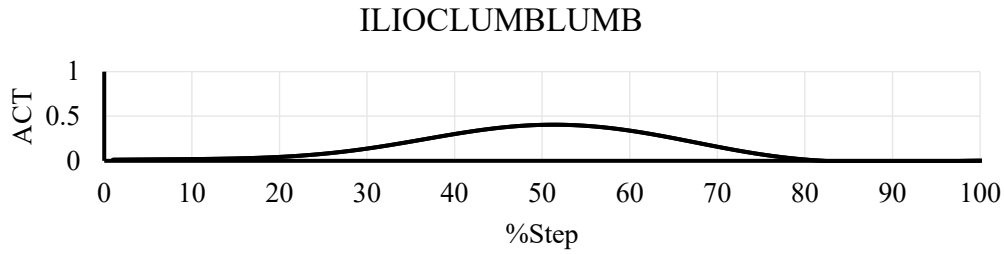

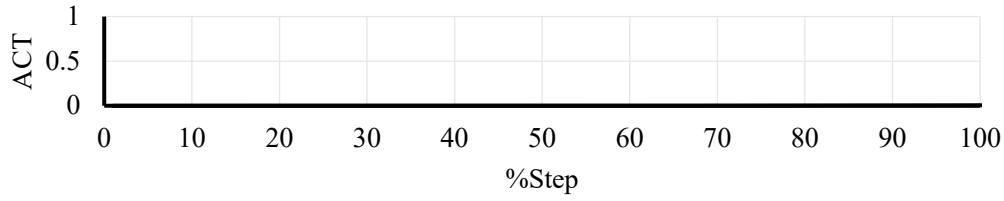

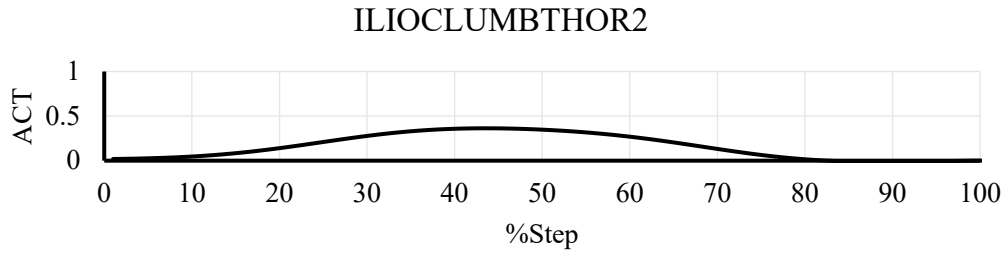

LONGISTHORLUMB

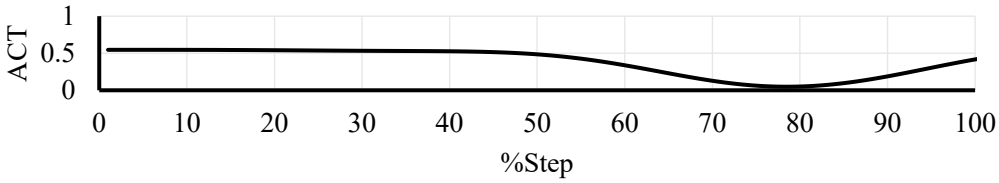

LONGISTHORTHOR1

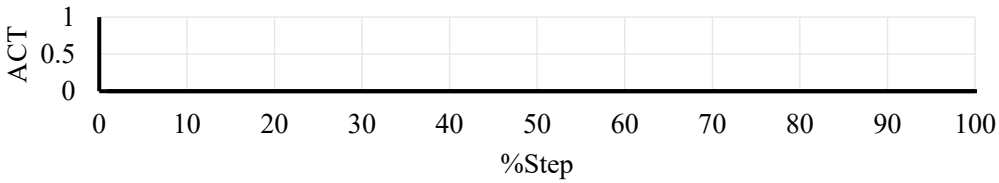

LONGISTHORTHOR2

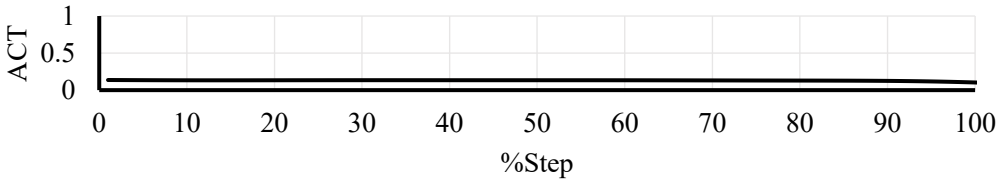

LONGISTHORTHORRIB1

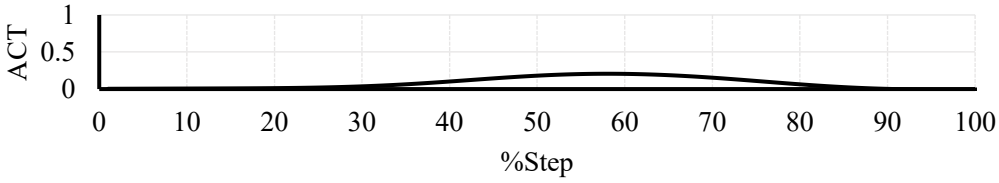

LONGISTHORTHORRIB2

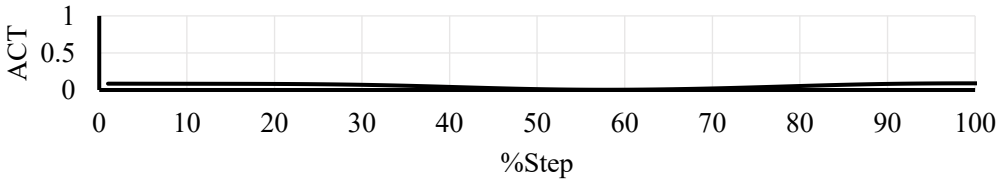

QUADLUMBPOST

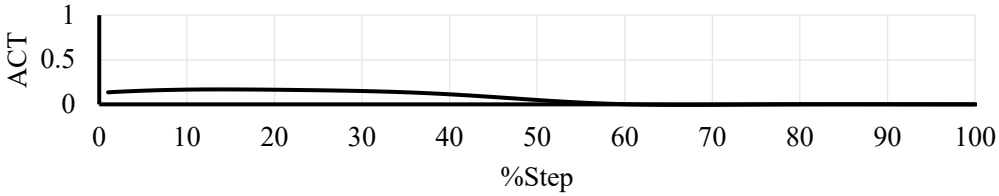

QUADLUMBMID

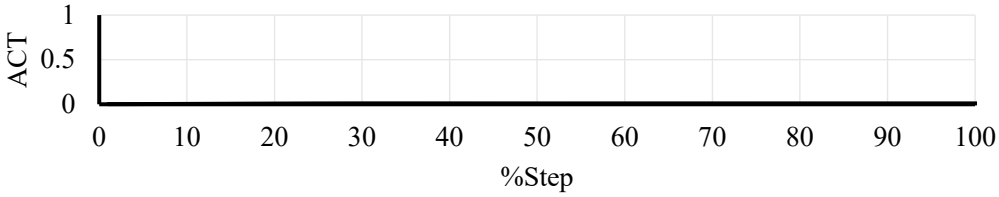

QUADLUMBANT

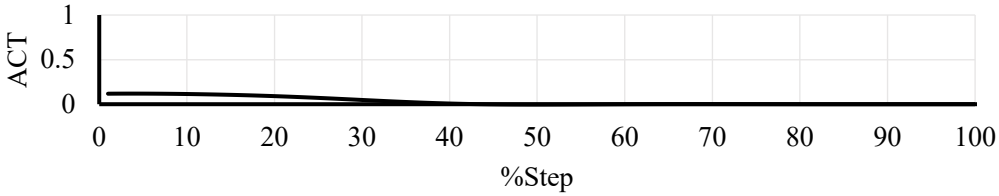

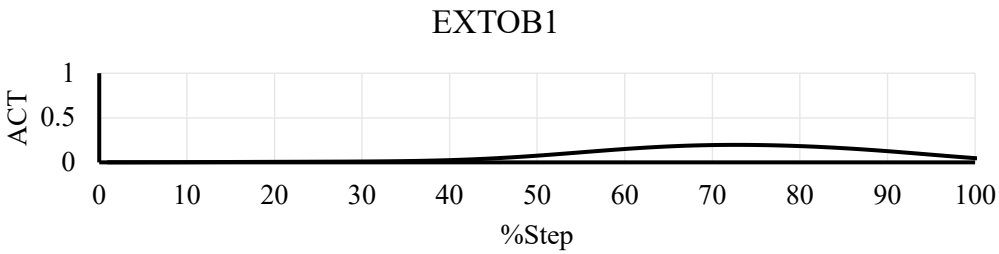
EXTOB1
ACT
1
0.5
0
0
10
20
30
40
50
60
70
80
90
100
%Step

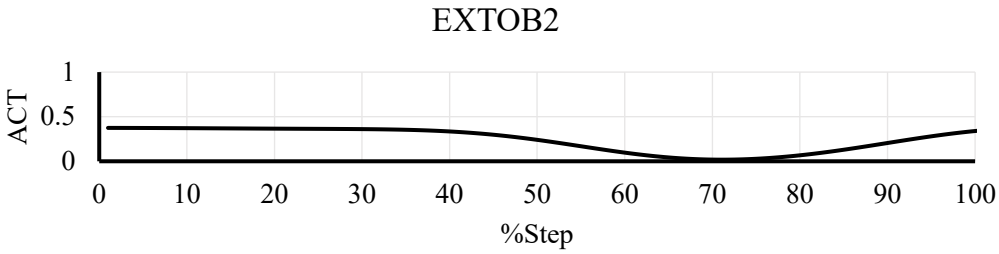
EXTOB2
ACT
1
0.5
0
0
10
20
30
40
50
60
70
80
90
100
%Step

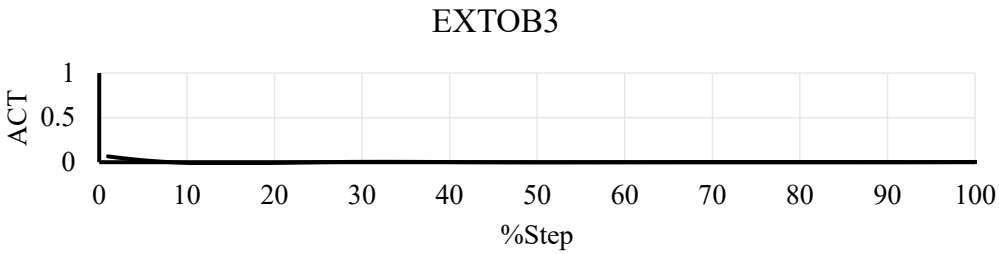
EXTOB3
ACT
1
0.5
0
0
10
20
30
40
50
60
70
80
90
100
%Step

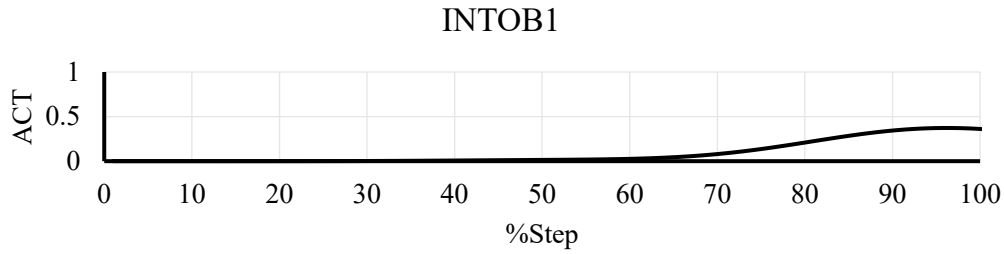
INTOB1
ACT
1
0.5
0
0
10
20
30
40
50
60
70
80
90
100
%Step

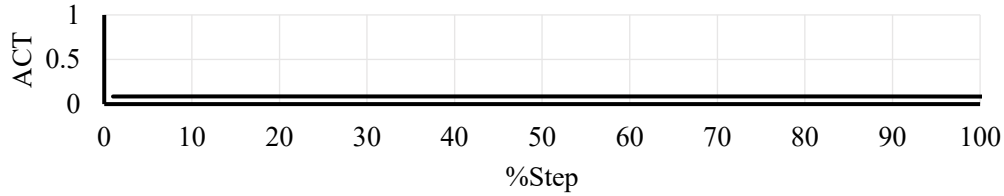
INTOB2
ACT
1
0.5
0
0
10
20
30
40
50
60
70
80
90
100
%Step

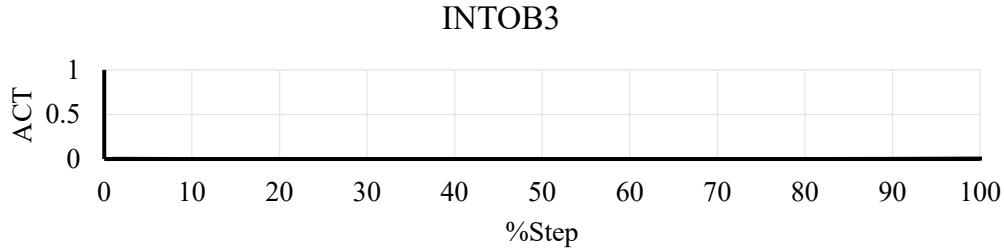
INTOB3
ACT
1
0.5
0
0
10
20
30
40
50
60
70
80
90
100
%Step

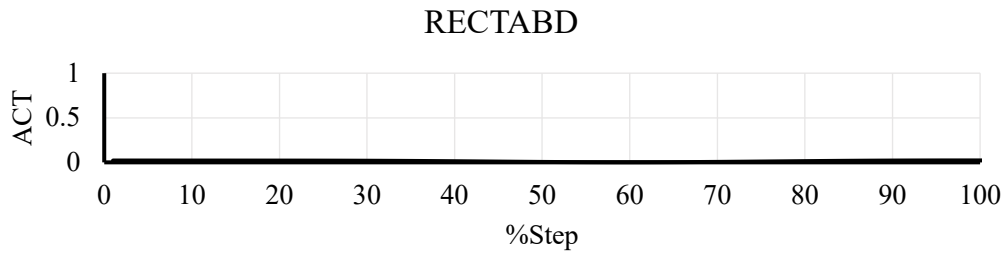
RECTABD
ACT
1
0.5
0
0
10
20
30
40
50
60
70
80
90
100
%Step

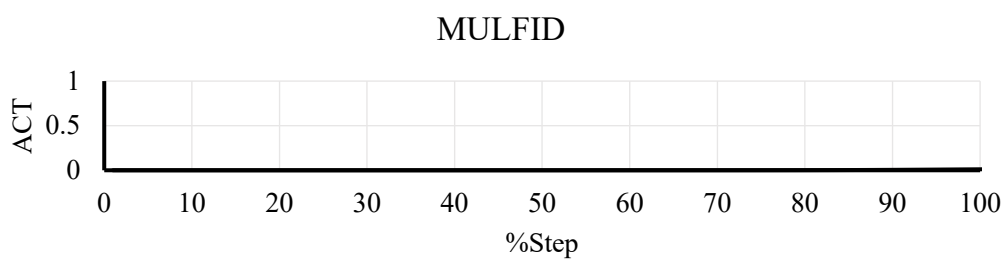
MULFID
ACT
1
0.5
0
0
10
20
30
40
50
60
70
80
90
100
%Step

Appendix E: Muscle force profiles of the trunk muscles during walking

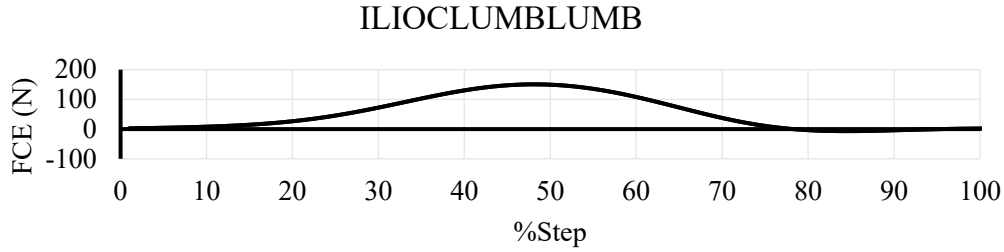

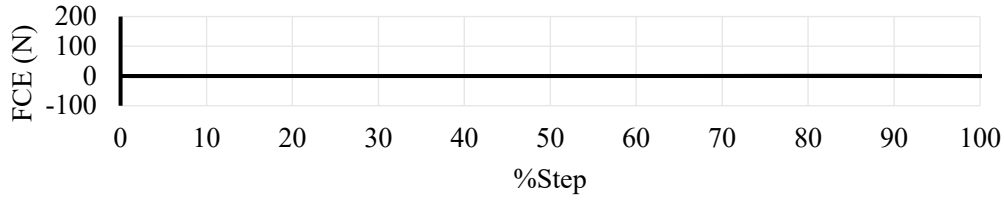

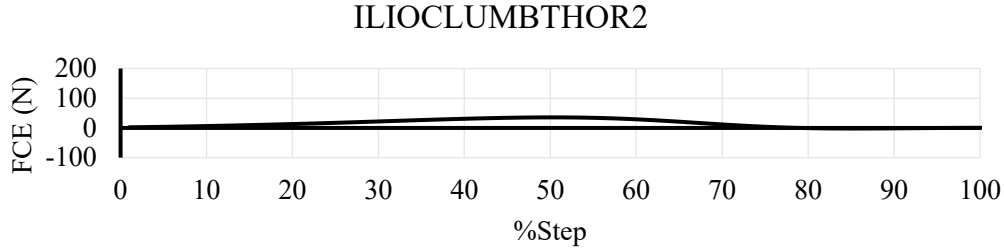

LONGISTHORLUMB

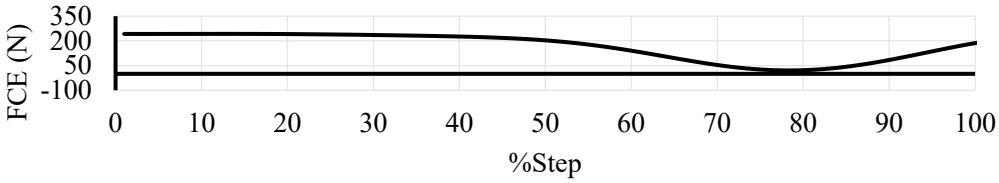

LONGISTHORTHOR1

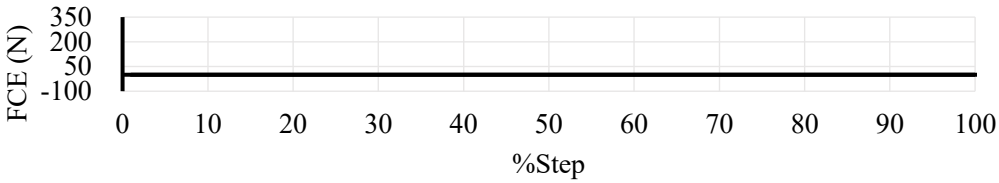

LONGISTHORTHOR2

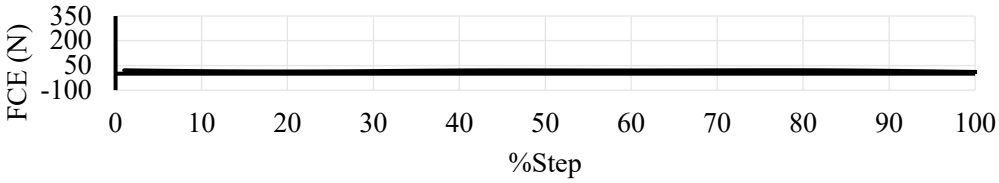

LONGISTHORTHORRIB1

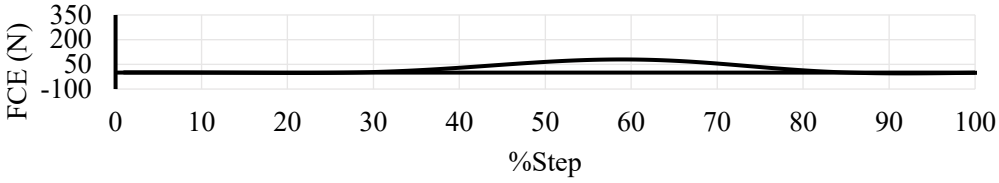

LONGISTHORTHORRIB2

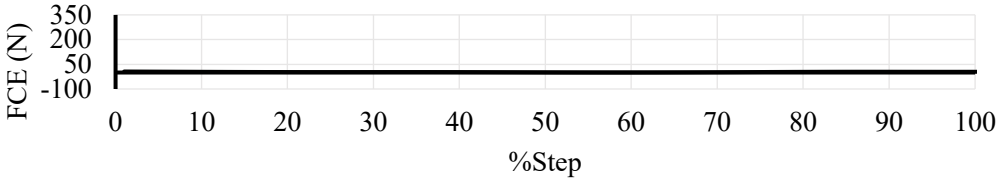

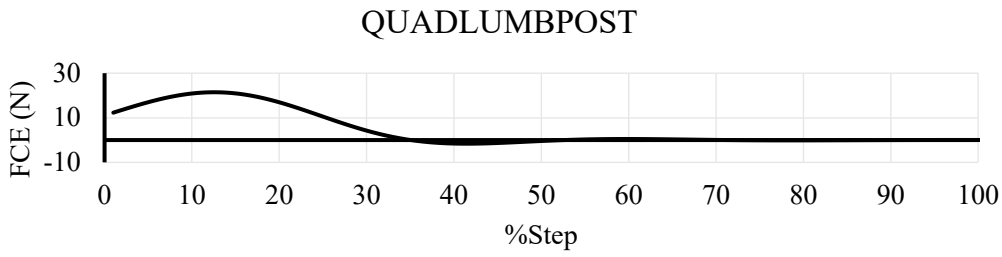
QUADLUMBPOST
FCE (N)
30
10
-10
0
10
20
30
40
50
60
70
80
90
100
%Step

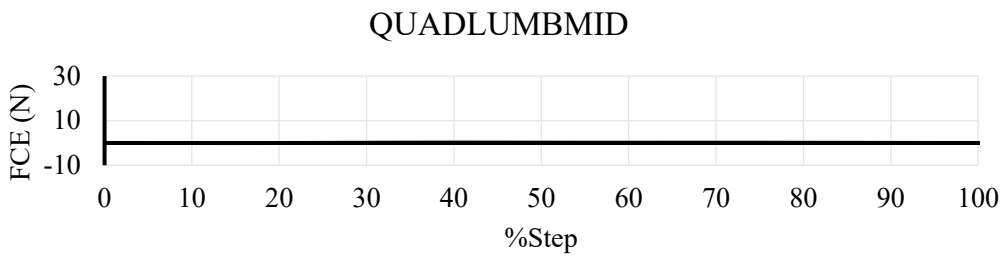
QUADLUMBMID
FCE (N)
30
10
-10
0
10
20
30
40
50
60
70
80
90
100
%Step

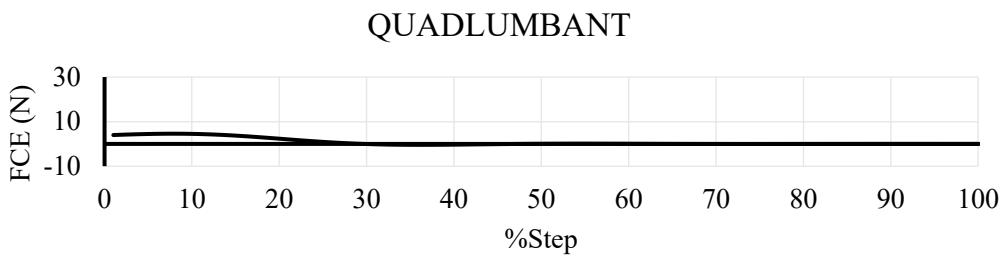
QUADLUMBANT
FCE (N)
30
10
-10
0
10
20
30
40
50
60
70
80
90
100
%Step

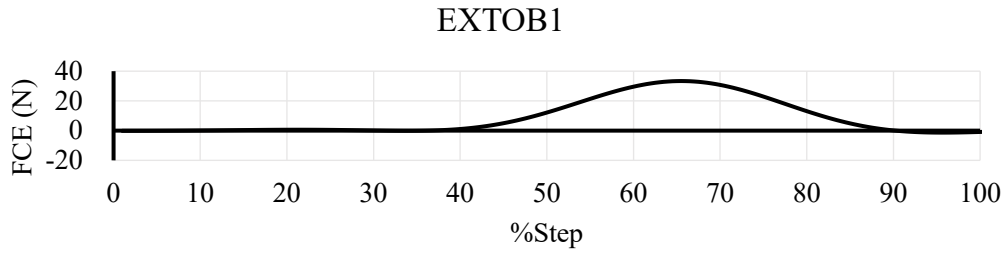
EXTOB1
FCE (N)
40
20
0
-20
0
10
20
30
40
50
60
70
80
90
100
%Step

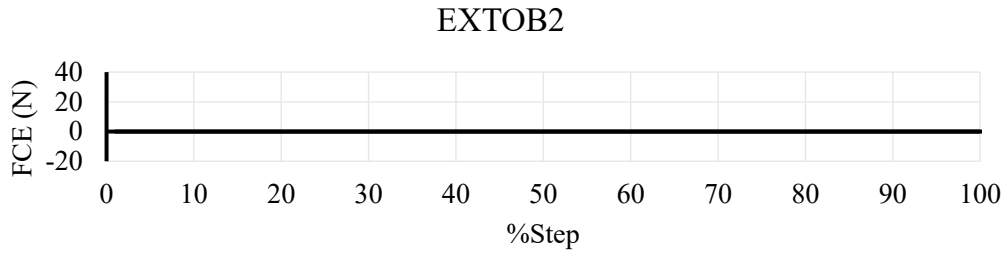
EXTOB2
FCE (N)
40
20
0
-20
0
10
20
30
40
50
60
70
80
90
100
%Step

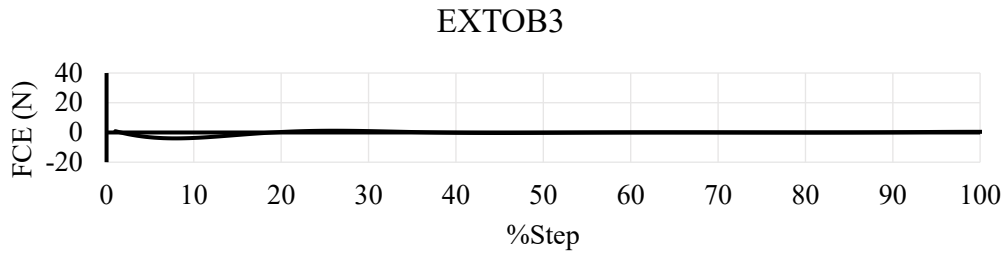
EXTOB3
FCE (N)
40
20
0
-20
0
10
20
30
40
50
60
70
80
90
100
%Step

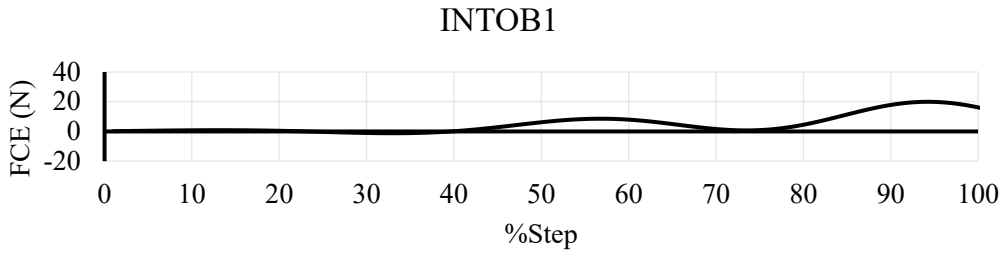
INTOB1
FCE (N)
40
20
0
-20
0
10
20
30
40
50
60
70
80
90
100
%Step

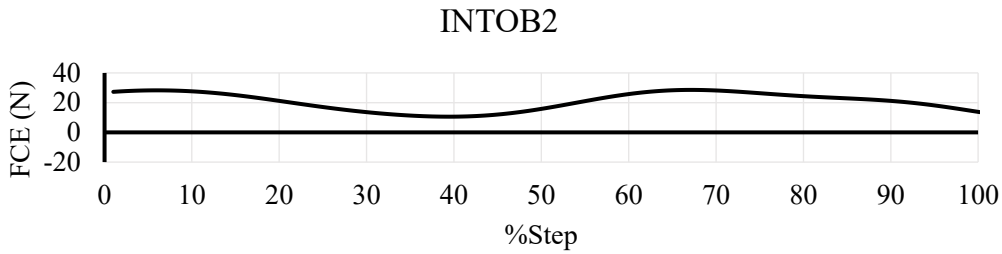
INTOB2
FCE (N)
40
20
0
-20
0
10
20
30
40
50
60
70
80
90
100
%Step

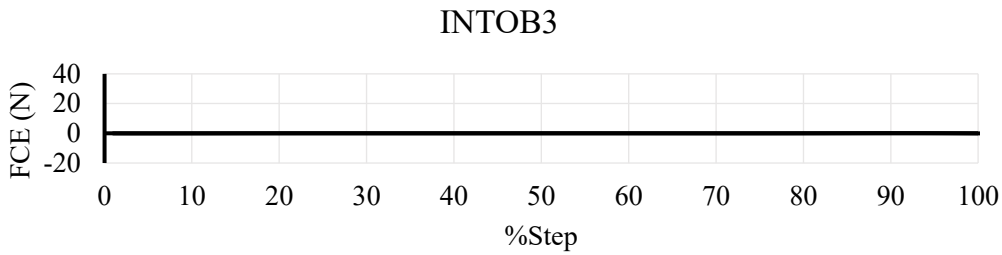
INTOB3
FCE (N)
40
20
0
-20
0
10
20
30
40
50
60
70
80
90
100
%Step

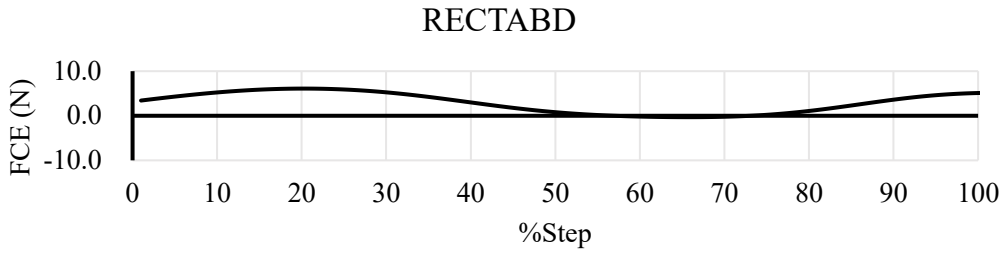
RECTABD
FCE (N)
10.0
0.0
-10.0
0
10
20
30
40
50
60
70
80
90
100
%Step

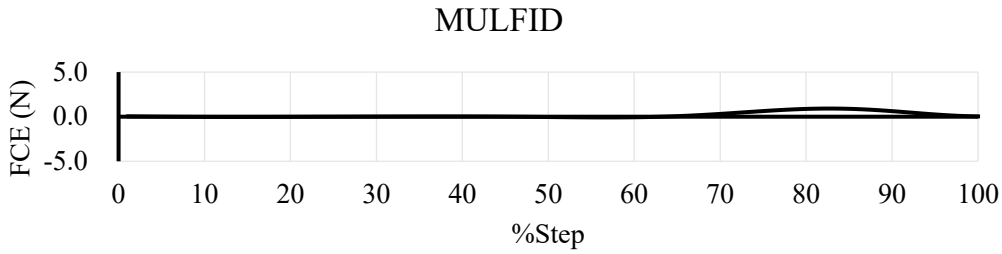
MULFID
FCE (N)
5.0
0.0
-5.0
0
10
20
30
40
50
60
70
80
90
100
%Step

Appendix F: Muscle property and geometry data

/*----------*/

The properties of the muscle implemented in the neuromusculoskeletal model used in this study were specified with: (1) maximum isometric strength of the muscle, (2) optimal fiber length of contractile element, (3) slack length of the tendon, (4) percentage of first twitch fibers, (5) pennation angle, and (6) number of muscle points. These parameters were described as (1) F_{max}, (2) LCE_{opt}, (3) L_{slack}, (4) %FT, (5) α, and (6) Novi, respectively.

The geometry of the muscle implemented in the neuromusculoskeletal model used in this study was specified with (1) the segment which the point of the origin and insertion are located, (2) x, y, z, generalized coordinate for muscle path, (3) the joint for via-points that appear/disappear, and (4) range for via-points that appear/disappear. These parameters were described as (1) Segment_ID, (2) Povi, (3) Joint_ID, and (4) Viapoint_range, respectively. Detailed information for each parameter were listed below.

Segment_ID : 1. Head, 2. Thorax, 3. Abdomen, 4. Pelvis, 5. Thigh, 6. Shank,
7. Hind foot, 8. Fore foot

Povi : x, y, z, generalized coordinate for muscle path (origin, via, and insertion points)
(these coordinates were specified from the center of mass of segments)

Joint_ID : Range ID for via-points that appear/disappear
(0: does not disappear, 1: Hip Flexion, 2: Knee Extension)

Viapoint_range : Range for via-points that appear/disappear (specified in degrees)

/*----------*/

muscle_name RECABD

Fmax (N) 260.82 /* maximum isometric strength of the muscle */

LCEopt (m) 0.2986 /* optimal fiber length */

Lslack (m) 0.0810 /* slack length of the tendon */

%FT (%) 55 /* percentage of first twitch fibers */

α (radian) 0.0000 /* pennation angle */

Novi 2 /* number of muscle points for the origin, via, insertion */

/* beginpoints */

/* Segment_ID, Povi (x, y, z), Joint_ID, Viapoint_range (lower limit), Viapoint_range (upper limit) */

2 0.0920 0.2220 0.0310 0 0.0 0.0

4 - 0.0260 - 0.0700 0.0110 0 0.0 0.0

/*endpoints*/

muscle_name ILIOCLUMB_LUMB

Fmax (N) 566.64

LCEopt (m) 0.0515

Lslack (m) 0.0019

%FT (%) 35

α (radian) 12.600

Novi 2

/* beginpoints */

3 - 0.0063 - 0.0695 0.0310 0 0.0 0.0

4 - 0.1170 0.0650 0.0560 0 0.0 0.0

/* endpoints */

muscle_name ILIOCLUMB_THOR1

Fmax (N) 375.97

LCEopt (m) 0.0731

Lslack (m) 0.0366

%FT (%) 40

α (radian) 12.600

Novi 2

/* beginpoints */

2 - 0.0320 0.0950 0.0670 0 0.0 0.0

4 - 0.1110 0.0820 0.0670 0 0.0 0.0

/* endpoints */

muscle_name ILIOCLUMB_THOR2

Fmax (N) 113.69

LCEopt (m) 0.1459

Lslack (m) 0.1536

%FT (%) 40

α (radian) 13.800

Novi 6

/* beginpoints */

2 - 0.0750 0.2610 0.0650 0 0.0 0.0

2	- 0.0810	0.2390	0.0640	0	0.0	0.0
2	- 0.0800	0.2010	0.0630	0	0.0	0.0
2	- 0.0800	0.1720	0.0630	0	0.0	0.0
3	- 0.0373	- 0.0264	0.0610	0	0.0	0.0
4	- 0.1190	0.0690	0.0580	0	0.0	0.0

/* endpoints */

muscle_name	LONGISTHOR_LUMB
Fmax (N)	446.68
LCEopt (m)	0.0515
Lslack (m)	0.0019
%FT (%)	35
α (radian)	12.600
Novi	2

/* beginpoints */

3	- 0.0047	-0.1007	0.0258	0	0.0	0.0
4	- 0.1285	0.0461	0.0455	0	0.0	0.0

/* endpoints */

muscle_name	LONGISTHOR_THOR1
Fmax (N)	365.23
LCEopt (m)	0.0980
Lslack (m)	0.1494
%FT (%)	40
α (radian)	12.600
Novi	5

/* beginpoints */

2	- 0.0590	0.1617	0.0176	0	0.0	0.0
3	- 0.0346	- 0.0254	0.0198	0	0.0	0.0
3	- 0.0320	- 0.0504	0.0209	0	0.0	0.0
3	- 0.0292	- 0.0801	0.0219	0	0.0	0.0
4	- 0.1476	0.0137	0.0240	0	0.0	0.0

/* endpoints */

muscle_name LONGISTHOR_THOR2

Fmax (N) 196.04

LCEopt (m) 0.1061

Lslack (m) 0.2550

%FT (%) 40

α (radian) 12.600

Novi 2

/* beginpoints */

2 -0.0550 0.3860 0.0265 0 0.0 0.0

3 -0.0356 -0.0438 0.0038 0 0.0 0.0

/* endpoints */

muscle_name LONGISTHOR_THOR_RIB1

Fmax (N) 365.20

LCEopt (m) 0.1045

Lslack (m) 0.1313

%FT (%) 40

α (radian) 12.600

Novi 5

/* beginpoints */

2 -0.0650 0.1477 0.0456 0 0.0 0.0

3 -0.0326 -0.0243 0.0356 0 0.0 0.0

3 -0.0280 -0.0500 0.0326 0 0.0 0.0

3 -0.0286 -0.0791 0.0294 0 0.0 0.0

4 -0.1477 0.0137 0.0240 0 0.0 0.0

/* endpoints */

muscle_name LONGISTHOR_THOR_RIB2

Fmax (N) 68.90

LCEopt (m) 0.1357

Lslack (m)	0.1847
%FT (%)	40
α (radian)	12.600
Novi	8

/* beginpoints */

2	-0.0690	0.2900	0.0400	0	0.0	0.0
2	-0.0730	0.2710	0.0400	0	0.0	0.0
2	-0.0770	0.2420	0.0373	0	0.0	0.0
2	-0.0760	0.2130	0.0347	0	0.0	0.0
2	-0.0760	0.1870	0.0310	0	0.0	0.0
3	-0.0346	-0.0244	0.0140	0	0.0	0.0
3	-0.0319	-0.0492	0.0108	0	0.0	0.0
3	-0.0295	-0.1092	0.0002	0	0.0	0.0

/* endpoints */

muscle_name	QUADLUMB_POST
Fmax (N)	115.46
LCEopt (m)	0.0361
Lslack (m)	0.0303
%FT (%)	35
α (radian)	7.4000
Novi	2

/* beginpoints */

3	-0.0109	-0.0443	0.0303	0	0.0	0.0
4	-0.0980	0.0890	0.0660	0	0.0	0.0

/* endpoints */

muscle_name	QUADLUMB_MID
Fmax (N)	29.90
LCEopt (m)	0.0631
Lslack (m)	0.0328
%FT (%)	35

α (radian) 7.4000

Novi 2

/* beginpoints */

2 -0.0413 0.1282 0.0312 0 0.0 0.0

3 -0.011 -0.0422 0.0304 0 0.0 0.0

/* endpoints */

muscle_name QUADLUMB_ANT

Fmax (N) 46.46

LCEopt (m) 0.1033

Lslack (m) 0.0537

%FT (%) 35

α (radian) 7.4000

Novi 2

/* beginpoints */

2 -0.0100 0.1310 0.0190 0 0.0 0.0

4 -0.0980 0.0890 0.0660 0 0.0 0.0

/* endpoints */

muscle_name MULFID

Fmax (N) 488.06

LCEopt (m) 0.0809

Lslack (m) 0.0246

%FT (%) 35

α (radian) 0.0000

Novi 2

/* beginpoints */

3 -0.0336 -0.0472 0.0036 0 0.0 0.0

4 -0.1340 0.0490 0.0470 0 0.0 0.0

/* endpoints */

muscle_name EXTOB1

Fmax (N)	516.63					
LCEopt (m)	0.0384					
Lslack (m)	0.0466					
%FT (%)	55					
α (radian)	0.0000					
Novi	2					
/* beginpoints */						
2	0.0785	0.1005	0.1136	0	0.0	0.0
3	0.1053	-0.0472	0.0330	0	0.0	0.0
/* endpoints */						

muscle_name	EXTOB2					
Fmax (N)	155.84					
LCEopt (m)	0.0471					
Lslack (m)	0.0515					
%FT (%)	55					
α (radian)	0.0000					
Novi	2					
/* beginpoints */						
2	0.0010	0.1100	0.1120	0	0.0	0.0
4	-0.0550	0.0820	0.1020	0	0.0	0.0
/* endpoints */						

muscle_name	EXTOB3					
Fmax (N)	226.63					
LCEopt (m)	0.0565					
Lslack (m)	0.0571					
%FT (%)	55					
α (radian)	0.0000					
Novi	2					
/* beginpoints */						
2	-0.0110	0.0930	0.1000	0	0.0	0.0

4 -0.0690 0.0930 0.0980 0 0.0 0.0

/* endpoints */

muscle_name INTOB1

Fmax (N) 426.17

LCEopt (m) 0.0517

Lslack (m) 0.0783

%FT (%) 55

α (radian) 0.0000

Novi 2

/* beginpoints */

3 0.1035 -0.0322 0.0490 0 0.0 0.0

4 -0.0390 0.0690 0.1170 0 0.0 0.0

/* endpoints */

muscle_name INTOB2

Fmax (N) 337.58

LCEopt (m) 0.0697

Lslack (m) 0.0470

%FT (%) 55

α (radian) 0.0000

Novi 2

/* beginpoints */

2 0.0660 0.1080 0.1210 0 0.0 0.0

4 -0.0530 0.0820 0.1000 0 0.0 0.0

/* endpoints */

muscle_name INTOB3

Fmax (N) 138.93

LCEopt (m) 0.0544

Lslack (m) 0.0367

%FT (%) 55

α (radian)	0.0000					
Novi	2					
/* beginpoints */						
2	0.0000	0.0860	0.1000	0	0.0	0.0
4	-0.0900	0.0880	0.0660	0	0.0	0.0
/* endpoints */						

muscle_name	PSOASM					
Fmax (N)	1113.11					
LCEopt (m)	0.1841					
Lslack (m)	0.1647					
%FT (%)	50					
α (radian)	10.700					
Novi	5					
/* beginpoints */						
3	-0.0233	0.0142	0.0226	0	0.0	0.0
4	-0.0238	-0.0570	0.0759	0	0.0	0.0
4	-0.0288	-0.0805	0.0816	1	-90	45
5	0.0016	-0.0507	0.0038	0	0.0	0.0
5	-0.0188	-0.0597	0.0104	0	0.0	0.0
/* endpoints */						

muscle_name	ILIA					
Fmax (N)	1357.4					
LCEopt (m)	0.1000					
Lslack (m)	0.1000					
%FT (%)	50					
α (radian)	7.0000					
Novi	5					
/* beginpoints */						
4	-0.0674	0.0365	0.0854	0	0.0	0.0
4	-0.0258	-0.0550	0.0811	0	0.0	0.0

4	-0.0288	-0.0805	0.0816	1	-90	45
5	0.0017	-0.0543	0.0057	0	0.0	0.0
5	-0.0193	-0.0621	0.0129	0	0.0	0.0

/* endpoints */

muscle_name	GMAXI
Fmax (N)	2359.1
LCEopt (m)	0.1420
Lslack (m)	0.1250
%FT (%)	50
α (radian)	5.0
Novi	4

/* beginpoints */

4	-0.1195	0.0612	0.0700	0	0.0	0.0
4	-0.1291	0.0012	0.0886	0	0.0	0.0
5	-0.0457	-0.0248	0.0392	0	0.0	0.0
5	-0.0277	-0.0566	0.0470	0	0.0	0.0

/* endpoints */

muscle_name	GMEDI
Fmax (N)	2421.11
LCEopt (m)	0.0535
Lslack (m)	0.0780
%FT (%)	50
α (radian)	8.0
Novi	2

/* beginpoints */

4	-0.0408	0.0304	0.1209	0	0.0	0.0
5	-0.0218	-0.0117	0.0555	0	0.0	0.0

/* endpoints */

muscle_name GMINI

Fmax (N)	1044.93					
LCEopt (m)	0.0380					
Lslack (m)	0.0510					
%FT (%)	50					
α (radian)	1.0					
Novi	2					
/* beginpoints */						
4	-0.0834	-0.0063	0.0856	0	0.0	0.0
5	-0.0135	-0.0083	0.0550	0	0.0	0.0
/* endpoints */						

muscle_name	ADDLO					
Fmax (N)	881.64					
LCEopt (m)	0.1380					
Lslack (m)	0.1100					
%FT (%)	35					
α (radian)	6.0					
Novi	2					
/* beginpoints */						
4	-0.0316	-0.0836	0.0169	0	0.0	0.0
5	0.0050	-0.2111	0.0234	0	0.0	0.0
/* endpoints */						

muscle_name	ADDMA					
Fmax (N)	2359.05					
LCEopt (m)	0.0870					
Lslack (m)	0.060					
%FT (%)	45					
α (radian)	5.0					
Novi	2					
/* beginpoints */						
4	-0.0732	-0.1174	0.0255	0	0.0	0.0

5	-0.0045	-0.1211	0.0339	0	0.0	0.0

/* endpoints */

muscle_name	ADDBR
Fmax (N)	446.83
LCEopt (m)	0.1330
Lslack (m)	0.0200
%FT (%)	55
α (radian)	0.0
Novi	2

/* beginpoints */

4	-0.0587	-0.0915	0.0164	0	0.0	0.0
5	0.0009	-0.1196	0.0294	0	0.0	0.0

/* endpoints */

muscle_name	PIRI
Fmax (N)	796.69
LCEopt (m)	0.0260
Lslack (m)	0.1150
%FT (%)	50
α (radian)	10.0
Novi	3

/* beginpoints */

4	-0.1396	-0.0003	0.0235	0	0.0	0.0
4	-0.1193	-0.0276	0.0657	0	0.0	0.0
5	-0.0148	-0.0036	0.0437	0	0.0	0.0

/* endpoints */

muscle_name	QUAD
Fmax (N)	1065.1
LCEopt (m)	0.0540
Lslack (m)	0.0240

%FT (%)	50					
α (radian)	0.0					
Novi	2					
/* beginpoints */						
4	-0.1143	-0.1151	0.0520	0	0.0	0.0
5	-0.0381	-0.0359	0.0366	0	0.0	0.0
/* endpoints */						

muscle_name	RECTF					
Fmax (N)	1666.3					
LCEopt (m)	0.1140					
Lslack (m)	0.3100					
%FT (%)	55					
α (radian)	5.0					
Novi	3					
/* beginpoints */						
4	-0.02950	-0.03110	0.09680	0	0.0	0.0
5	0.03340	-0.40300	0.00190	2	-150	-85
6	0.06176	0.02098	0.00140	0	0.0	0.0
/* endpoints */						

muscle_name	BIFEL					
Fmax (N)	1060.45					
LCEopt (m)	0.1090					
Lslack (m)	0.3410					
%FT (%)	35					
α (radian)	0.0					
Novi	3					
/* beginpoints */						
4	-0.1260	-0.1026	0.0694	0	0.0	0.0
6	-0.0301	-0.0360	0.0294	0	0.0	0.0
6	-0.0234	-0.0563	0.0343	0	0.0	0.0

/* endpoints */

muscle_name	SEMM
Fmax (N)	1797.02
LCEopt (m)	0.0800
Lslack (m)	0.3590
%FT (%)	50
α (radian)	15.0
Novi	3

/* beginpoints */

4	-0.1192	-0.1015	0.0695	0	0.0	0.0
6	-0.348	-0.0352	-0.0189	2	-32	10
6	-0.0243	-0.0536	-0.0194	0	0.0	0.0

/* endpoints */

muscle_name	SEMT
Fmax (N)	902.58
LCEopt (m)	0.2010
Lslack (m)	0.2620
%FT (%)	50
α (radian)	5.0
Novi	5

/* beginpoints */

4	-0.1237	-0.1043	0.0603	0	0.0	0.0
6	-0.0420	-0.0286	-0.0228	2	-19	10
6	-0.0332	-0.0528	-0.0229	0	0.0	0.0
6	-0.0113	-0.0746	-0.0245	0	0.0	0.0
6	0.0027	-0.0956	-0.0193	0	0.0	0.0

/* endpoints */

muscle_name	VASL
Fmax (N)	2498.3

LCEopt (m) 0.0840

Lslack (m) 0.1570

%FT (%) 55

α (radian) 5.0

Novi 5

/* beginpoints */

5	0.00480	-0.18540	0.03490	0	0.0	0.0
5	0.02690	-0.25910	0.04090	0	0.0	0.0
5	0.03610	-0.40300	0.02050	2	-150	-70
5	0.02530	-0.42430	0.01840	2	-150	-110
6	0.05996	0.01959	0.01650	0	0.0	0.0

/* endpoints */

muscle_name VASI

Fmax (N) 3180.57

LCEopt (m) 0.0870

Lslack (m) 0.1360

%FT (%) 50

α (radian) 3.0

Novi 4

/* beginpoints */

5	0.02900	-0.19240	0.03100	0	0.0	0.0
5	0.03350	-0.20840	0.02850	0	0.0	0.0
5	0.03430	-0.40300	0.00550	2	-150	-80
6	0.05546	0.02529	0.00180	0	0.0	0.0

/* endpoints */

muscle_name VASM

Fmax (N) 2593.72

LCEopt (m) 0.0890

Lslack (m) 0.1260

%FT (%) 50

α (radian) 5.0

Novi 5

/* beginpoints */

5	0.01400	-0.20990	0.01880	0	0.0	0.0
5	0.03560	-0.27690	0.00090	0	0.0	0.0
5	0.03700	-0.40480	-0.01250	2	-150	-70
5	0.02740	-0.42550	-0.01310	2	-150	-100
6	0.05596	0.02179	-0.01460	0	0.0	0.0

/* endpoints */

muscle_name BIFES

Fmax (N) 315.73

LCEopt (m) 0.1730

Lslack (m) 0.1000

%FT (%) 35

α (radian) 23.0

Novi 3

/* beginpoints */

5	0.0050	-0.2111	0.0234	0	0.0	0.0
6	-0.0301	-0.0360	0.0294	0	0.0	0.0
6	-0.0101	-0.0725	0.0406	0	0.0	0.0

/* endpoints */

muscle_name GASM

Fmax (N) 1962.6

LCEopt (m) 0.0450

Lslack (m) 0.4080

%FT (%) 45

α (radian) 17.0

Novi 3

/* beginpoints */

5	-0.0190	-0.3929	-0.0235	0	0.0	0.0

5 -0.0300 -0.4022 -0.0258 2 -44 6

7 0.0000 0.0310 -0.0053 0 0.0 0.0

/* endpoints */

muscle_name GASL

Fmax (N) 554.66

LCEopt (m) 0.0640

Lslack (m) 0.3850

%FT (%) 45

α (radian) 8.0

Novi 3

/* beginpoints */

5 -0.0220 -0.3946 0.0272 0 0.0 0.0

5 -0.0300 -0.4018 0.0274 2 -44 6

7 0.0000 0.0310 -0.0053 0 0.0 0.0

/* endpoints */

muscle_name TIBAN

Fmax (N) 654.73

LCEopt (m) 0.0980

Lslack (m) 0.2230

%FT (%) 30

α (radian) 5.0

Novi 3

/* beginpoints */

6 0.0179 -0.1624 0.0115 0 0.0 0.0

6 0.0329 -0.3951 -0.0177 0 0.0 0.0

7 0.1166 0.0178 -0.0305 0 0.0 0.0

/* endpoints */

muscle_name SOLEU

Fmax (N) 7238.9

LCEopt (m)	0.0300					
Lslack (m)	0.2680					
%FT (%)	25					
α (radian)	25.0					
Novi	2					
/* beginpoints */						
6	-0.0024	-0.1533	0.0071	0	0.0	0.0
7	0.0044	0.0310	-0.0053	0	0.0	0.0
/* endpoints */						

muscle_name	TIBPOS					
Fmax (N)	1018.9					
LCEopt (m)	0.0310					
Lslack (m)	0.3100					
%FT (%)	45					
α (radian)	12.0					
Novi	4					
/* beginpoints */						
6	-0.0094	-0.1348	0.0019	0	0.0	0.0
6	-0.0144	-0.4051	-0.0229	0	0.0	0.0
7	0.0417	0.0334	-0.0286	0	0.0	0.0
7	0.0772	0.0159	-0.0281	0	0.0	0.0
/* endpoints */						

muscle_name	PERL
Fmax (N)	956.1
LCEopt (m)	0.0490
Lslack (m)	0.3450
%FT (%)	40
α (radian)	10.0
Novi	7
/* beginpoints */	

6	0.0005	-0.1568	0.0362	0	0.0	0.0
6	-0.0207	-0.4205	0.0286	0	0.0	0.0
6	-0.0162	-0.4319	0.0289	0	0.0	0.0
7	0.0438	0.0230	0.0221	0	0.0	0.0
7	0.0681	0.0106	0.0284	0	0.0	0.0
7	0.0852	0.0069	0.0118	0	0.0	0.0
7	0.1203	0.0085	-0.0184	0	0.0	0.0

/* endpoints */

muscle_name	PERB
Fmax (N)	760.6
LCEopt (m)	0.0500
Lslack (m)	0.1610
%FT (%)	55
α (radian)	5.0
Novi	5

/* beginpoints */

6	-0.0070	-0.2646	0.0325	0	0.0	0.0
6	-0.0198	-0.4184	0.0283	0	0.0	0.0
6	-0.0144	-0.4295	0.0289	0	0.0	0.0
7	0.0471	0.0270	0.0233	0	0.0	0.0
7	0.0677	0.0219	0.0343	0	0.0	0.0

/* endpoints */

muscle_name	FHAL
Fmax (N)	718.34
LCEopt (m)	0.0430
Lslack (m)	0.3800
%FT (%)	50
α (radian)	10.0
Novi	7

/* beginpoints */

6	-0.0079	-0.2334	0.0244	0	0.0	0.0
6	-0.0186	-0.4079	-0.0174	0	0.0	0.0
7	0.0374	0.0276	-0.0241	0	0.0	0.0
7	0.1038	0.0068	-0.0256	0	0.0	0.0
7	0.1726	-0.0053	-0.0269	0	0.0	0.0
8	0.0155	-0.0064	-0.0265	0	0.0	0.0
8	0.0562	-0.0102	-0.0181	0	0.0	0.0

/* endpoints */

Achievement during doctoral course enrollment

Journal publications

1. **Kudo S,** Fujimoto M, Isaka T, Nagano A. Quantitative assessment of trunk deformation during running. J Biomech. 2017 Jul 5;59: 116-121.
2. **Kudo S.**, Fujimoto M., Sato T., Nagano A., 2018. Quantitative evaluation of linked rigid-body representations of the trunk., Gait & posture 63 119-123.
3. **Kudo S.**, Fujimoto M., Sato T., Nagano A., 2020. Determination of the optimal number of linked rigid-bodies of the trunk during walking and running based on Akaike's information criterion, Gait & posture 77, 264-268.

International conference presentations

1. **Kudo S**, Fujimoto M, Sato T, Nagano A., 2019, Kinetic characteristics of the trunk during walking, 25th congress of the European Society of Biomechanics.
2. **Kudo S**, Fujimoto M, Sato T, Nagano A., 2018, Determination of the optimal number of rigid-body segments to represent the trunk using Akaike's information criterion, the 36th International Conference on Biomechanics in Sports 2018
3. **Kudo S**, Fujimoto M, Sato T, Nagano A., 2018, Kinetic contribution of multi-segmental trunk during dynamic movements, 8th World Congress of Biomechanics.

Domestic conference presentations

1. **工藤将馬**，藤本雅大，佐藤隆彦，長野明紀, 2019, 歩行動作中の体幹部の運動力学的特徴 歩行動作における最適自由度を有する剛体リンクモデルを用いた解析, 第 1 回彗ひろば.
2. **工藤将馬**，藤本雅大，佐藤隆彦，長野明紀, 2018, 赤池情報量基準に基づいた体幹部の動作解析に適した剛体セグメントモデルの検討, 第 25 回日本バイオメカニクス学会大会.

Acknowledgements

本博士論文を執筆するにあたり，学部生 3 回生の頃から修士課程及び博士課程の 7 年間にかけて終始懇切丁寧なご指導を賜りました指導教員の長野明紀教授に心から厚く御礼申し上げます．長野先生の研究活動に対する姿勢や才能に憧れ，向上心を持って博士課程での日々を送ることが出来ました．長野先生に出会えたこと，長野先生から学んだこと，そのすべてが私の大切な財産です．有難うございました．

本博士論文の審査にあたり、ご多忙の中，副査をお引き受けいただきました立命館大学スポーツ健康科学部の金久博昭教授ならびに同学部の塩澤成弘教授，招聘副査としてご協力いただきました東京大学大学院総合文化研究科の吉岡伸輔准教授には，貴重なご指導，ご助言を賜りました．深く感謝申し上げます．

本博士論文の各研究課題において，共同研究者としてご協力賜りました産業技術総合研究所の藤本雅大先生，びわこリハビリテーション専門職大学の佐藤隆彦先生，立命館大学スポーツ健康科学部の伊坂忠夫教授に深謝いたします．藤本先生には学術論文を執筆する際に必要となる論理的な物事の考え方やその表現方法などをご教授いただきました．佐藤先生には，動作解析の方法や力学の知識など，バイオメカニクスの研究に必要な技術を習得する際に沢山のご支援を賜りました．伊坂先生には，本研究の発展性，応用性を考える上で沢山のアイデアやご助言をいただきました．先生方からご教授いただいた知識や研究者としての心得を常に忘れることなく，今後も精進していきます．

研究室での活動において，日々お世話になりましたスポーツサイバネティクス研究室の皆様に深謝の意を表します．特に，立命館大学共通教育機構の大島雄治先生，同大学スポーツ健康科学部の森下義隆先生，城西大学経営学部の篠原康男先生には日ごろの研究室ミーティングにおいて本研究に関わる有益なアドバイスを賜りました．また，同研究室の先輩，同期，後輩の皆様には，日頃から沢山の励ましの言葉をいただき，充実した研究生活を送ることが出来ました．皆様と過ごした濃密な時間は一生の宝物です．

最後になりましたが，これまで心身ともに手厚い支援をしていただいた家族（両親，姉，

愛犬なな）に対し，心から感謝の意を表します．家族の理解なくして，無事に博士課程を修了することはできなかったと思います．有難うございます．これからも精進し，少しずつではありますが，この恩を返していきます．

なお，本研究は文部科学省科学研究費補助金（特別研究員奨励費# 18J21267）の助成のもと実施いたしました．